Synthesis and characterization of unsaturated polyesters for use in multi-vesiculated particles (MVPs)

by

Jaylin Mitch Simpson

Thesis presented in partial fulfilment of the requirements for the degree Master of Science (Polymer Science) at the University of Stellenbosch

Supervisor: Prof. P. E. Mallon
Co-supervisor: Dr. J. B. McLeary
Faculty of Science
Department of Chemistry and Polymer Science

December 2010

Declaration

By submitting this thesis/dissertation electronically, I declare that the entirety of the work contained therein is my own, original work, and that I have not previously in its entirety or in part submitted it for obtaining any qualification.

December 2010

ABSTRACT

Unsaturated polyesters resins (UPRs) of maleic anhydride (MA), phthalic anhydride (PA) and propylene glycol (PG) were synthesized using the fusion polycondensation process for use in Multi-vesiculated Particles (MVPs). The UPRs were synthesized using different MA:PA mole ratios and process parameters, including heating rates, agitation speed, exotherm rate and maximum processing temperature. Design of Experiments (DoE) software (Design Expert 7) was employed to find the optimum experimental space, i.e. least amount of experiments, but covering all the factors. The variations in the formulation and process parameters had a significant effect on the molecular structure and physical properties of the UPRs. The molecular structure and physical properties of the UPRs was successfully determined using various techniques including viscometry, acid-base titration, Proton Nuclear Magnetic Resonance (^{1}H NMR) spectroscopy, Size-Exclusion Chromatography (SEC), Fourier Transform Infrared (FTIR) spectroscopy and Differential Scanning Calorimetry (DSC). Furthermore, the carboxyl and hydroxyl end-group concentrations of the UPRs were determined by derivatization of the groups with trichloroacetyl isocyanate (TAI) and analysis by ^{1}H NMR.

As a second part of the study, the effect of the above-mentioned monomer ratio and process factors of the UPRs, on the properties of the MVPs (produced from the UPRs), was investigated. Results showed that these factors had a significant effect on the particle size and degree of vesiculation of the MVPs. The degree of vesiculation of the MVPs was determined by Scanning Electron Microscopy (SEM). Attempts were also made to determine the relative hardness of the MVPs by AFM and microhardness testing to determine a relationship with UPRs properties (e.g. molecular weight, degree of unsaturation and chain branching). These techniques were however found to be unsuitable due to the physical nature of the MVPs.

OPSOMMING

Onversadigde poliësters (OPs) van maleïensuuranhidried (MA), fataalsuuranhidried (PA) en propileen glikol (PD) is berei deur die fusie polikondensasie-proses vir gebruik in multi-vesikulerende partikels (MVPs). Die OPs is berei deur gebruik te maak van verskillende MA:PA molverhoudings en reaksie faktore wat verhittingstempo's, roerspoed, eksoterm tempo en maksimum reaksie temperatuur, insluit. As gevolg van die groot hoeveelheid faktore is eksperimentontwerp sagteware (Design Expert 7) gebruik om die aantal eksperimente te verminder, maar ook waardevolle afleidings van die data te maak. Die verskille in die formulasie en reaksie faktore het 'n merkwaardige effek op die molekulêre struktuur en fisiese eienskappe van die OPs gehad. Hierdie eienskappe is bepaal m.b.v. verskeie tegnieke, naamlik viskometrie, suur-basis titrasie, Proton Kern-Magnetiese Resonansie (^{1}H KMR) spektroskopie, Grootte-Uitsluitings-Chromatografie (SEC), Fourier Transform Infrarooi (FTIR) spektroskopie en Differensiële Skandeerings Kalorimetrie (DSC). Die hidroksiel en karboksielgroep konsentrasies van die OPs is bepaal deur hul reaksie met trichloroasetiel-isosianaat (TAI) gevolg deur ^{1}H KMR analise.

In die tweede deel van hierdie studie is die invloed van bogenoemde faktore op die eienskappe van die MVPs ondersoek. Die resultate het getoon dat hierdie faktore 'n merkwaardige effek op die partikel grootte en graad van "vesiculation" van die MVPs gehad het. Die graad van "vesiculation" van die MVPs is bepaal met behulp van Skandeer Elektron Mikroskopie (SEM). Pogings is ook gemaak om die relatiewe hardheid van die MVPs te bepaal deur middel van AFM en Mikro-hardheid toetsing. Dit is gedoen om die verhouding van die OPs eienskappe (molekulêre gewig, graad van onversadigheid en sy-kettings) vas te stel. Hierdie tegnieke is egter ongeskik bevind as gevolg van die inherente fisiese aard van die OPs.

ACKNOWLEDGEMENTS

I would first like to thank God for the health and strength to carry out this study.

Secondly, I would like to thank my parents for all their support during my studies.

I would also like to thank my promoters Prof. P. E. Mallon and Dr. J. B. McLeary for their help and support, and the opportunity to carry out this MSc study.

I would also like to thank the following people for their contributions:

1. Mr. Mohammed Jaffer (University of Cape Town) for the microtoming assistance
2. Mrs. M. R. Franzenburg for the SEM assistance
3. Dr. M. Meincken (University of Stellenbosch) for the AFM assistance
4. Dr. J. Brand and Elsa Malherbe (University of Stellenbosch) for the NMR assistance
5. Dr. N. Mautjana for the SEC assistance.

Lastly, I would like to thank my Plascon colleagues, especially Bertus Smit and Stephen Clarke, for all their support.

Dedicated to my mother and father

LIST OF CONTENTS

LIST OF CONTENTS i

LIST OF FIGURES iv

LIST OF TABLES vii

LIST OF ABBREVIATIONS viii

LIST OF SYMBOLS x

CHAPTER 1: INTRODUCTION AND OBJECTIVES 1

1.1 Introduction 1

1.2 Objectives 2

1.3 References 3

CHAPTER 2: HISTORICAL AND THEORETICAL BACKGROUND 4

2.1 **Polycondensation: Polyesters** 4

2.1.1 Introduction *4*

2.1.2 Polycondensation *6*

2.1.3 *Reactions* *9*

2.2 Suspension polymerization 16

2.2.1 *Introduction* *16*

2.2.2 History *17*

2.2.3 Process of suspension polymerization *17*

2.2.4 Control of particle size in suspension polymerization *21*

2.2.5 *Bead-suspension polymerization kinetics* *23*

2.3 Suspension polymerization – Vesiculated particles 24

2.3.1 Introduction *24*

2.3.2 Single vesicle particles *24*

2.3.3 *Multi-vesiculated particles (MVPs)* *25*

2.4 Design of Experiments (DoE) **30**

2.4.1 Introduction *30*

2.5 References **32**

CHAPTER 3: EXPERIMENTAL **39**

3.1 Introduction **39**

3.2 Materials **40**

3.3 Unsaturated polyester (UPR) synthesis **40**

3.4 Design of Experiments (DoE) **42**

3.5 Multi-vesiculated particle (MVP) synthesis **43**

3.6 Analytical techniques and measurements **44**

3.6.1 *Size-Exclusion Chromatography (SEC)* *45*

3.6.2 *Dynamics Scanning Calorimetry (DSC)* *45*

3.6.3 *Nuclear Magnetic Resonance (NMR) Spectroscopy* *45*

3.6.4 *Scanning Electron Microscopy (SEM)* *45*

3.6.5 *Microtoming* *46*

3.6.6 *Laser diffraction (*LD*)* *46*

3.6.7 *Acid-value* *46*

3.6.8 *Solids conten*t *47*

3.6.9 *Viscosity* *47*

3.6.10 Contrast ratio (opacity) *48*

3.6.11 *Hardness – microhardness and Atomic Force Microscopy (AFM*) *48*

CHAPTER 4: RESULTS AND DISCUSSION 50

4.1 Design of Experiments (DoE) analysis 50

4.1.1 Introduction 50

4.1.2 Results and discussion – UPRs 50

4.1.2.1 Brookfield viscosity 54

4.1.2.2 Acid-value 61

4.1.2.3 Number- and weight-average molecular weights (M_n and M_w) 64

4.1.2.4 Polydispersity index (PDI) 68

4.1.2.5 Preliminary conclusion: UPRs 70

4.1.3 Results and discussion – MVPs 71

4.1.3.1 SMD-values 73

4.1.3.2 VMD-values 74

4.1.3.3 Preliminary conclusion: MVPs 79

4.2 Detailed analysis of selected DoE runs 80

4.3 Effect of UPR maximum processing temperature on properties of the UPR and the resultant MVPs 85

4.4 Determination of hardness of MVPs 92

4.5 Chain-branching 94

4.6 End-group analysis by isocyanate derivatization and ^{1}H NMR 97

4.7 References 101

CHAPTER 5: CONCLUSIONS 103

5.1 Conclusions 103

5.2 Recommendations for future work 105

LIST OF FIGURES

CHAPTER 2

Figure 2.1: Generalized reaction scheme of esterification. 6
Figure 2.2: Reaction scheme of polyesters via self-condensation of ω-hydroxy acids. 6
Figure 2.3: Reaction scheme of polyesters via condensation of diols with diacids. 7
Figure 2.4: Reaction scheme of polyesters via ester exchange with a diol. 7
Figure 2.5: Reaction scheme of polyesters via ring-opening of lactones. 7
Figure 2.6: Reaction scheme of polyesters via alcoholysis. 7
Figure 2.7: Formation of the UPR, poly (propylene fumarate phthalate). 8
Figure 2.8: Reaction scheme of monoester formation. 9
Figure 2.9: Reaction scheme of polyesterification. 9
Figure 2.10: Reaction scheme of cis-trans isomerization (maleate to fumarate). 10
Figure 2.11: Reaction scheme of the Ordelt saturation of monoester by diol (short chain branches) 12
Figure 2.12: Reaction scheme of the Ordelt saturation of monoester by monoester (long chain branches). 13
Figure 2.13: Reaction scheme of transesterification side reaction during polyesterification. 14
Figure 2.14: Illustrative scheme of breakage and coalescence mechanisms involved in suspension polymerization. 20
Figure 2.15: Schematic diagram of the Ropaque opaque polymer particle. 25
Figure 2.16.1: Scanning electron micrograph of Spindrift particles. 26
Figure 2.16.2: Scanning electron micrograph of a cross-section of a Spindrift particle. 26
Figure 2.17: Micelle formation. 28
Figure 2.18: Crosslink reaction of unsaturated polyester and styrene. 29

CHAPTER 4

Figure 4.1: Two component mix graph for the formulation factors affecting the viscosity of the UPR-STY mixtures. 55
Figure 4.2: Contour mix-process graph of the interaction effect (BC) of heating rate 1 and %MA in MA:PA mole ratio on the Brookfield viscosity of UPR-STY mixtures. 57
Figure 4.3: Contour mix-process graph of the interaction effect (BD) maximum temperature and %MA in MA:PA mole ratio on the Brookfield viscosity of UPR-STY mixtures. 58

Figure 4.4: Pertubation graph for the process factors affecting viscosity of the UPR-STY mixtures (fixed MA:PA ratio at 26.19: 13.18). 60
Figure 4.5: Two component mix graph for the formulation factors affecting the acid-value of UPRs. 62
Figure 4.6: Contour mix-process graph of the interaction effect (AF) of %PA in MA:PA mole ratio and agitation speed on the acid-value of UPRs. 63
Figure 4.7: Contour mix-process graph of the interaction effect (BF) of %MA and agitation speed on acid-value of UPRs. 64
Figure 4.8: Two component mix graph for the formulation factors affecting the M_w-value of UPRs. 66
Figure 4.9: Contour mix-process graph of the interaction effects AD and ABD, i.e. interactions between %PA, MA:PA mole ratio and maximum temperature on M_w-value of UPRs. 67
Figure 4.10: Two component mix graph for the formulation factors affecting the PDI-value of UPRs. 69
Figure 4.11: Contour mix-process graph of the interaction effect ABD, interaction between MA:PA ratio and the maximum temperature on PDI-value of UPRs. 70
Figure 4.12: : Two component mix graph for the formulation factors of the UPRs affecting SMD-value of the MVPs. 74
Figure 4.13: Contour mix-process graph of the interaction effect BD, i.e. interaction between %MA and the maximum temperature of the UPRs on SMD-value of MVPs. 75
Figure 4.14 Two component mix graph for the formulation factors of the UPRs affecting VMD-value of the MVPs. 77
Figure 4.15: Contour mix-process graph of the interaction effect BD, i.e. interaction between %MA and the maximum temperature of the UPRs on VMD-value of MVPs. 78
Figure 4.16: Contour mix-process graph of the interaction effect BE, i.e. interaction between %MA and the heating rate 2 of the UPRs on VMD-value of MVPs. 79
Figure 4.17: SEM images of (a) MVPs of RUN 6 at 100× magnification and (b) microtomed MVPs of RUN 6 at 1790 × magnification. 82
Figure 4.18: SEM images of (a) MVPs of RUN 26 at 100× magnification and (b) microtomed MVPs of RUN 26 at 735 × magnification. 82
Figure 4.19: Surface area- and cumulative distributions of the particle sizes of MVPs of DoE run 6 and DoE run 26. 84
Figure 4.20: SEC chromatograms of UPRs prepared at different maximum processing temperatures. 86

Figure 4.21: Schematic diagram of the effect of chain branching on the acid-value of the UPRs. 87
Figure 4.22: DSC curves of the UPRs prepared at different maximum processing temperatures. 88
Figure 4.23: SEM micrograph of microtomed MVPs of a) RUN 29 at 622× magnification and (b) RUN 33 at 913× magnification. 89
Figure 4.24: Surface area- and cumulative distributions of the particle sizes of MVPs of runs 29 (red) and 33 (blue). 91
Figure 4.25: AFM 3D image (a) and force-distance curve (b) of a sub-micron MVP of RUN 29. 93
Figure 4.26: AFM 3D-image (a) and force-distance curve (b) of a sub-micron MVP of RUN 33. 94
Figure 4.27: ^{1}H NMR spectrum of polyester with phthalic anhydride. 95
Figure 4.28: ^{1}H NMR spectrum of polyester with maleic anhydride. 95
Figure 4.29: ^{1}H NMR spectrum of UPR of RUN 29. 96
Figure 4.30: Derivatization of OH-groups of UPRs with TAI. 98
Figure 4.31: Derivatization of COOH-groups of UPRs with TAI. 98
Figure 4.32: FTIR spectrum of the UPRs of RUN 29 and RUN 29 derivatized with TAI. 99
Figure 4.33: ^{1}H NMR spectrum of UPR of RUN 29 derivatized by TAI. 100

LIST OF TABLES

CHAPTER 2

Table 2.1: Isomeration vs glycol type. 11

Table 2.2: Isomerization vs reaction temperature. 11

Table 2.3: Level of unsaturation. 15

Table 2.4: Typical properties of Ropaque. 24

CHAPTER 3

Table 3.1: Standard unsaturated polyester formulation. 41

Table 3.2: Formulation and process factors for unsaturated polyester synthesis. 42

Table 3.3: Standard MVPs formulation. 44

CHAPTER 4

Table 4.1: Experimental design space for UPR synthesis. 52

Table 4.2: Significant factors affecting the Brookfield viscosity of UPR-STY mixtures. 54

Table 4.3: Significant factors affecting the acid-value of UPRs. 61

Table 4.4: Significant factors affecting the M_w-value of UPRs. 65

Table 4.5: Significant factors affecting the PDI-value of UPRs. 68

Table 4.6: Particle size results of MVPs. 72

Table 4.7: Significant factors affecting SMD-value of the MVPs. 73

Table 4.8: Significant factors affecting VMD-value of the MVPs. 76

Table 4.9: Formulation and process parameters of DoE runs 6 and 26. 80

Table 4.10: Properties of UPRs of DoE runs 6 and 26. 80

Table 4.11: Properties of MVPs with UPRs of DoE runs 6 and 26. 80

Table 4.12: Effect of UPR maximum processing temperature on properties of the UPRs of runs 29 – 33. 85

Table 4.13: Effect of UPR maximum processing temperature of runs 29 – 33 on properties of the MVPs. 88

Table 4.14: Degree of branching results of UPRs of runs 29 and 33 via ^{1}H NMR and SEC. 96

Table 4.15: Relative hydroxyl -and carboxyl group percentages of UPRs of runs 29 to 33. 100

LIST OF ABBREVIATIONS

AV	Acid-value
AFM	Atomic Force Microscopy
ANOVA	Analysis of variance
CHP	Cumene hydroperoxide
DB	Degree of branching
DCPD	Dicyclopentadiene
DEG	Diethylene glycol
DSC	Differential Scanning Calorimetry
DoE	Design of Experiments
DETA	Diethylene triamine
EG	Ethylene glycol
FTIR	Fourier Transform Infra-red spectroscopy
HEC	Hydroxy ethyl cellulose
HPLC	High Performance Liquid Chromatography
IPA	Isophthalic acid
KOH	Potassium hydroxide
LD	Laser Diffraction
LMA	Lauryl methacrylate
MA	Maleic anhydride
MALDI-MS	Matrix-Assisted-Laser-Desorption-Ionization-Mass-Spectrometry
MEKP	Methyl-ethyl ketone peroxide
MMA	Methyl methacrylate
MVPs	Multi-vesiculated particles
NMR	Nuclear magnetic resonance
OH	Hydroxyl
PA	Phthalic anhydride
PET	Poly (ethylene terephthalate)
PG	Propylene glycol
PVA	Poly (vinyl acetate)
PVOH	Poly (vinyl alcohol)

RSM	Response surface methodology
SEM	Scanning Electron Microscopy.
STY	Styrene
TAI	Trichloroacetyl isocyanate
TBC	Tert-butyl catechol
T_g	Glass transition temperature
THF	Tetrahydrofuran
TiO_2	Titanium dioxide
UPR	Unsaturated polyester resin
ZnO	Zinc oxide

LIST OF SYMBOLS

D	NMR intensity of branched unit in polyester chain
DP_n	Degree of polymerization
L	NMR intensity of linear unit in polyester chain
M_n*	Growing polymer chain
M_n	Number average molecular weight
M_w	Weight average molecular weight
N	Normality of KOH solution
PDI	Polydispersity index
SMD	Sauter Mean Diameter
$S_{UPR\text{-}STY}$	Solids content of UPR-STY mixture
V_{KOH}	Volume of KOH solution used in acid-base titration
VMD	Volume Mean Diameter
w_i	Sample weight
$W_{UPR\text{-}STY}$	Weight of UPR-STY mixture
R*	Radical generated by dissociation of the initiator
P_n	Polymer with n repeat units
d	Average particle size
k	Parameters e.g. apparatus design, type of stirrer
D_v	Diameter of vessel
D_s	Diameter of stirrer
R	Volume ratio of droplet phase / suspension medium
N	Stirring speed (or power of mixing)
v_a	Viscosity of the droplet phase
v_m	Viscosity of the suspension medium
ε	Interfacial tension between two immiscible phases
C_s	Stabilizer concentration

CHAPTER 1

INTRODUCTION AND OBJECTIVES

1.1 Introduction

Titanium dioxide (TiO_2) is the primary opacifying pigment in the coatings industry. The cost of the TiO_2 pigment have soared in the past few decades due to increased consumption in a variety of applications, therefore alternatives are attractive [1]. It is known that opacity of a coating can be increased by incorporating microvoids or micro-vesicles into a coating as they scatter light[1]. Micro-voids can be incorporated into a coating by introducing organic opacifying particles, such as the commercial products Multi-vesiculated particles® (MVPs) produced by Plascon and single-vesiculated particles like Ropaque Opaque Polymer® produced by Rohm & Haas.

The present study focuses on MVPs which are dispersions of crosslinked (thermosetting) non-film forming particles in water. The particles are formed by the reaction of the unsaturated polyester resin (UPR) with reactive diluent styrene (STY) and diethylene triamine (DETA) in a continuous aqueous phase containing water, poly (vinyl alcohol) (PVOH) and hydroxyl ethyl cellulose (HEC), via suspension polymerization [2]. These particles contain air voids which form by the reaction between the UPR and DETA [2]. The voids/vesicles are filled with water in the wet-state. The water from the voids diffuses through the particle-wall upon drying, resulting in the air voids/vesicles. These vesicles have the ability to scatter light (and thus impart opacity and "hiding power" to a surface coating) due to the difference in the refractive index between the particle shell and the air voids [1, 3].

MVPs are used in surface coating formulations as matting agents and can be used to partially replace the primary but expensive opacifying pigment, TiO_2, depending on their particle size[1, 3]. Generally, two versions of MVPs are commercially available which have average particle sizes of 5µm (used in silk/satin finish paints) and 25µm (used in matt finish paints) [1].

Numerous processing- and formulation factors affect the properties and performance of the MVPs. These include process parameters such as temperature, addition rate, mass

and heat transfer, agitation, stabilizer system, and reaction kinetics [4-5]. The effect of the properties of the UPR is also a major factor affecting the properties of MVPs such as particle size and particle size distribution, viscosity, and degree of particle vesiculation [4-5].

The UPR used in the synthesis of the MVPs is commercially produced by the polycondensation reaction between maleic anhydride (MA), phthalic anhydride (PA) and propylene glycol (PG) at 220°C. A reactive diluent (styrene) is added which reduce the viscosity of the resins to assist processing, and copolymerize with the resin in order to cure the material [6].

1.2 Objectives

Despite the commercial production of the particular UPR and the MVPs, little is understood about the effect of the UPR molecular structure on the properties of the MVPs (e.g. particle size or degree of vesiculation). It is known that the molecular structure and inherent properties of the UPRs (e.g. molecular weight and degree of chain branching) are greatly affected by the ratio of the monomers and process parameters such as reaction temperature, agitation speed and heating rate [7-8]. The present study attempts to relate the UPR molecular structure with the MVP properties by synthesizing MVPs from UPRs with varying monomer ratios and process parameters. Due to the large number of factors affecting the properties of the UPRs, statistical Design of Experiments (DoE) is employed to reduce the number of experiments and isolate the most significant factors affecting the UPR and MVP properties.

The major objectives of this study are as follows:

1.2.1 Investigation of the effects of varying the MA:PA mole ratio and process parameters, e.g. heating rates, agitation speeds, etc. on the properties of the UPR, via DoE.

1.2.2 Synthesis of MVPs using the different synthesized UPRs to investigate the effects of varying the PA: MA ratio and process parameters on the properties of the MVPs.

1.2.3 Determination of the molecular composition/ structure of the UPR and relate to specific properties of MVPs.

1.3 References

1. Goldsbrough, K.; Simpson, L. A.; Tunstall, D. F. *Progress in Organic Coatings* **1982,** 10, 35.
2. Engelbrecht, J. F.; De Wet-Roos, D.; Smit, A. C.; Cooray, B. Vesiculated polymer particles. US 2006/0111474 A1, **2006**.
3. Ritchie, P., *Spindrift Pigmented Vesiculated Beads*, In *Surface Coatings. Raw materials and their usage*, The New South Wales University Press: Kensington, NSW, Australia, **1993**; pp 351 - 355.
4. Terblanche, J. C. The development of vesiculated beads. MScEng, University of Stellenbosch, **2002**.
5. Gous, K. Continuous processing of vesiculated beads. MScEng, University of Stellenbosch, **2003**.
6. Johnson, K. G.; Yang, L. S. *Preparation, Properties and Applications of Unsaturated Polyesters,* In *Modern Polyesters: Chemistry and Technology of Polyesters and Copolyesters*, Scheirs, J.; Long, T. E., Eds. John Wiley & Sons: West Sussex, England, **2003**; p 699.
7. *Processing Unsaturated Polyesters based on Amoco Isophthalic acid*; IP-43b; Amoco Chemical Co.: **1989**; pp 1 - 19.
8. *How Ingredients Influence Unsaturated Polyester properties*; IP-70; Amoco Chemical Co.: pp 1 - 27.

CHAPTER 2

HISTORICAL AND THEORETICAL BACKGROUND

2.1 Polycondensation: Polyesters

2.1.1 Introduction

Polyesters are a class of polymers that can be formulated to be hard or soft, brittle or flexible depending on the structure and can therefore be used in various applications. These applications include fibers (e. g. polyethylene terephthalate (PET)) [1-3], coatings[4-5], plasticizers [6], adhesives [5-6], polyurethane based resins [6], films [6], laminates [5], industrial construction [5], insulation[5], molding compounds [5], etc. Polyesters are used for these applications because of their low cost [2-3, 5, 7], ease of process [7], ease of combination with reinforcements [2-3, 7]. In addition, these polymers cure rapidly without any volatile products [2-3, 7-8], have excellent dimensional stability [7], have high impact resistance [5], transparency [5] and good weathering resistance [5].

Polyesters do however have disadvantages including poor adhesion, high cure shrinkage and inhibition of the curing reaction by air and certain fillers [5], as well as poor resistance to hydrolysis by water [8].

History suggests that the first saturated polyesters were synthesized by Berzelius in 1847 from tartaric acid and glycerine [9-10], Berthelot in 1853 from glycerol and camphoric acid [11], and Lorenzo in 1863 from ethylene glycol and succinic acid [12]. UPRs were first prepared by Vorlander in 1894 who studied glycol maleates [9].

In the 1920s, Wallace Carothers studied linear polyesters [6, 8, 13] among which were unsaturated derivatives from ethylene glycol and unsaturated carboxylic acids and anhydrides such as MA and fumaric acid. The resins synthesized by Carothers were either extremely viscous or solid [14]. Carlton Ellis discovered that a diluent monomer such as styrene (STY) can be added to the UPR to produce a low viscosity mixture that will also copolymerize (under certain conditions) at rates much faster than that of the homopolymerization [14]. In 1947, during the Second World War, styrenated polyesters were reinforced with glass fibers to yield high strength materials [8, 14].

The first major commercial polyesters were PET discovered by Whinfield and Dickson [8, 15] and polyadipates (for polyurethane resins) [16].

Commercial polyester resins are classified as follows [17]:

- General-purpose orthophthalic resins – PA, MA and glycol resins.
- Isophthalic resins – isophthalic acid (IPA), MA and glycol resins.
- Dicyclopentadiene (DCPD)-capped resins.

These polyesters are generally produced via four main processes:

- ***Fusion process*:** In the fusion process, monomers are polymerized at very high temperatures. The main advantage is that the process is robust but the process is disadvantageous because great difficulties are experienced due to slow-down of polycondensation reaction in the final reaction phase due to increase in viscosity of reaction mixture [18]. In addition, the use of esterification catalysts is not possible because the reaction is carried out at very high temperatures [18]. Large excesses of acidic or alcoholic components are also not possible, since these components cannot be removed from the reaction mass in an economic manner [18].

- ***Azeotropic solvent process*:** The azeotropic solvent process involves the addition of an aromatic hydrocarbon, e.g. xylene (concentration = 3 – 6 wt. %), to the reaction mixture during polymerization to increase the rate of water removal by increasing the vapor pressure of the volatile compounds [18]. It also results in a decrease in the solubility of water in the system and a reduction of the overall viscosity to some extent [18]. Aromatic hydrocarbons are water-insoluble, so that separation of the water phase from the organic phase occurs very rapidly and the organic phase can be recycled immediately to the reactor or to the distillation element above the reactor [18]. The main advantages of the azeotropic solvent process include reducing the polyesterification time by 30-50 % and producing polyesters with improved color, and in some cases narrower molecular weight distribution [18].

- ***Inert gas transport process*:** In the inert gas transport process, inert gas (usually nitrogen or carbon dioxide) is sparged through the reaction mass during the fusion process to aid water removal [19-21]. Reduction in polyesterification is comparable to that of the azeotropic solvent process [18]. The main disadvantage of the inert gas transport process is that other volatile components e.g. PA are also removed from the reaction

mass during this process [18].

- ***Vacuum process*:** The vacuum process involves the dehydration of the reaction mass by reducing the interior pressure of the reactor [18]. The main advantage of the vacuum process is the fact that water, the azeotropic component, and other volatile compounds are converted into the gas phase more readily [18]. The vacuum process also results in an increase in the rate of acid-value reduction[18]. The rate at which the acid value decreases is proportional to the rate at which the reaction mass is dehydrated. The main disadvantage of vacuum polyesterification is the formation of additional molecular structures, which are not present when polyesterification is carried out at atmospheric pressure.

2.1.2 Polycondensation

Polyesters are condensation polymers with ester/ carboxylate repeating units in the main chain. Figure 2.1 shows the generalized reaction scheme of esterification, where N: is nucleophile eg. OR', where R' is an alkyl group. The rate of reaction is dependent on R, X and N and whether or not the reaction is catalyzed [1, 22-25].

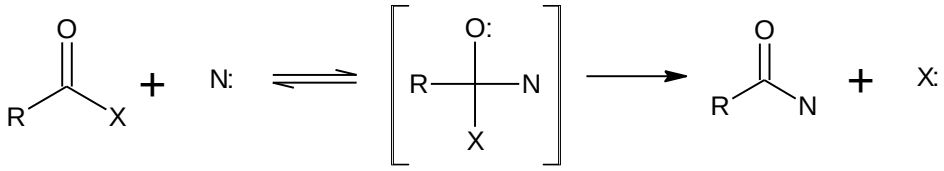

Figure 2.1: Generalized reaction scheme of esterification (R = alkyl).

Polyesters can be synthesized via a variety of pathways, these include:

1. Self-condensation of ω-hydroxy acids [8]

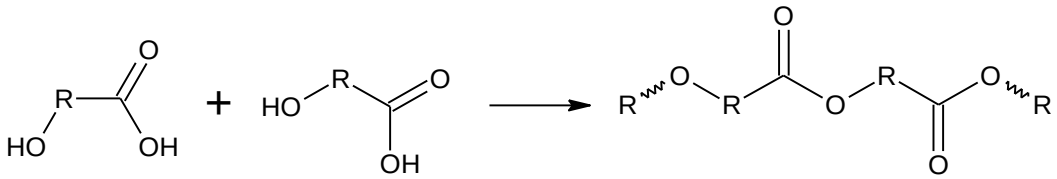

Figure 2.2: Reaction scheme of polyesters via self-condensation of ω-hydroxy acids (R = alkyl).

2. Condensation of a diol with a dicarboxylic acid [8]

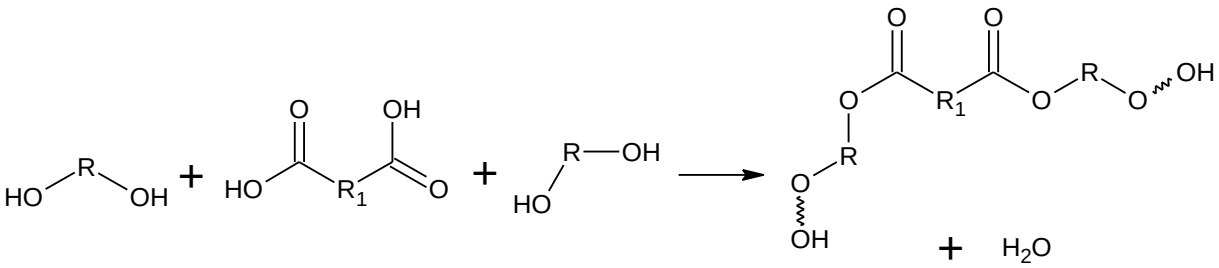

Figure 2.3: Reaction scheme of polyesters via condensation of diols with diacids (R, R_1 = alkyl groups).

3. Ester exchange [8]

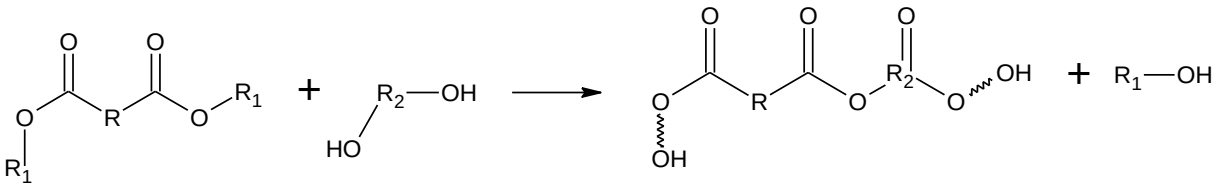

Figure 2.4: Reaction scheme of polyesters via ester exchange with a diol (R, R_1, R_2 = alkyl groups).

4. Ring opening of a lactone, e.g. of e-caprolactone with dihydroxy or trihydroxy initiators [8]:

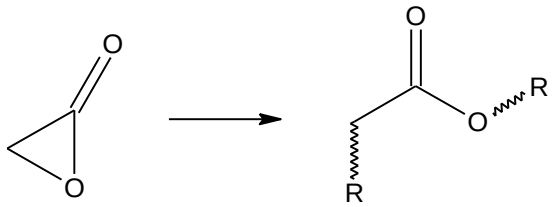

Figure 2.5: Reaction scheme of polyesters via ring-opening of lactones (R = alkyl group).

5. Alcoholysis of the acid chloride of a dicarboxylic acid with a polyhydroxy alcohol [8]

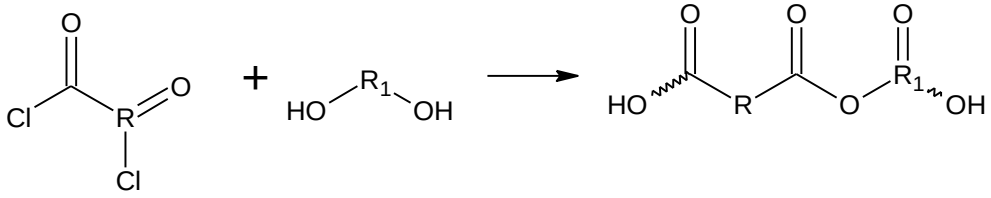

Figure 2.6: Reaction scheme of polyesters via alcoholysis (R, R_1 = alkyl groups).

UPRs, which are the focus of this study, are polymers obtained by the polycondensation reaction of a difunctional unsaturated acid or anhydride, e.g. MA and a difunctional saturated acid or anhydride, e.g. PA with a diol, e.g. propylene glycol (PG) [14,26-28] at 150 - 280 °C, predominantly at atmospheric pressure due to the disadvantages of reduced pressure reactions (e.g. vacuum process) (see Section 2.1.1). Water is the main by-product of the condensation reaction and is removed from the reaction to drive it to completion [14, 26]. Figure 2.7 shows the formation of the UPR, poly (propylene fumarate phthalate).

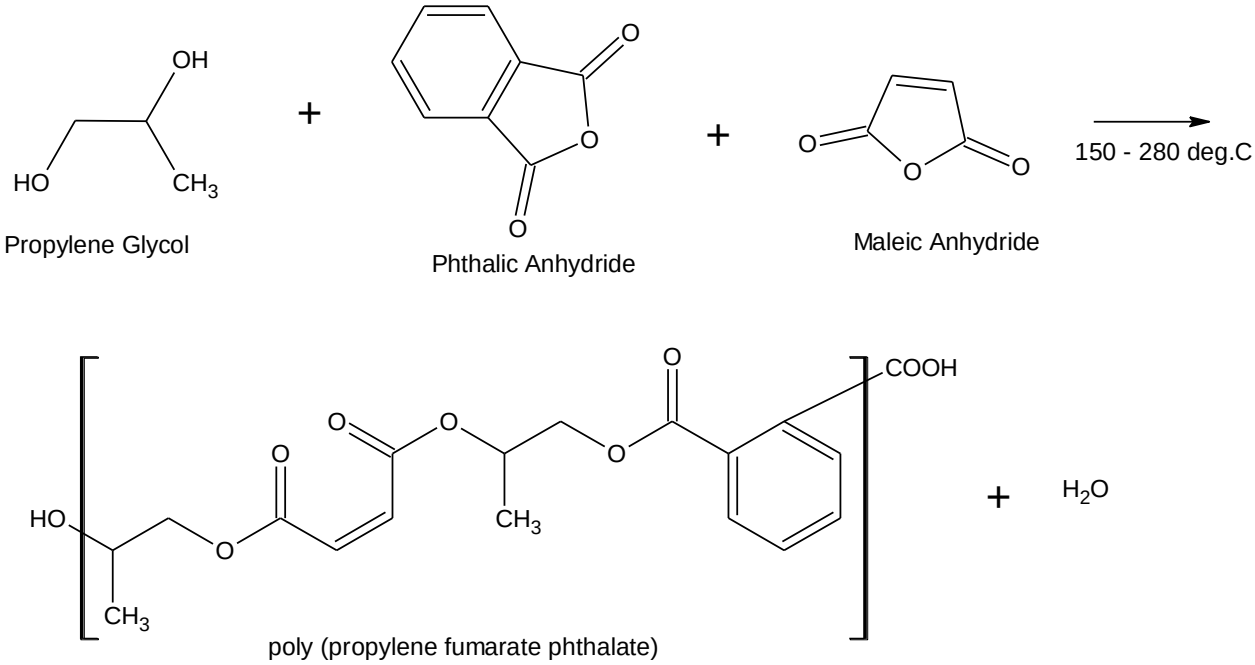

Figure 2.7: Formation of the UPR, poly (propylene fumarate phthalate).

As mentioned previously in Section 2.1.1, UPRs are usually diluted with a reactive diluent, e.g. styrene (STY) or methyl methacrylate (MMA) [2, 18]. The STY or MMA reduces the viscosity of the resins to assist processing, and copolymerizes with the resin in order to cure the material [17].

UPRs are produced by the formation of monoesters or ring-opening of the anhydrides in the first reaction step which reacts to form di-esters after the temperature is increased. These diesters react further through polycondensation to produce the final polyester and water as by-product. The reaction mechanisms throughout polyesterification depend on the reaction temperature, monomer ratio, catalyst system, and processing variables such as water removal and agitation [27]. Detailed description of the reactions involved in the synthesis of UPRs, i.e. ring-opening or monoester formation, polyesterification and side reactions, are discussed in the Section 2.1.3.

2.1.3 Reactions

2.1.3.1 Ring-opening (monoester formation)

Monoesters are formed by the reaction between the anhydride (A) and the glycol (G) to form acid and alcohol end groups (COOH and OH) and an ester bridge with no water formation [27-28]. Figure 2.8 shows the monoester formation during polyesterification.

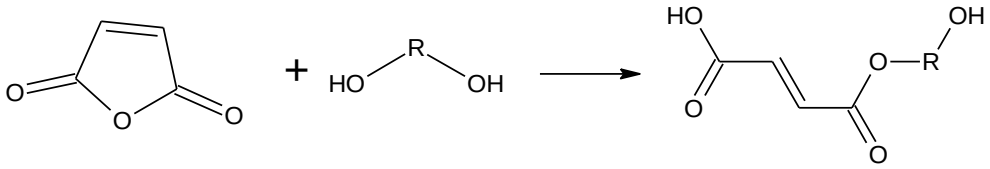

Figure 2.8: Reaction scheme of monoester formation (R = alkyl group).

The monoester formation reaction normally occurs in the temperature range of 60 – 130 °C. The kinetics of this reaction suggests that it is a second order reaction and irreversible. The formation of monoesters depends on the reactivities of the glycols towards the anhydrides, for example, ethylene glycol (EG) and PG are assumed to have the same reactivity towards ring-opening, but anhydrides have different reactivities. The rates at which MA react with EG and PG during ring-opening are equal, but different for when they react with PA [29]. In most cases, monoester formation is followed by the main polyesterifcation reaction between the formed esters and acids and alcohols, with the elimination of water as by-product [18].

2.1.3.2 Polyesterification

The esterification reaction proceeds by reaction of a hydroxyl end-group of one molecule with a carboxylic acid end group to form an ester and water [29]. Figure 2.9 illustrates the polyesterification which occurs in the temperature range of 160 to 220 °C[28]. A high degree of polyesterification is obtained upon efficient removal of water. The removal of water is, however, hampered due to an increase of its solubility in organic substances with increasing temperature [18, 28].

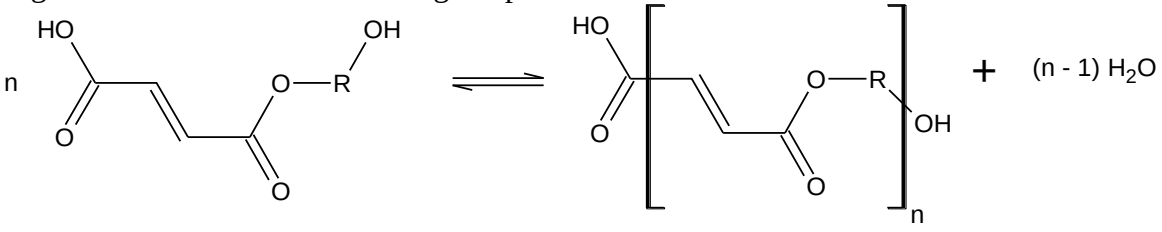

Figure 2.9: Reaction scheme of polyesterification (R = alkyl group).

A number of side-reactions take place during the polyesterification stage. These reactions are discussed in Section 2.1.3.3.

2.1.3.3 Side reactions

2.1.3.3.1 Isomerization

Side reactions in the later stages of the polyesterification reaction prevent high degrees of polymerization [30]. These side reactions are related to a cis-trans isomerization [30]. Figure 2.10 illustrates the cis-trans isomerization reaction which involves the rapid isomerization of maleate (cis) to fumarate (trans) (from the MA component) at a reaction temperature of approximately 200 °C[17, 31].

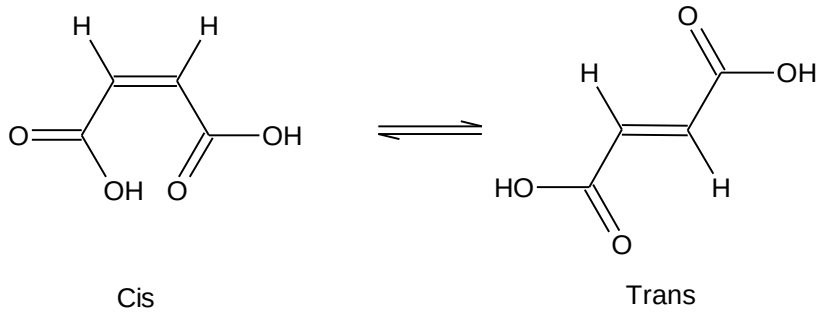

Figure 2.10: Reaction scheme of cis-trans isomerization (maleate to fumarate).

The kinetics suggest that the isomerization reaction is acid catalyzed and obeys a second-order rate law with respect to the acid. The activation energy of isomerization is 63.2 kJ/mol [32].

Furthermore, it is known that more than 90 % of the cis maleate (highly strained structure) isomerizes to the trans-fumarate isomer (less strained, lower energy level)[7, 14]. The fumarate isomer is also much more (about 20 times) reactive to the crosslinking reaction with styrene than the maleate isomer [7, 14, 36-38]. The increased reactivity of the fumarate isomer is due to lesser "crowding" of chains in the trans-configuration [17], which leads to products with improved mechanical [33-34], (improved tensile strength [35] greater hardness, high moduli or stiffness, lower elongation) [36] and thermal [33-34] properties (higher heat distortion temperature, reduced gel and propagation time and higher exotherms) [36] and better chemical resistance [35].

Table 2.1 shows the effect of the glycol type on the percentage isomerization of the maleate groups UPRs. It can be seen from Table 2.1 that the structure of the glycol starting material has a marked influence on the maleate-fumarate isomerization [30, 34], i.e. the reaction is favored by secondary glycols e.g. PG [14]. Primary glycols such as EG are less favorable [14]. It has been shown experimentally that isomerization decreased by around 10-15 % when replacing ethylene glycol (EG) with 1,3-propylene glycol [37], due to the steric hindrance between hydroxyl groups, the glycol chain-length and the "intramolecular spatial interaction between ester groups" which are closely arranged [38].

Isomerization is also affected by reaction temperature and time, i.e. greater isomerization is favored by high temperatures and long reaction times [14, 34]. Other factors influencing isomerization include the nature of the starting materials [39], the concentration of catalyst (e.g. piperidine and morpholine) [33, 40-41] and stereochemical agents [33]. The addition of aromatic acids (e.g. phthalic acid) also has a favorable effect on the degree of isomerization[33-34].

Table 2.1: Isomerization vs glycol type[# 32].

Glycol	Type	Isomerization, %
1,2-propylene	Secondary	96
Ethylene	Primary	64
Diethylene	Primary	53
1,6-Hexamethylene	Primary	36

[#] Reaction Temperature constant = 180 ˚C

Table 2.2 shows the effect of reaction temperature on the percentage of isomerization of the maleate groups of UPRs. It can be seen from Table 2.2 that the percentage of isomerization increases with an increase in the reaction temperature as in the case of poly (propylene glycol maleate) at temperatures ranging from 105-180 ˚C [32].

Table 2.2: Isomerization vs reaction temperature [32].

Reaction temperature (˚C)	Isomerization to fumerate (%)
105	34
125	56
140	75
180	96

2.1.3.3.2 Double bond saturation (Ordelt reaction)

The Ordelt reaction is the main side reaction in the polyesterification reaction. The Ordelt reaction involves the double bonds of the maleate or fumarate component becoming saturated by the addition of hydroxyl groups via electrophilic addition (hydroxyl-alkoxy addition) [42-45] from the glycol. The kinetics of this electrophilic addition were studied by Fradet and Marechal (1982) [46]. It was shown that the reaction is acid catalyzed and follows a first order rate law with respect to the acid and the alcohol [46].

The saturation reaction occurs during the isomerization of maleate to fumarate [28] and may reach 10-20 % [29, 34]. Paci et. al. studied this saturation reaction of UPRs from diethylene glycol (DEG), PG, MA and PA [47]. The saturation reaction effectively leads to branched structures (side chains) and deviation from the stoichiometry of the reactants and is known to affect the mechanical properties of the final cured polyester resin [28, 34]. The side chains may consist of one diol molecule or more than one diol molecule or long ester chains [28]. Theoretically the chain end number is 2 for linear chains, although in practice it is 2 plus the sum of chain ends due to short and long chain branches [28].

The probability of monoester saturation by diol is greater than saturation by monoester. The greater probability of saturation by diol is due to the fact that hydroxyl group of the diol monomers is more reactive than that of the monoester [28]. It has been shown that a polyesterification system only shows Ordelt saturation when the diol consists of more than two carbons [48]. Figures 2.11 and 2.12 show the Ordelt saturation reactions via monoester and diol (short chain branches), and monoester and monoester (long chain branches), respectively.

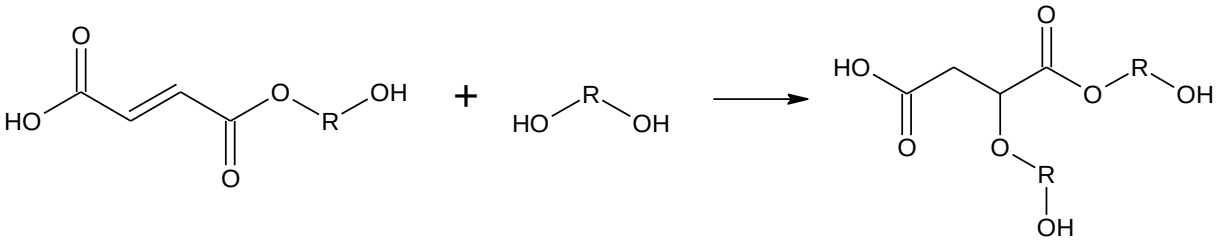

Figure 2.11: Reaction scheme of the Ordelt saturation of monoester by diol (short chain branches) [28] (R = alkyl group).

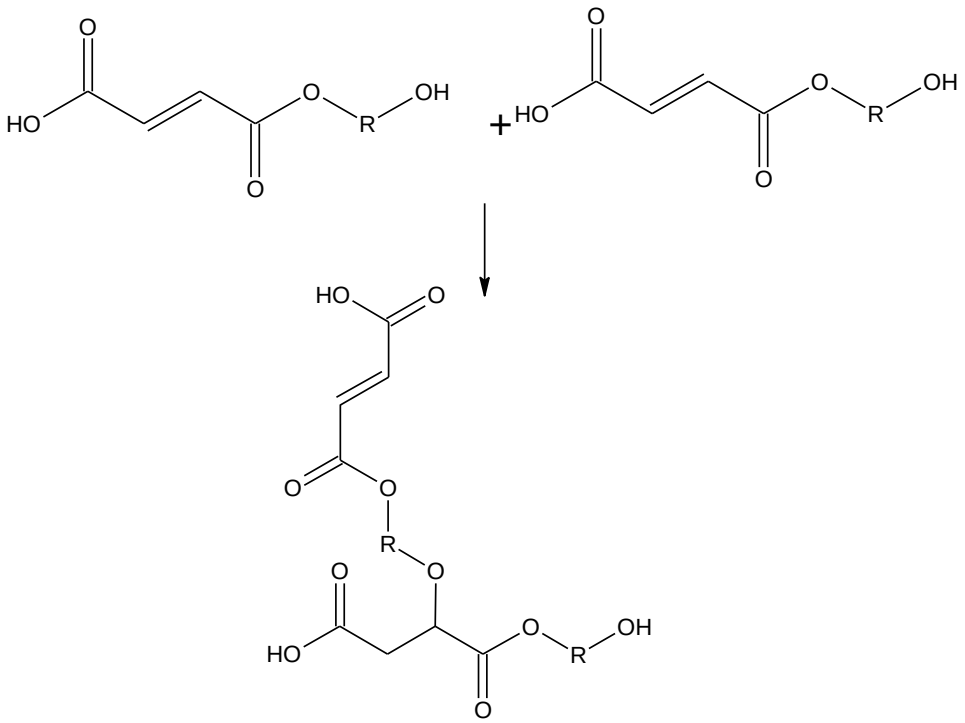

Figure 2.12: Reaction scheme of the Ordelt saturation of monoester by monoester (long chain branches) [28] (R = alkyl group).

2.1.3.3.3 Transesterification

Transesterification occurs when the polyester chains undergo alcoholysis or acidolysis by the hydroxyl or carboxyl groups of the diols and acids or the oligomers at high temperature. Transesterification results in a statistical distribution of repeating units and functional end-groups [28]. Figure 2.13 illustrates the transesterification side reaction during polyesterification.

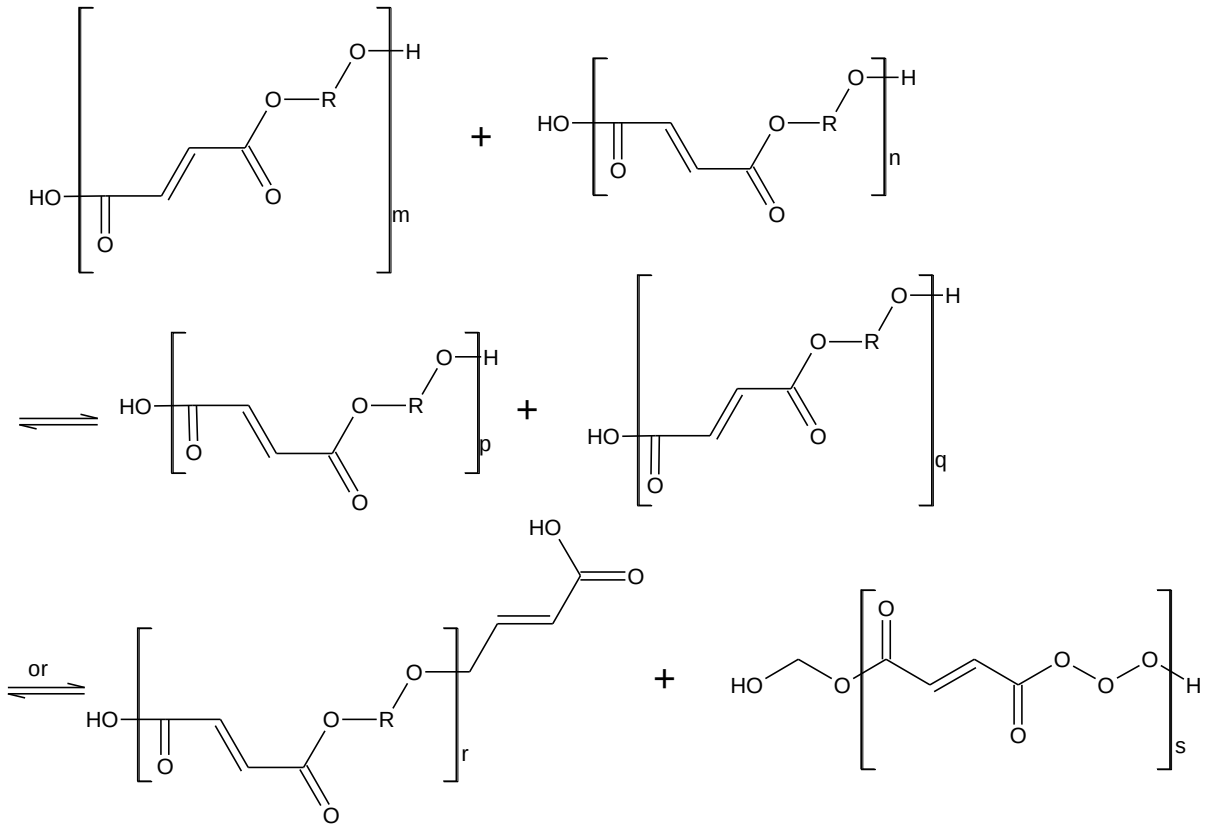

Figure 2.13: Reaction scheme of transesterification side reaction during polyesterification (R = alkyl group).

2.1.3.3.4 α-Diol dehydration

Higher molar mass diols may be formed during α-diol dehydration such as DEG and dipropylene glycol from 1,2-ethanediol and 1,2-propanediol [49]. The α-diol dehydration reaction also results in low boiling point compounds such as THF [50]. The structure of the diol is effectively modified and the reactant ratio of diol to acid changes, although the linear structure is maintained [28].

2.1.3.3.5 Formation of cyclic structures

The formation of cyclic structures during polyesterification is heavily affected by the flexibility of the main chains. These structures can be formed in two major ways:
The structures can be formed at the beginning of the polycondensation reaction when the functional end-groups of the same chain react (ring closure)[51].
The carboxylic end-group can react with the ester component of the same chain (back-biting)[51].

2.1.4 Curing of unsaturated polyester-styrene solution

The crosslinking reaction of UPRs with STY has been extensively studied. Crosslinking takes place between the double bond of the unsaturated acid component (maleate or fumarate) in the polyester chains and the double bond of STY (reactive diluent) through a free-radical reaction [2, 8-9, 14, 36, 52-55].

Molecularly, the UPR-STY solution may be described as "coiled polyester chains in styrene solution". The copolymerization reaction commences by the decomposition of the initiator molecules to produce free radicals in the system. The UPR molecules are linked to the styrene molecules by the free radicals to create long chain molecules, which forms spherical-type structures as a result of the intra-molecular cross-linking between the maleate / fumarate groups of the pendant polyester chains [52].

The crosslinking reaction normally takes place at room temperature [7, 54] with a combination of catalyst/initiator usually methyl-ethyl ketone peroxide (MEKP) and accelerator, usually cobalt napthenate (4 % solution in styrene) [7]. During the accelerated crosslinking reaction, vinylene, STY-STY and polyester-vinylene-polyester-vinylene bonds can be formed [52]. Linear polystyrene chains form at the unsaturation site of the polyester chain, which extends to the unsaturation site of another polyester chain, essentially crosslinking the polyester chains [56]. The length of the polystyrene chains has been estimated to be 2 – 3 monomer units long [57-58] and the styrene to double bond ratio in general purpose resins are 2:3 [14].

The degree of crosslinking or crosslink density (controlled by the concentration of unsaturated acid –or glycol) [5, 36] and the length of these polystyrene chains (can be controlled by the type and concentration of the monomer, initiators, and catalyst) [5] affect the properties of the cured resin[59].
Table 2.3 illustrates the calculation of the level of unsaturation in UPRs [36]. It is generally accepted that higher levels of unsaturation results in a faster crosslinking reaction, although a decrease in the unsaturation level leads to increase in the impact resistance [36].

Table 2.3: Level of unsaturation of a UPR.

Reactant	mol	Mass (kg)
IPA	3.0	0.498
MA	2.0	0.196
PG	5.5	0.418
Less water	-8.0	-0.144
Yield	2.5	0.968
Unsaturation = 2.0 / 0.968 = 2.07 mol/kg		

UPRs can be crosslinked with styrene via suspension polymerizations resulting in a dispersion of micro-particles or beads in water [60-61]. Depending on the production process, these particles may contain single or multiple air voids or vesicles, which are used as organic opacifying particles [62]. These particles can be used as a partial replacement for pigments, extenders and additives in surface coatings [62]. Suspension polymerization theory and the production of the vesiculated micro-particles are discussed in Section 2.2.

2.2 Suspension polymerization

2.2.1 Introduction

Suspension polymerization, also called pearl or bead polymerization [63], refers to a system in which droplets of monomer (s) are suspended in a medium (usually water) by means of controlled agitation and a suspension stabilizer (suspending agent or protective colloid or dispersant) [63]. These materials are usually water-soluble polymers, e.g. PVOH [66-68] or cellulose derivatives [63-64] and inorganic salts e.g. Talc.

Suspension polymerization can be considered a bulk polymerization in small monomer droplets, typically 10-1000 μm in diameter [63, 65]. Monomer-soluble initiators are used [63, 65-66] and the reaction is carried out above room temperature but below the boiling point of the water phase [65-66]. Under these conditions, the monomer droplets are converted to polymer particles [66]. Suspension polymerization obeys the kinetics of solution polymerization if the particles are not too small and polymerization is initiated in the monomer phase [63, 67]. The kinetics becomes more like that of emulsion polymerization

if the particles become too small in size, so that polymerization is only initiated by a few free radicals in the particles [63].

The size of the suspension particles, typically 50-200 µm in diameter, depends on the monomer type, suspending agent, and agitation in the reactor [65]. Micro-suspension processes can yield particles in a range of 20-30 µm [65].

The applications of products made by suspension polymerization includes, chromatographic separation media [68], ion-exchange resins [65, 68] supports for enzyme immobilization [68] and poly(vinyl chloride) (PVC) and poly (vinylidene chloride-co-vinyl chloride) for molding applications [65].

2.2.2 History

Hofman and Delbruck developed the first suspension polymerization in 1909 [69-71]. In 1931, Bauer and Lauth performed the first suspension polymerization which led to the formation of beads from acrylic monomers [72]. Hohenstein and Mark, Trommsdorff and coworkers discussed the basic aspects of suspension polymerization in early papers [73]. The first commercial resin obtained by suspension polymerization was poly (vinyl chloroacetate) [74].

The major challenge experienced by Voss et. al. was coalescence of the droplets which led to large polymeric masses [76]. Cooling of these polymeric masses to remove the heat of polymerization was difficult. Water-soluble polymers were used to overcome this problem [75]. Other dispersants e.g. talc, barium sulfate, magnesium hydroxide and other materials were discovered in later years [76].

2.2.3 Process of suspension polymerization

2.2.3.1 General

Suspension polymerization involves the mixing of two immiscible phases by mechanical agitation. Droplets are formed and their size is determined by the balance between breakup and coalescence between the droplets [68, 77]. Suspension droplets are not thermodynamically stable, as these droplets do not remain dispersed for long time periods like in emulsion systems [65]. Suspension droplets (50 – 200 µm) tend to coalesce

rapidly when agitation of the monomer phase is discontinued [65]. The process of coalescence is controlled by the balance of agitation and stabilizer system [65]. The size of the droplets are affected to a large degree by the properties of the continuous (water) and dispersed (oil/ monomer) phases [68, 78] like interfacial tension [68, 78-79], density [78] and viscosity [78-79], type and concentration of stabilizer [68, 77-79], monomer-phase hold-up [68, 77], impeller type and agitation speed [68, 77-79], apparatus design [66] and the polymerization kinetics [68].

Arshady and Ledwith [80], Hopff et. al. [81], Kavarov and Babanov [82], Mersmann and Grossman [83], and Sculles [84] reported the relationship between particle size and the factors mentioned in the following equation:

$$\bar{d} = k\frac{D_v \cdot R \cdot v_d \cdot \varepsilon}{D_s \cdot N \cdot v_m \cdot C_s} \qquad (2.1)$$

Where d = average particle size, k = parameters such as apparatus design, type of stirrer, self stabilization, etc., D_v = diameter of vessel, D_s = diameter of stirrer; R = volume ratio of the droplet phase to suspension medium; N = stirring speed (or power of mixing); v_d = viscosity of the droplet phase; v_m = viscosity of the suspension medium; ε = interfacial tension between the two immiscible phases; and C_s = stabilizer concentration.

The agitation speed is the most convenient way to control the particle size among the parameters in Equation 2.1 [66]. Generally, the size of suspension polymerized particles ranges between 10 µm and 5 mm, although much smaller particles, which are unintended, are also present. Suspension based particles are known to display broad or bimodal particle size distributions [68].

2.2.3.2 Droplet formation

The formation and the maintenance of individual monomer droplets in the continuous phase throughout the polymerization process is the most important feature in suspension polymerization [85]. The dispersion of the monomer droplets is usually achieved by mechanical agitation [85]. The main problems in suspension polymerization are reduction of droplet coalescence and the formation of suspension droplets of equal sizes [65].

In order to form droplets, the monomer must be water-insoluble [65]. Typically these monomers have a lower surface tension than water [65]. Dispersion of these monomers in the continuous phase without surfactants or stabilizers results in an unstable dispersion as a result of the break-up-coalesce process of the monomer droplets [65]. The monomer-water system separates into the individual phases once agitation is discontinued [65].

The coalescence of monomer droplets or agglomeration of particles varies during the reaction [65]. The dispersion of monomer droplets is stable in the initial stages of polymerization [65]. At conversion levels of about 20 %, agglomeration of the particles can occur if they collide, as the surfaces of the droplets (which contain polymer and monomer) become "tacky"/ sticky [65]. The droplets become tacky due to the fact that the monomer is soluble in the polymer or the polymer is swollen by the monomer (e.g. PVC in vinyl chloride) [65]. As polymerization continues, the particles become less "tacky", resulting in reduced particle agglomeration [65].

2.2.3.3 Droplet/ particle stabilization

Reduction of the surface tension of the droplets and minimization of the force at which the droplets collide can prevent the large coagulation during the "tacky" stage [64, 85]. The addition a small of amount droplet stabilizer and choosing the correct apparatus design [85], may prevent the coagulation. The droplet stabilizer is usually a water-insoluble inorganic salt (e.g. talc, bentonite, calcium sulfate, etc.) or an organic polymer (e.g. poly(vinyl pyrolidone) [64, 85], PVOH [63-64, 85], salts of acrylic acid polymers [64], cellulose ethers [63-64] and natural gums [64]. The inorganic salt reduces coagulation of the droplets by forming a thin layer around the droplets [85]. The organic polymer must be insoluble in the monomer phase and have low solubility in the water phase [85]. Organic polymers can be removed more easily from the polymer bead particles, and are therefore preferred to inorganic salts [85].

2.2.3.4 Particle size

The process of coalescence – breakup/ dispersion in the droplets dictates the final particle size [65, 68, 77-78]. The breakage of the droplets occurs as a result of the high-shear stresses at the impeller blades or pressure fluctuations and turbulence at the surface of the droplets [78]. The "turbulent flow field" dictates the coalescence process [78]. The

coalescence process is assumed to be negligible in dilute dispersions with very high stabilizer concentrations [86-87].

Figure 2.14 shows the breakage and coalescence mechanisms involved in suspension polymerization [88]. It can be seen from Figure 2.14(a) when drop breakage occurs as a result of "viscous shear forces", the droplet becomes elongated to a threadlike form [89]. The deformed droplet subsequently splits into two drops of equal size and small droplets due to the breakage of the fluid thread between the two fluid lumps [78].

Figure 2.14(b) shows that erosive breakage of the droplets can also occur due to pressure and relative velocity fluctuations [78].

Coalescence of droplets can occur by two different mechanisms [78]. Coalescence can occur by collision of two droplets with the continuous phase being trapped initially between the drops. Figure 2.14(c) shows that the continuous phase is eventually drained from between the droplets by the attractive forces, resulting in complete drop coalescence [86, 90].

Figure 2.14(d) shows that immediate coalescence can also occur when the turbulent energy of the collision between droplets is greater than that of the surface energy of the droplets [91].

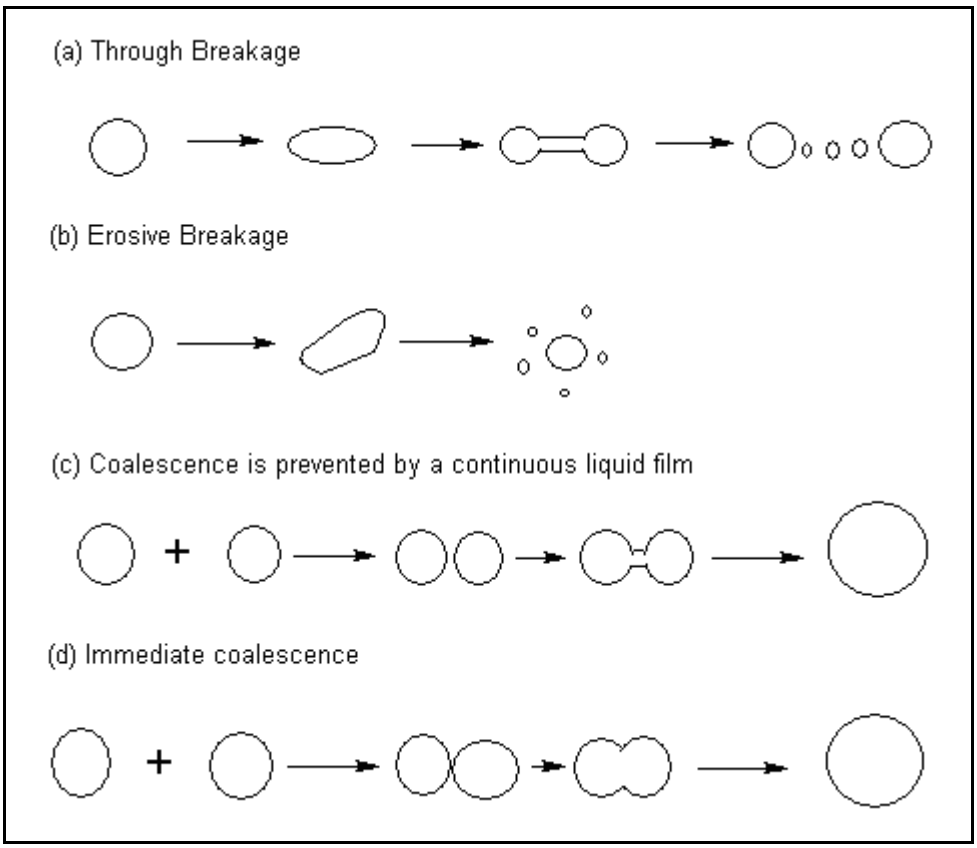

Figure 2.14: Illustrative scheme of breakage and coalescence mechanisms involved in suspension polymerization [88].

2.2.3.5 Particle morphology

Suspension polymer particles or beads or pearls, may be hard or soft in nature. The relative hardness of the beads depend on the monomer composition and whether miscible diluents are present [64]. The morphology of suspension polymerized particles is largely affected by the coalescence and dispersion of droplets before and during polymerization, the change in specific gravity between the monomer and the polymer phases, and the solubility of the monomer in the polymer [65].

Suspension polymer particles have smooth surfaces and relatively uniform texture (non-porous) when the polymer is soluble or swellable in its monomer (e.g. poly (styrene) dissolve in its own monomer and smooth and translucent beads are produced) [64, 66]. On the other hand, porous beads with a rough surface are expected when the polymer is insoluble or not swellable in its monomer (e.g. PVC is insoluble in vinyl chloride) [64, 66].

Suspension polymerized particles, or, "beads" can be made porous by the addition of inert diluents or porogens, to the monomer phase during polymerization. The porogen

diluents are generally alkanes, aromatics (e.g. toluene), alcohols and carboxylic acids [64]. The porogen is extracted at the end of polymerization [64, 77]. The size of the pores depends on the mutual solubility of monomer and diluents, chemical structure of the diluents, chemical nature of the monomer phase, type of stabilizer, and the concentration of the crosslinking monomer [64].

Particles may also collapse inward (e.g. PVC particles [67]) and can be attributed to "the change in the specific gravity between the monomer and the polymer" [65]. If the density of the polymer is higher than that of the monomer and the shape of the particle is not maintained by crosslinking, then less volume must be occupied by the final polymer particle relative to the original monomer droplet [65]. The collapse of the particle inwards relieves the strain induced by the difference in specific gravity between the polymer and monomer, when the surface area of the particle is fixed upon surface skin formation [65].

2.2.4 Control of particle size in suspension polymerization

2.2.4.1 Stabilizer

The type and concentration of the stabilizer plays a vital role in the particle formation stage of suspension polymerization [68, 78, 92]. The stabilizer must prevent aggregation or coagulation of the droplet-particle by maintaining complete coverage of the droplet-particle surface by physical adsorption and/or adsorption by anchoring [69, 84, 96].

As mentioned previously, the stabilizers used in suspension polymerization are usually either water-soluble polymeric materials or inorganic materials [68]. Water-soluble stabilizers aids droplet break-up by dropping the interfacial tension [64, 68]. One of the most commonly used water-soluble stabilizers is partially hydrolyzed poly (vinyl acetate) (PVA) or PVOH. The best grade of PVOH for use as a suspension stabilizer is one with a high degree of hydrolysis (80-90 %) and molecular weight in excess of 70000 g/mol [93]. The mentioned PVOH grade provides a thicker and stronger layer around the monomer droplet/particle and the tendency to be desorbed is less [68]. The polymer particles coalesce and agglomerate forming lumps when PVOH grades with a lower degree of hydrolysis (less than 80 %) or lower molecular weight is used [68]. On the other hand, unstable dispersions are obtained when a PVOH grade with a very high degree of hydrolysis (>90 %) is used [68]. The ability of PVOH to stabilize suspensions is

also influenced by the stereochemistry, degree of branching and distribution of acetate and hydroxyl groups [94]. Generally an increase in the concentration of the stabilizer, results in a more stable dispersion due to steric [64, 68] and Marangoni effects [68]. An increase in the PVOH concentration also leads to smaller average droplet/ particle size with a narrow distribution [68].

2.2.4.2 Agitation

Droplets are formed when two immiscible phases are mixed [68]. The size of the droplets is affected by the agitation speed [68, 77]. The role of agitation is to balance coalescence/ dispersion of the droplets/particles, suspension of the droplets/ particles and the effects of heat transfer[65]. The rate at which droplets are broken-up is enhanced by an increase in the agitation speed, and therefore the formation of smaller droplets is therefore favored[68, 95]. However, there is a U-shaped relationship between the average droplet size and agitation speed as the droplet size may increase at very high agitation speeds due to an increase in the rate at which the droplets coalesce [68]. The increased droplet coalescence can be explained by the large surface area of these droplets and the reduced effectiveness of the stabilizer molecules at the interface [68] at high agitation speeds.

2.2.4.3 Monomer hold-up

The kinetics of the reaction are affected by the solubility of the monomer in the water phase. When the monomer is insoluble in water (e.g. styrene) the kinetics of suspension polymerization is similar to that of bulk polymerization. In cases where the monomer is moderately to highly soluble in water, the kinetics deviate from that of bulk polymerization as some monomer molecules reside in the water phase, which means that monomer transfers from the water phase to replace monomer in the polymerizing droplets [68].

2.2.4.4 Temperature

Monomer and oil phase properties are affected by the variation in reaction temperature[68]. It is known that the rate of polymerization can be increased by two-to-three fold by increasing the reaction temperature by 10 °C [96].

PVOH shows a decrease in its ability to stabilize droplets with increasing temperature[97]. An increase in the agitation speed, monomer hold-up and temperature leads to an increase in the ratio of final particle/droplet size $D_{32,s}/ D_{32,d}$ [95]. On the other hand, an increase in the stabilizer and initiator concentrations leads to a decrease in the final particle/ drop size ratio [95].

2.2.5 Bead-suspension polymerization kinetics

Suspension polymerizations are considered bulk polymerizations in the monomer droplets when the "initiators and chain transfer agents are soluble only in the monomer phase". The particle size and type of stabilizer used in the suspension polymerization of beads do not greatly influence the rate of the bead-polymerization. The following reactions occur in the monomer phase:

Initiation $$I \xrightarrow{k_d} 2R^* \quad (2.2)$$

$$R^* + M \xrightarrow{k_i} R - M^* \quad (2.3)$$

Propagation $$M_n^* + M \xrightarrow{k_p} M_{n+1}^* \quad (2.4)$$

Chain transfer (to monomer) $$M_n^* + M \xrightarrow{k_{tr,m}} P_n + M^* \quad (2.5)$$

Termination

(Coupling) $$M_m^* + M_n^* \xrightarrow{k_{tc}} P_{m+n} \quad (2.6)$$

(Disproportionation) $$\xrightarrow{k_{td}} P_m + P_n \quad (2.7)$$

Where I is the initiator, R* is the radical generated by dissociation of the initiator (with rate constant k_d), M is the monomer concentration, M_n* is growing polymer chain having n repeat units, P_n is the polymer with n repeat units. The rate constants k_d, k_i, k_p, $k_{tr,m}$, k_{tc}, and k_{td} refer to the rate equations for Eqs. 1-6 [65].

2.3 Suspension polymerization – Vesiculated particles

2.3.1 Introduction

Titanium dioxide (TiO_2) is the primary opacifying pigment in the coatings industry [92]. The amount of opacity it imparts to a coating depends on its crystal and particle size, relative refractive index, and the degree of which it is dispersed in the dry film [92]. The cost of the TiO_2 pigment have soared in the past few decades due to increased consumption in a variety of applications (e.g. paints), therefore alternatives are attractive [92]. The opacity of a coating can also be increased by incorporating microvoids into a coating as they also scatter light. Willkie produced a microvoid coating in 1923 [98]. As in the case of TiO_2, the size, concentration, etc. of microvoids determines its light-scattering efficiency. Furthermore, combinations of microvoids and the TiO_2 are effective in achieving and/ or increasing opacity of a coating [62]. Microvoids increase opacity due to the air contained in the matrix which increases the refractive index difference between the pigment and the matrix [92].

The major developments in the field of air-void technology include the Spindrift process which is used by Dulux Australia to commercially produce multi-vesiculated particles (MVPs) and single vesiculated particles (Ropaque opaque polymer) which are manufactured by Rohm & Haas Company. The processes involved in the production of these particles are discussed in Section 2.3.2.

2.3.2 Single vesicle particles

Single-void polymer micro-particles were successfully developed by the Rohm & Haas Company in the early 1980s. These micro-particles, commercially known as Ropaque opaque polymer, are produced via emulsion polymerization where water is encapsulated in the core of the polystyrene particles. Figure 2.15 shows the Ropaque particle with a polymer shell and the air void or vesicle. When these particles are dried, the water in the core irreversibly evaporates and is replaced with air. The resultant opaque particles have the ability to scatter light, which is due to the refractive index difference between the polymer shell and the air filled void. Table 2.4 shows the typical properties of Ropaque[61].

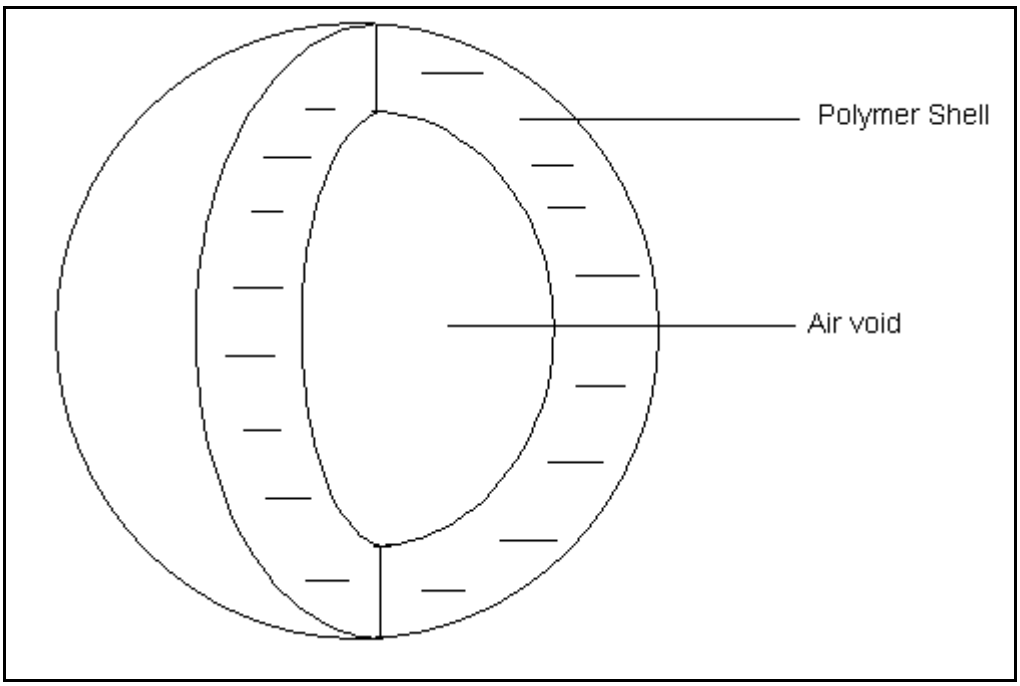

Figure 2.15: Schematic diagram of the Ropaque opaque polymer particle[61].

Table 2.4: Typical properties of Ropaque [61].

Property	Value
Solids content (%)	37 - 38
Dry relative density	0.741
Wet relative density	1.038
Average particle size (μm)	0.4
Viscosity (cPs)	100

2.3.3 Multi-vesiculated particles (MVPs)

In 1976, Kershaw filed a patent describing the process of producing vesiculated polymer beads with an average particle size of 10 μm [99]. The vesicles or small air pockets/ bubbles encapsulated in the beads were approximately 0.7 μm in diameter which displaced 50 % of the total bead volume. A double emulsion technique, water-in-oil-in-water emulsion, was used to prepare the beads. Water was dispersed in a mixture of UPR and STY, and this dispersion was added to an aqueous solution of polymeric stabilizers, eventually forming the water-in-oil-in water emulsion. The organic phase droplets were cured using a redox-free radical system to form the crosslinked polymer particles or beads. Interfacial tensions, phase volumes and agitation were optimized to control the bead and vesicle sizes [99].

Kershaw then used an aqueous TiO_2 dispersion in the first stage of the process [101]. In this way, the TiO_2 pigment is introduced into the beads, which resulted in an increased scattering efficiency of this pigment. The beads can also be incorporated into emulsion paints without sacrificing the integrity of the paint film due to the presence of air. These pigmented vesiculated beads, marketed under the tradename Spindrift [92, 100], contain TiO_2 pigment and vesicles (filled with water) encapsulated in crosslinked UPR-STY matrix. Figures 2.16.1 and 2.16.2 show the scanning electron micrographs of Spindrift pigmented vesiculated particles and the microvoids or vesicles (indicated by the holes or indentations), respectively [100]. As with Ropaque opaque polymer, when the paint film is dried, water in the vesicles evaporates by diffusion through the matrix wall, due to the difference in the vapor pressure between that inside the vesicle and the surface of the paint film. When the difference in vapor pressure diminishes, the process is discontinued [92]. During this process, micro-void cells are formed which can be monitored by an increase in the opacity of the paint film. Furthermore, no water diffuses back into the vesicles of the beads when water is applied to the paint film [92].

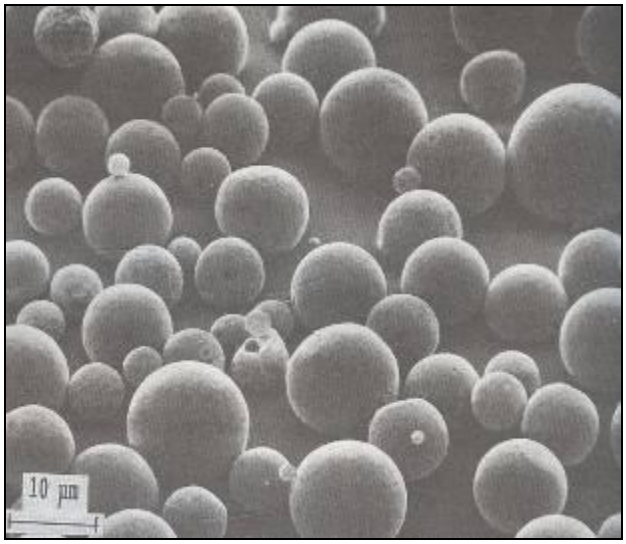

Figure 2.16.1: Scanning electron micrograph of Spindrift particles [100].

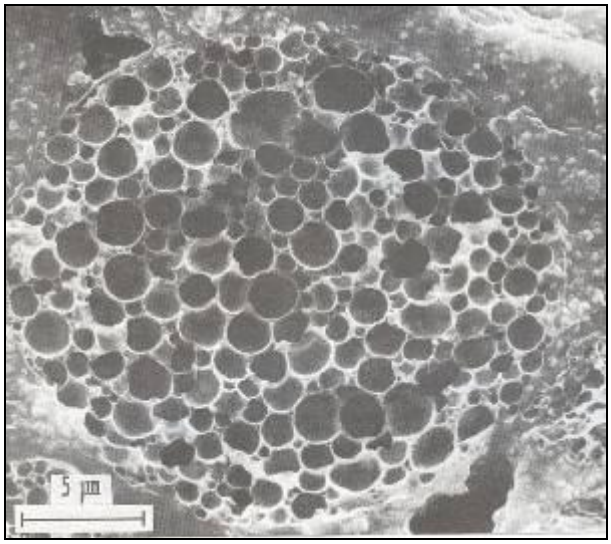

Figure 2.16.2: Scanning electron micrograph of a cross-section of a Spindrift particle [100].

The vesicles of the beads contain a high partial pressure of water, although it has become common practice to assume that the vesicles are filled with air when the paint is dry. Approximately 50 % of the dry bead volume is occupied by air [92]. An increase in the volume of the voids can increase light-scattering power, but leads to a decrease in the mechanical strength of the beads [92].

The average particle size of beads can be controlled and two versions are commercially available based on the size distributions, namely beads with average particle size of 5 μm (suitable for paints with silk/ satin finish) and 25 μm (suitable for paints with matt finish)[92].

In 2006, Engelbrecht et. al. filed a patent for the production of MVPs via a single-emulsification process in the presence of a hydrophobic monomer, for the beneficial replacement of TiO_2, extenders and additives [101]. Vesiculated beads or MVPs are currently being manufactured and used in coatings by Plascon South Africa.

The process steps for the manufacture of the MVPs are as follows:

- Pigment particles are in a UPR-STY solution at high speed,
- The UPR-STY mixture (with dispersed pigment) is dissolved in a suitable monomer (e.g. STY) in the presence of a water-soluble base, e.g. diethylene triamine (DETA),
- The UPR-STY-DETA mixture is then added to a mixture of water, stabilizer, e.g. PVOH and thickener, e.g. hydroxyl ethyl cellulose (HEC), forming a stable emulsion of oil droplets in water,
- A hydrophobic monomer, e.g. laurel methacrylate (LMA) is added to the emulsion, after which UPR is polymerized with the co-polymerizable monomer (e.g. STY), producing a dispersion of opaque cross-linked vesiculated particles in water.

The proposed mechanisms for the vesicle formation and the crosslink-reaction between the UPR and STY are as follows:

2.3.3.1 Vesicle formation

The addition of the polyamine, DETA, to the mixture of UPR, STY and LMA, results in the neutralization of the main and side-chain carboxylic groups of the polyester chains (Equation 2.8).

$$R\text{-}COOH + R'\text{-}NH_2 \rightarrow R\text{-}COO^- + R'\text{-}NH_3^+ \qquad (2.8)$$

The neutralization reaction in Equation 2.8 causes the negatively charged carboxylic groups of multiple polyester chains to orientate themselves toward the positively charged amine groups of DETA, forming stable macro-molecular structures, also referred to as micelles. Figure 2.17 shows that the formed micelles possess hydrophilic character due to the neutralized groups in the centre, i.e. when the organic phase is added to the aqueous phase (comprising of water, HEC, PVOH and a small amount of DETA), the organic phase becomes "soluble" in the aqueous phase. Water molecules from the aqueous phase can migrate or diffuse to the centre of the micelles, resulting in the aqueous voids or entrapped water molecules in the organic phase droplets.

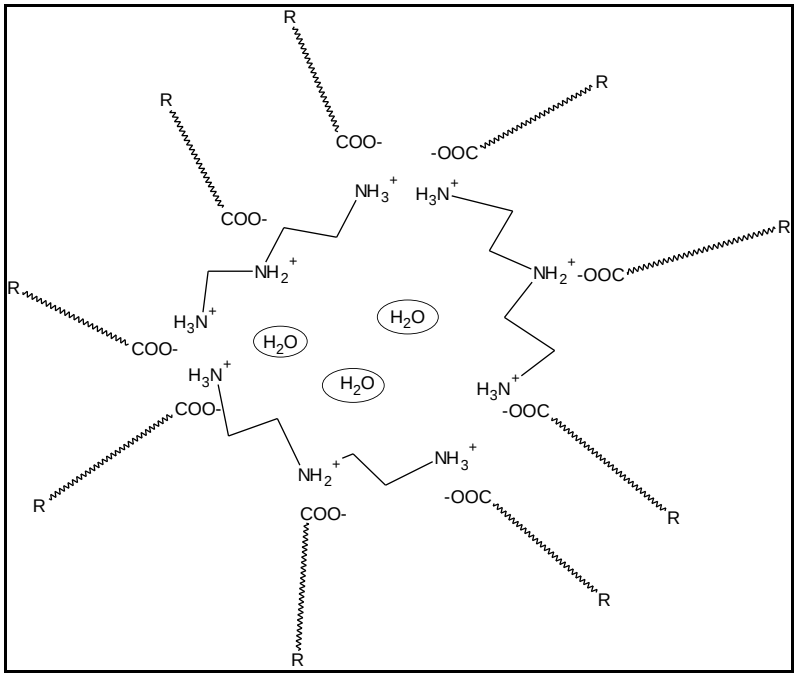

Figure 2.17: Micelle formation by interaction between carboxyl groups of UPR and ammonium groups of DETA [102].

Gous [102] showed that the amount of DETA plays an important role, as an increased amount of amine added to the organic phase results in an increased amount of neutralized groups, which in turn may lead to increase in the amount of water molecules attracted to the organic phase droplets. The small amount of DETA added to the aqueous phase prevents the system from experiencing pH-shock when the organic phase is added.

The steric stabilizer PVOH in the aqueous phase also plays an important role in the formation of vesicles of the MVPs. The PVOH chains orientate themselves so that the hydrophilic acetate groups are orientated toward the aqueous phase and hydrophobic groups are orientated toward the surface of the organic phase droplets, to ensure that no water molecules leave the micelles.

2.3.3.2 Curing reaction of UPR and STY.

Polymerization is initiated by the reaction of the organic peroxide cumene hydroperoxide (CHP) with ferrous sulphate ($FeSO_4.7H_2O$). The peroxide molecules react with the ferrous ions via single-electron transfer, leading to the splitting of the peroxide molecules into a stable anion and a reactive free radical [103]. The initiation reaction believed to take place is illustrated by Equation 2.9.

$$ROOH + Fe^{2+} \rightarrow RO\cdot + OH^- + Fe^{3+} \qquad (2.9)$$

The free radicals formed by the reaction in Equation 2.9 initiate the crosslinking reaction between the fumarate (and maleate) double bonds of the UPR chains and STY, leading to the MVPs. Figure 2.18 shows the reaction between the UPR chains and styrene [78].

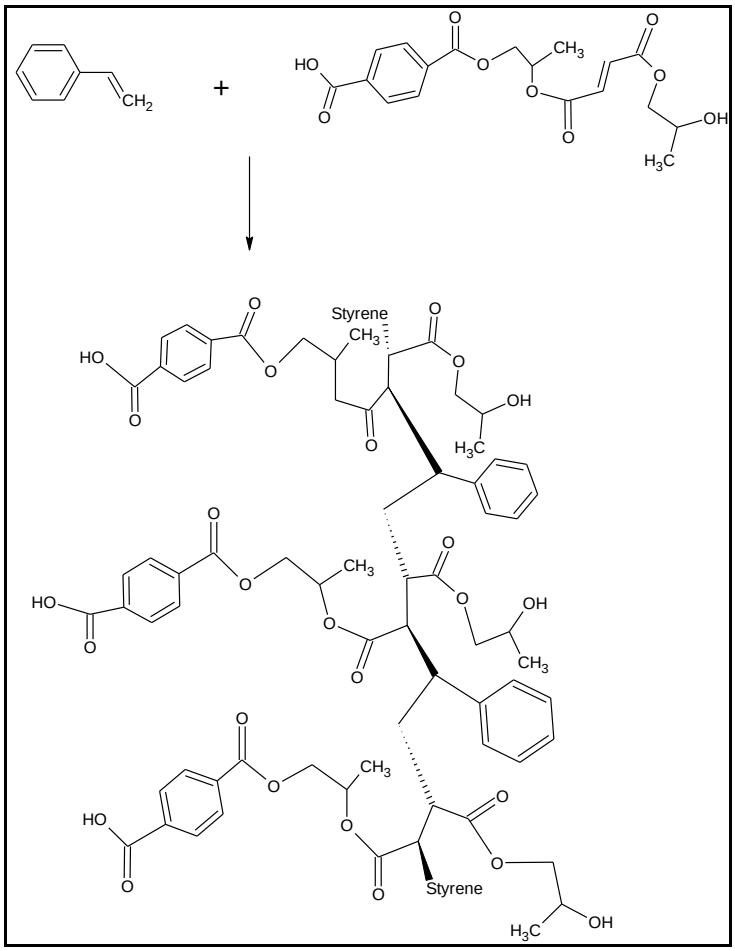

Figure 2.18: Crosslink-reaction of unsaturated polyester (UPR) and styrene (STY)[78].

Numerous factors influence the properties of the MVPs which include process factors such as temperature, addition rate, mass and heat transfer, agitation, stabilizer system, properties of the UPR and reaction kinetics [102, 104]. One of the main objectives of this study is to determine the effect of the polyester chemistry on the properties of the MVPs. Due to the large number of factors that affect the properties of the UPR (and ultimately the properties of MVPs), statistical design of experiments was used to minimize the amount of experiments and draw meaningful conclusions from the results. Statistical design of experiments (DoE) is discussed in Section 3.

2.4 Design of Experiments (DoE)

2.4.1 Introduction

Statistical design was led by work of Sir Roland A. Fisher in the agricultural industry in the 1920s and the early 1930s. Fisher introduced several experimental design principles which include factorial design and analysis of variance (ANOVA) concepts[107-109].

Statistical design, first applied in industry in the 1930s, was promoted by Box and Wilson (1951) with the development of the response surface methodology (RSM) [105]. RSM can be defined as a group of mathematical and statistical techniques used to model and analyze results/data in which the response/property of interest is affected by numerous factors and the aim is to obtain an optimum response [106]. RSM and other designs spread throughout several industries over the next 30 years.

Statistical design for quality improvement began in the 1970s. The use of experimental design was expanded by Genichi Taguchi and others [107-109]. Today, statistical design is applied in many areas including industries such as the chemical, automotive and electronics industry and the service sector of business and financial services [106].

Statistical design of experiments refers to the process of planning a series of experiments so that appropriate data can be analyzed by statistical methods, to draw meaningful conclusions from the data [106, 110]. Statistical and experimental design is applied in product and process development to improve process yields, and minimize variability, development time and overall cost [106, 110].

Two approaches (apart from statistical design) exist when conducting an experiment:

- Best-guess approach: The best-guess approach involves the selection and testing of an arbitrary combination of factors. The best-guess approach often works well when the experimenters have advanced technical or theoretical knowledge as well as considerable practical experience. The best guess approach does not always produce

the desired results and there is no guarantee that when an acceptable result is found, it is the best solution [106].

- One-factor-at-a-time approach: In the one-factor-at-a-time approach, a starting point (or a baseline of set levels) is selected for each factor, whereby each factor is varied successively while the other factors are held constant. The disadvantage of the one-factor-at-a-time approach is that no interaction effects are considered. An interaction is when one factor fails to reproduce an effect on the response at different levels of another factor [106].

These approaches are always less efficient than statistical design methods. The most common statistical design is the factorial statistical design in which all combinations of levels of factors are varied together, instead of one at a time [106]. Other statistical designs include factorial screening designs, response surface methods, mixture designs (the factors are the ingredients of a product (e.g. paint formulation) and the levels of the factors/ingredients are dependent on each other, i.e. the levels of ingredients add up to 100 percent) [106] and combinations thereof.

A screening design, which is used in the present study, is a fraction of a full design and is often employed first when a process or product is affected by a large number of factors, to determine the major factors that affect a particular response, the range of the factors and the curvature of the response. The major advantages of screening designs are the fact that a minimal number of experiments are required, and that information obtained can be used in subsequent designs to optimize or fine-tune a process or product.

2.5 References

1. Goodman, I., In *Encyclopedia of Polymer Science and Technology*, **1969**; Vol. 11, p 62.
2. Ahamad, A.; Lubic, M.; Mohan, A.; Safeer, M.; Thachil, E. T. *Designed Monomers and Polymers* **2001,** 4, 3, 261.

3. Thachil, B. C.; Thachil, E. T. *Polymer - Plastics Technology and Engineering* **2005,** 44, 931.
4. von Boenig, H., In *Encyclopedia of Polymer Science and Technology*, **1969**; Vol. 11, p 129.
5. Tawfik, S. Y.; Asaad, J. N.; Sabaa, M. W. *Polymer Testing* **2003,** 22, 747.
6. Sandler, S. R.; Karo, W., Polyesters. In *Polymer Syntheses*, 2nd ed.; Academic Press, Inc.: Boston, 1992; Vol. 1, pp 68 - 86.
7. Cherian, B.; Thachil, E. T. *International Journal of Polymeric Materials* **2004,** 53, 829.
8. Brydson, J. A., Polyesters. In *Plastics Materials*, 7th ed.; **1999**; pp 694 - 743.
9. von Boenig, H., *Unsaturated Polyesters*. Elsevier: New York, **1964**.
10. Berzelius, J. *Rapport Annuel sur les Progres des Sciences Physiques et Chimiques* **1847,** 26, 1.
11. Berthelot, M. M. *Comptes Rendus* **1853,** 37, 398.
12. Lorenzo, A. V. *Annales De Chimie Et De Physique* **1863,** 67, 2, 293.
13. Bjorksten, J., *Polyesters and Thier Applications*. Reinhold: New York, **1956**.
14. Zaske, O. C.; Goodman, S. H., Unsaturated Polyester and Vinyl ester resins. In *Handbook of Thermoset Plastics*, **1999**; pp 97-168.
15. Whinfield, J. R., In *Nature*, London, **1946**; Vol. 158, p 930.
16. Bayer, O. *Justus Liebigs Annalen Der Chemie* **1941,** 549, 286.
17. Johnson, K. G.; Yang, L. S., Preparation, Properties and Applications of Unsaturated Polyesters. In *Modern Polyesters,: Chemistry and Technology of Polyesters and Copolyesters*, Scheirs, J.; Long, T. E., Eds. John Wiley & Sons: **2003**.
18. Kaska, J.; Lesek, F. *Progress in Organic Coatings* **1991,** 19, 283.
19. United States Patent 3, 109, 831, **1961**.
20. United States Patent 3, 109, 832, **1962**.
21. United States Patent 3, 109, 834, **1962**.
22. Hawthorne, J. M.; Heffelfinger, C. J., In *Encyclopedia of Polymer Science and Technology*, **1988**; Vol. 11, p 1.

23. Goodman, I., In *Encyclopedia Polymer Science and Engineering*, **1988**; Vol. 12, p 1.
24. von Boenig, H., In *Encyclopedia of Polymer Science and Technology*, **1969**; Vol. 11, p 729.
25. Korshak, V. V.; Vinogradova, S. V., *Polyesters*. Elsevier: Amsterdam, **1953**.
26. Korbor, J.; Golob, J.; Sebenik, A. *Polymer Engineering and Science* **1993,** 33, 18, 1212.
27. Jedlovcnik, R.; Sebenik, A.; Golob, J.; Korbar, J. *Polymer Engineering and Science* **1995,** 35, 17, 1413.
28. Yang, Y. S.; Pascault, J. P. *Journal of Applied Polymer Science* **1997,** 64, 133.
29. Shah, M.; Zondervan, E.; de Haan, A. B. *Journal of Applied Sciences* **2010**, 10, 21, 2551.
30. Larez, C. V.; Perdomo, M. G. A. *Polymer Bulletin* **1990,** 23, 577.
31. Lehtonen, J.; Immonen, K.; Salmi, T.; Paatero, E.; Nyholm, P. *Chemical Engineering Science* **1996,** 51, 11, 2799.
32. Vanso-Szmercsanyi, I.; Marcos, L. K.; Zahran, A. A., *Journal of Applied Polymer Science* **1948,** 10, 5, 513.
33. Matynia, T.; Worzakowska, M.; Tarnawski, W. *Journal of Applied Polymer Science* **2006,** 101, 3143.
34. Grobelny, D.; Kotas, A. *Polymer* **1995,** 36, 7, 1363.
35. Gamstedt, E. K.; Skrifvars, M.; Jacobsen, T. K.; Pyrz, R. *Composites: Part A* **2002,** 33, 1239.
36. *Processing Unsaturated Polyesters based on Amoco Isophthalic acid*; IP-43b; Amoco Chemical Co.: **1989**; pp 1 - 19.
37. Larez, C. J.; Mendoza, G. A. P., *Polymer Bulletin* **1990,** 23, 577.
38. Larez, C. J.; Mendoza, G. A. P. *Journal of Applied Polymer Science* **1991,** 43, 1605.
39. Vancso-Szmercsanyi, I.; Manx, L. K.; Zahran, A. A. *Journal of Applied Polymer Science* **1966,** 10, 5, 513.
40. Grobelny, J. *Polymer* **1995,** 36, 22, 4215.

41. Savicheva, O. I.; Sedov, L. N.; Khramova, T. S.; Urman, Y. G.; Slonim, I. Y., *Vysokomelkulyarnye Soedineniya Seriya A & Seriya B* **1973,** A15, 96, 1.
42. Ordelt, Z. *Vysokomelkulyarnye Soedineniya Seriya A & Seriya B* **1962,** 4, 1110.
43. Ordelt, Z. *Chemicky Prumsyl* **1966,** 16, 22, 97.
44. Ordelt, Z. *Makromolekulare Chemie* **1963,** 63, 153.
45. Ordelt, Z. *Makromolekulare Chemie* **1963,** 68, 166.
46. Fradet, A.; Marechal, E. *Makromolekulare Chemie* **1984,** 188, 319.
47. Paci, M.; Crescenzi, V.; Supino, N. *Makromolekulare Chemie* **1982,** 183, 377.
48. Piras, A. Universite´ Pierre et Marie Curie (Paris VI), France, **1988**.
49. Herrmann, D.; Kimmer, W.; Sauer, W. *Acta Polymer* **1984,** 35, 277.
50. Robins, R. G. *Australian Journal of Applied Science* **1954,** 5, 187.
51. Ahjopaloa, L.; sterholm, H. O.; Ja¨rvinen, H.; Pietila¨, L. O. *Polymer* **2000,** 41, 8283.
52. Hsu, C. P.; Lee, L. J. *Polymer* **1991,** 32, 12, 2263.
53. Eisenberg, P.; Lucas, J. C.; Williams, R. J. J. *Unsaturated polyesters*, John Wiley & Sons, Inc. **1997**, 755 - 760.
54. Parkyn, B., Chemistry of polyester resins. *Composites* **1972**, 29 - 33.
55. Rieckmann, T. H.; Volker, S., Poly (ethylene Terephthalate) Polymerization - Mechanism, catalysis, kinetics, mass transfer and reactor design. In *Modern Polyesters: Chemistry and Technology of Polyesters and Copolyesters*, J. Scheirs, T. E. L., Ed. John Wiley & Sons Ltd.: West Sussex, England, **2003**; pp 31-115.
56. Goodman, I., John Wiley: New York, **1972**; Vol. 11.
57. Brydson, J. A. *Plastic Materials*. Butterworths: USA, **1973**.
58. Jadhav, J. Y.; Kantor, S. W., In *Encyclopedia of Polymers Science and Engineering*, 3rd ed.; John Wiley: New York, **1964**; Vol. 12, pp 256 - 290.
59. Auria, B. D. *Journal of Polymer Materials* **1988,** 25, 125.
60. Narkis, M., Size distribution of Suspension-Polymerized Unsaturated Polyester Beads. *Journal of Applied Polymer Science* **1979,** 23, 2043 - 2048.
61. Stewart, D. M. D., Opacifiers for Latex Paints. Microvoid Polymer Particles. In *Surface Coatings. Raw materials and their usage*, The New South Wales University Press: Kensington, NSW, Australia, **1993**; pp 343-350.

62. El-Aasser, M. S., *Polymer News* **1977,** 3, 4, 209.
63. Polymerization Conditions. In *Experiments in Polymer Science*, E. A. Collins, J. B., F. W. Billmeyer, Ed. John Wiley & Sons: **1973**; p 33.
64. Dowding, P. J.; Vincent, B. *Colloids and Surfaces A: Physicochemical and Engineering Aspects* **2000,** 161, 259.
65. Grulke, E. A., Suspension Polymerization. In *Encyclopedia of Polymer Science and Engineering*, Mark, H. F., Ed. John Wiley & Sons: **1988**, Vol. 16, pp 443 - 473.
66. Arshady, R., Leading Contribution: *Colloid Polymer Science* **1992,** 270, 717.
67. Yuan, H. G.; Kalfas, G.; Ray, W. H. *Journal of Macromolecular Science - Reviews in Macromolecular Chemistry & Physics* **1991,** C31, 215.
68. Jahanzad, F.; Sajjadi, S.; Brooks, B. W. *Chemical Engineering Science* **2005,** 60, 5574.
69. Hofman, F.; Delbruck, K. German Patent, 250,690, **1909**.
70. Hofman, F.; Delbruck, K. German Patent, 254,672, **1912**.
71. Hofman, F.; Delbruck, K. German Patent, 255,129, **1912**.
72. Bauer, W.; Lauth, H. German Patent, 656.134, **1931**.
73. Hohenstein, M., *Journal of Polymer Science* **1946,** 1, 127.
74. Voss, A.; Eisfeld, K.; Freundenberger, H. United States Patent, 210,9981, **1938**.
75. Crawford, J. W. C.; McGrath, J. United States Patent, 210,8044, **1938**.
76. Rohm, O.; Trommsdorff, E. German Patent, 735,284, **1943**.
77. Dowding, P. J.; Goodwin, J. W.; Vincent, B. *Colloids and Surfaces A: Physicochemical and Engineering Aspects* **1998,** 145, 263.
78. El-Nahas, H. H.; Khalil, F. H.; Ibrahim, G. M.; El-Gammal, B. *Journal of Applied Polymer Science* **2007,** 104, 1149.
79. Winslow, F. H.; Matreyek, W. *Industrial Engineering Chemistry 1951* **1951,** 43, 5, 1108.
80. Arshady, R.; Ledwith, A., *Reactive Polymers* **1983,** 1, 159.
81. Hopff, H.; Lussi, H.; Hammer, E., *Makromolekulare Chemie* **1965,** 82, 175, 184.
82. Kavarov, V. V.; Babanov, B. M., *Journal of Applied Chemistry USSR (Engl Translation)* **1959,** 32, 810.

83. Mersmann, A.; Grossman, H., *Chemical Engineering and Technology* **1980,** 52, 621.
84. Sculles, D. B., *Journal of Applied Polymer Science* **1976,** 20, 2299.
85. Arshady, R. *Journal of Chromatography* **1991,** 586, 181.
86. Kotoulas, C.; Kiparissides, C. *Chemical Engineering and Technology* **2006,** 61, 332.
87. Chatzi, E. G.; Gavrielides, A. D.; Kiparissides, C. *Industrial and Engineering Chemistry Research* **1989,** 28, 1704.
88. Niwas, R.; Khan, A. A.; Varshney, K. G. *Colloids and Surfaces A* **1999,** 7, 150.
89. Taylor, G. *Proceedings of the Royal Society A (London)* **1934,** 1, 46A, 501.
90. Shinnar, R.; Church, J. M. *Industrial and Engineering Chemistry Research* **1960,** 35, 253.
91. Howarth, W. *Chemical Engineering Science* **1964,** 19, 33.
92. Goldsbrough, K.; Simpson, L. A.; Tunstall, D. F. *Progress in Organic Coatings* **1982,** 10, 35.
93. Castellanos, J. R.; Mendizabal, E.; Puig, J. E. *Journal of Applied Polymer Science* **1991,** 49, 91.
94. Dawkins, A., Chain Polymerization II. In *Comprehensive Polymer Science*, A. Ledwith, S. R. a. P. S., Ed. Pergamon Press: Oxford, **1989**; Vol. 4, p 231.
95. Jahanzad, F.; Sajjadi, S.; Brooks, B. W. *Industrial and Engineering Chemistry Research* **2005,** 44, 11, 4112.
96. Odian, G., *Principles of Polymerisation*. 3rd ed.; Wiley: New York, **1991**.
97. Lazrak, N.; Bolay, N. L.; Ricard, A. *European Polymer Journal* **1998,** 34, 1637.
98. Willkie, H. F. United States Patent, 144,9157, **1923**.
99. Kershaw, R. W., *Australian Oil and Colour Chemists Association Proceedings* **1971**, 4.
100. Ritchie, P., Spindrift Pigmented Vesiculated Beads. In *Surface Coatings. Raw materials and their usage*, The New South Wales University Press: Kensington, NSW, Australia, **1993**; pp 351 - 355.
101. Engelbrecht, J. F.; De Wet-Roos, D.; Smit, A. C.; Cooray, B. Vesiculated polymer particles. US 2006/0111474 A1, **2006**.

102. Gous, K. Continuous processing of vesiculated beads. MScEng, University of Stellenbosch, **2003**.

103. Kolthoff, I. I.; Aiedalia, A. I., Determination of Organic Peroxides by Reaction with Ferrous Iron. *Analytical Chemistry* **1951,** 23, 4, 595.

104. Terblanche, J. C. The development of vesiculated beads. MScEng, University of Stellenbosch, **2002**.

105. Box, G. E. P.; Wilson, K. G. J*ournal of the Royal Statistical Society B* **1951,** 13, 1.

106. Montgomery, D. C., *Design and Analysis of Experiments*. 6th ed.; John Wiley & Sons, Inc.: **2005**.

107. Taguchi, G.; Wu, Y., Introduction to Off-line Quality Control. In *Central Japan Quality Control Association*, Nagoya, Japan, **1980**.

108. Taguchi, G., System of Experimental Design: Engineering Methods to Optimize Quality and Minimize Cost. In UNIPUB, New York, **1987**.

109. Taguchi, G., Introduction to Quality Engineering. In *Asian Productivity Organization*, UNIPUB, New York, **1991**.

110. Rekab, K.; Shaikh, M., *Statistical Design of Experiments with Engineering Applications*. Taylor & Francis Group, LCC: London, **2005**.

CHAPTER 3

EXPERIMENTAL

3.1 Introduction

In this chapter the experimental methods used to synthesize and characterize a series of UPRs (poly (propylene fumarate phthalate)), which vary in terms of molecular structure, are described. UPRs with different molecular structures were obtained by polymerizing PG with varying MA:PA mole ratios and different processing parameters (e.g. heating rates, stirring rates and maximum temperatures). The resultant polymers were added to a mixture of STY and a polymerization inhibitor, tertiary butyl catechol (TBC).

The resultant UPR-STY mixtures were then used in the synthesis of MVPs by suspension polymerization, to determine the effect of the UPR molecular structure on the properties (e.g. particle size and degree of vesiculation) of the MVPs.

Due to the large number of factors that affect the molecular structure and properties of the UPR, DoE software (Design Expert 7) was employed. The Design Expert software was used to find the optimum experimental space, i.e. least amount of experiments, but covering all the factors. The software allows the results to be analyzed in a statistical manner, i.e. the percentage contribution of each factor can be determined and their interaction with other factors.

The properties of the UPRs including molecular weight and molecular weight distribution, molecular structure (end-group concentration, % chain branching) and glass-transition temperature (Tg) was determined by SEC, NMR and DSC respectively.
SEM was used to directly visualize the MVPs morphology, while SEM with microtoming was used to determine the degree of vesiculation of the MVPs. Laser diffraction was used to determine the particle size– and distributions of the MVPs. In the following sections the

formulations, experimental procedures and characterization of the UPRs and MVPs are described.

3.2 Materials

The UPRs were synthesized using maleic anhydride (MA), phthalic anhydride (PA), propylene glycol (PG), styrene (STY) and tertiary butyl catechol (TBC). The MVPs raw materials included the UPRs obtained from DoE series, STY, lauryl methacrylate (LMA), diethylene triamine (DETA), poly (vinyl alcohol) (PVOH) (10.7% solution in water), hydroxy ethyl cellulose (HEC) (2.5% solution in water), distilled water (DI), cumene hydroperoxide (CHP), ferrous sulphate ($FeSO_4.7H_2O$), anionic surfactant (sulfosuccinate based on a fatty alcohol ether, disodium salt), ammonia (12.5% solution in water), hydrophobically modified anionic thickener (50% solution in water), biocide based on 2-bromo-2-nitropropandiol and zinc oxide (ZnO) dispersion. All the above mentioned raw materials were used as received from Plascon SA.

Trichloroacetyl isocyanate (Aldrich 96%) and deuterated chloroform (CIL 99.8%) were used as received.

3.3 UPR Synthesis

PG, MA and PA are charged into a 1L reactor under continuous agitation. The mixture is heated from room temperature to 120 °C (heating rate 1), when the exotherm sets in. (nitrogen is blown into the reactor before heating starts for approximately 15 minutes to displace any oxygen, and then the N_2 is blown throughout the whole process). A “slow” heating rate involves increasing the temperature of the heating mantle in increments of 10 °C from room temperature to 120 °C, after which heating is discontinued when the exotherm sets in. A “fast” heating rate involves setting the heating mantle at 120 °C from room temperature. The maximum exotherm temperature is generally between 160 °C – 175 °C depending on heating rate 1.

The reactor is allowed to cool back to 160 °C for a slow exotherm rate, whilst a fast exotherm rate involves heating the reactor to the maximum reaction temperature as soon as the maximum exotherm temperature is reached.

After the exotherm, the mixture is heated to the maximum reaction temperature, heating rate 2. Fast heating rate 2 means heating immediately after the maximum exotherm temperature is reached, whilst a slow heating rate 2 means setting the heating mantle in increments of 10 °C from the exotherm to the maximum reaction temperature.

The distillation column temperature is approximately 100 °C while water and a small amount of glycol are continuously removed from the reaction by distillation. As soon as the column temperature subsides to below 60 °C (no water is condensed), vacuum is applied (average of 3 times for 1 minute) using a Vacuubrand MZ 2C diaphragm vacuum pump at 9.0 mbar together with a 1L glass solvent vapor trap, to remove residual water and un-reacted monomers from the system, effectively lowering the acid-value and increasing the viscosity of the polyester until the specifications are reached.

The mixture is allowed to cool to approximately 160 °C, at which it is slowly discharged into a mixture of STY and TBC, maintaining the polyester/styrene mixture at approximately 60 °C. Once the discharge is complete, the mixture is allowed to cool to room temperature. A typical unsaturated polyester resin formulation is tabulated in Table 3.1.

Table 3.1: Standard UPR formulation.

Reagents	Weight (%)
PG	30.74
MA	26.19
PA	13.18
STY	27.25
Additional STY	2.62
TBC	2.00×10^{-3}

3.4 Design of Experiments (DoE)

A Combined response surface and mixture design was chosen to determine the effects of the formulation and processing factors on the properties of the resins. The Design Expert 7 software determined that 27 runs (which include multiple replicate runs) were sufficient to evaluate the effects of the tested factors. The following factors were varied:

Formulation factors

- MA:PA mole ratio

Process factors

- Heating rates
- Exotherm time/ rate
- Maximum temperature
- Agitation speed.

Table 3.2 illustrates the experimental design space used to synthesize the resins. Each factor was varied over three levels (lower, intermediate and high level)

Table 3.2: Formulation and process factors for UPR synthesis.

Factor	Lower level (-1)	Intermediate (0)	High level (+1)
% Phthalic anhydride	9.24	13.18	17.12
% Maleic anhydride	22.25	26.19	30.13
Average heating rate 1 (±18 °C to 120 °C) (°C/min)	3.20	6.20	5.90
Exotherm rate (120 °C to max. exotherm temp)	slow	-	fast
Average heating rate 2 (±160 °C to max.) (°C/min)	1.00	1.20	1.30
Maximum temperature (°C)	240	250	260
Agitation speed (rpm)	300	400	500

Notes: %Propylene glycol is kept constant at 30.74%.

All process parameters are affected by the formulation.

Exotherm rate depends heavily on heating rate 1.

The resultant UPR samples were used in the synthesis of Multi-vesiculated particles (MVPs) via suspension polymerization to determine the effect of UPR structure and properties on those of the MVPs.

3.5 MVP synthesis

The unsaturated polyester resin – styrene (UPR-STY) mixture is mixed with STY, followed by LMA and DETA. The LMA acts as a hydrophobic monomer and DETA is added to neutralize the main and side-chain carboxylic groups of the UPR and to increase the solubility of water of the mixture [1-2]. The UPR-STY-LMA-DETA mixture (hereafter the organic phase) is added to an aqueous phase made up of DI water, PVOH and HEC solutions and DETA over ± 10 minutes at room temperature (±23 °C) and whilst stirring at 330 rpm in a 2L round-bottom metal reactor suspended in a temperature-controlled water-bath (Dispersion stage). The PVOH acts as a polymeric stabilizer to ensure a stable oil-in-water emulsion and the HEC is added to increase the viscosity of the aqueous phase and prevent settling of the oil droplets [1-2].

The dispersion stage is followed by the "Emulsification stage" (± 20 minutes) where the organic phase droplets undergo the break-up-coalescence process to form stable droplet sizes and aqueous voids are formed in the droplets.

The crosslinking reaction of the UPR and STY is initiated by the addition of free-radical initiator CHP and catalyzed with $FeSO_4.7H_2O$. After the initiation stage, the stirring is discontinued for 30 minutes.

After the crosslinking reaction, the system is stirred again and heated up to 50 °C in the water-bath. After 60 minutes at 50 °C, the system is heated to 60 °C and kept at that temperature for 3 hours. The suspension is left to cool to room temperature over-night after which it is post treated with the surfactant, ammonia, anionic thickener, biocide and ZnO dispersion. Table 3.3 shows a typical MVPs formulation and the relative weight percentages of the reagents.

Table 3.3: Standard MVPs formulation.

Reagents	Weight (%)
UPR – STY mixture	15.07
STY	5.79
LMA	0.64
DETA	0.21
Water	51.26
PVOH solution (10.7%)	13.08
HEC solution (2.5%)	10.30
DETA	0.06
Water	0.21
$FeSO_4.7H_2O$	0.01
CHP	0.12
Anionic surfactant	0.99
Water	0.19
25 % Ammonia solution	0.19
Water	0.19
Anionic thickener	0.19
Biocide	0.24
ZnO dispersion	0.38

3.6 Analytical techniques and measurements

Various analytical techniques and measurements were used to characterize both the UPRs (no styrene) and MVPs. All analytical methods and the purpose of using them are listed in sections 3.6.1 – 3.6.11.

3.6.1 Size-Exclusion Chromatography

Size-Exclusion Chromatography (SEC) was used to determine the molecular weight and molecular weight distributions of the UPRs. The UPR was dried at ambient temperature and dissolved in HPLC-grade THF (1 mg/mL) for 24 h before being filtered through a

0.45 µm nylon filter. The SEC system used for the analyses consisted of a Waters 717 auto-sampler, Waters 600E system controller (run by Breeze software), Waters 610 fluid unit and a Waters 410 differential refractometer at 35 °C. THF (HPLC-grade) spurged with IR-grade helium was used as an eluent at a flow rate of 1 mL/min. Two PLgel 5-µm mixed-C columns and a pre-column PLgel 5-µm guard were used. The system was calibrated with narrow polystyrene standards ranging from 800 to 2×10^6 g. mol^{-1}. All SEC results are given relative to polystyrene standards.

3.6.2 Differential Scanning Calorimetry (DSC)

Differential Scanning Calorimetry was used to determine the glass-transition temperatures (Tg) of the UPRs. A Perkin Elmer Pyris 1 DSC was used and the sample (±12 mg) was heated under a nitrogen atmosphere (gas flow = 20 mL/min) from -50 °C to 50 °C at a heating rate of 20 °C/min.

3.6.3 Nuclear Magnetic Resonance (NMR) spectroscopy

Proton Nuclear Magnetic Resonance Spectroscopy (^{1}H NMR) was used to resolve the molecular structure of the UPRs. Dried UPR was dissolved in deuterated chloroform (with TMS as reference) (300 mg/mL) for 24h. The ^{1}H NMR analyses were performed on Varian VXR 300MHz Spectrometers (300 and 400 MHz).

3.6.4 Scanning Electron Microscopy (SEM)

Scanning Electron Microscopy (SEM) was used to determine the particle size and morphologies of the MVPs. A Leo® 1430VP Scanning electron microscope was used to obtain images of the MVPs at 7kV at a working distance of ±10 mm, using secondary electron imaging.

The samples were prepared by drying the MVPs at ambient temperature, placing the dried powder on SEM sample stubs and gold-plating the stubs.

3.6.5 Microtoming

Microtoming in conjunction with SEM was done to determine the internal morphology (degree of vesiculation) of the MVPs. Dried MVPs were mixed with a crosslinkable resin and dried in an oven at 50 °C for 24h. Thin layers (±0.1 μm thickness) of the cured resin-MVPs were sliced off or microtomed using a diamond blade, until the sliced/ cut MVPs were exposed at the resin surface. These microtomed resins were placed on stubs and the internal structure of the MVPs viewed via SEM.

3.6.6 Laser Diffraction (LD)

Laser Diffraction (LD) was used to determine the particle size and distribution of the MVPs. A Sympatec SUCELL HELOS/BF-OM laser diffraction sensor was used for the particle size and distribution analysis. The HELOS is equipped with a high precision optical bench, 31 channel multi-element detector and auto-alignment unit (auto-focus), on board data acquisition electronics, automatic laser beam diameter adaptation, 5 mW HeNe-laser with fibre optic light transmission and a high speed fibre optic data communication interface.

The method requires that a small amount of sample material is added in a well chosen liquid into the basin of the SUCELL. The resulting suspension or emulsion is homogenised by a speed-controllable, double-stirrer and dispersed by ultrasonication. It is transported through a cuvette with the help of a peristaltic pump. The suspension is examined by the HELOS laser beam. The SUCELL is a universal wet dispersion system which can detect particle sizes from 0.1 μm to 875 μm, representing ranges R1 up to R5 of the HELOS system. The R3 lens was used as it can detect particle sizes in the range of 0.5 to 175 μm. All operations are controlled and monitored by the WINDOX software via an RS485 interface.

3.6.7 Acid-value

The main chain and unreacted carboxylic acid concentration (acid-value) of the UPR-STY mixtures was determined visually by acid-base titration using a 4.95 *N* potassium

hydroxide (KOH) in a methanol solution and phenolphthalein as indicator. The acid-value (mg KOH per gram UPR) was calculated using the following equation:

$$\text{Acid} - \text{value} = \frac{V_{KOH} \times N}{W_{UPR-STY} \times \left(\frac{S_{UPR-STY}}{100} \right)} \quad (3.1)$$

Where:

V_{KOH} : Volume (mL) of KOH solution used in titration

N : Normality of KOH solution

$W_{UPR\text{-}STY}$: Weight (g) of UPR-STY mixture sample

$S_{UPR\text{-}STY}$: Solids content of UPR-STY mixture

3.6.8 Solids content

The solids content of the UPR-STY mixture was determined by drying ~ 1 g of the mixture at 105 °C in an oven for 2 h. The solids content of the MVPs dispersion was determined by drying ~ 1.5 g of the dispersion at 180 °C in a Mettler Toledo HR73 Halogen Moisture Analyzer for 11 min 40 sec. The solids content of both the UPR-STY mixture and the MVP dispersion was calculated using the following equation:

$$\text{Solids Content} = \frac{w_1 - w_2}{w_1} \quad (3.2)$$

where w_1 and w_2 are the sample weight before and after drying respectively.

3.6.9 Viscosity

Viscosity: The viscosities of the UPR-STY mixtures and MVP dispersions were determined at ambient temperature using a Brookfield DV-II+ Pro Viscometer with a LVDV-II+ Pro using spindles #3 and #4, at 50 and 30rpm respectively.

3.6.10 Contrast ratio (opacity)

The contrast ratio or opacity of material is a measure of the dry hiding power (or ability to completely cover/ obliterate a substrate) it possesses. The contrast ratio of a paint/ coating is usually determined by the reflectance ratio of a dried film applied to a black substrate relative to a white substrate:

$$\text{Opacity} = \frac{\text{reflective index of black surface}}{\text{reflective index of white surface}} \qquad (3.3)$$

Where opacity = 1, constitutes complete hiding/ obliteration of the substrate by the test material.

Test samples were prepared by drawing a thin film (200 µm) of the MVP dispersion, using an automatic film applicator, onto an opacity chart consisting of black and white colored surface. The thin film is left to dry in an oven at 50 °C for 15 minutes.
A reflectometer (at a 45° angle) was used to determine the reflective indices of the black and white colored surfaces, whereafter Equation 3.3 was used to determine the contrast ratio or opacity imparted by the MVPs.

3.6.11 Hardness of MVPs

The hardness of the MVPs was determined using two techniques, namely:

- Microhardness: The UHL VMH-002 microhardness tester was used to determine the hardness of MVPs at 25 °C, with indentation load of 0.01 N, indentation speed of 25 µm/s and dwell time of 15 seconds.

  The samples were prepared by sprinkling oven-dried MVPs onto a disk-shaped mold of semi-crosslinked alkyd resin, after which the resin was allowed to cure completely in an oven at 50 °C for 24h. The test was performed on the cured alkyd resin with dried MVPs exposed at the surface, to ensure that the indenter is in direct contact with the MVPs and to ensure that the MVPs remain stationary when they are indented. The microhardness of the MVPs would be equal to the sum of the hardness values of the MVPs embedded in the resin, minus the hardness value of the resin itself.

- Atomic Force Microscopy (AFM): The Veeco Multimode AFM in contact mode was the second technique used to determine the hardness of the MVPs.

  The test samples were prepared by sprinkling oven-dried MVPs on a thin layer semi-dry PVOH on a glass plate, after which the PVOH was allowed to dry completely. The MVPs were sprinkled onto the PVOH to ensure that the MVPs are directly exposed to the cantilever tip of the AFM, and to ensure that the MVPs remain stationary when the cantilever moves across them.

3.7 References

1. Terblanche, J. C. The development of vesiculated beads. MScEng, University of Stellenbosch, **2002**.
2. Gous, K. Continuous processing of vesiculated beads. MScEng, University of Stellenbosch, **2003**.

CHAPTER 4

RESULTS AND DISCUSSION

4.1 Design of Experiments (DoE) analysis

4.1.1 Introduction

A series of UPRs with varying chemical composition were synthesized by varying the process parameters as well as the MA:PA mole ratio. Due to the large number of variables that affect the polymer structure, statistical design of experiments (DoE) was used to minimize the number of experiments, but still allow for meaningful conclusions to be drawn from the data. Design Expert 7 software was used to generate a combined response surface and mixture design which is sufficient to determine the effects of the MA:PA mole ratio and processing factors on the properties of the UPRs. A total of 27 UPRs were synthesized to evaluate the effects of the factors. These UPRs (in styrene) were subsequently used to synthesize MVPs to indirectly determine the effect of the MA:PA mole ratio and processing factors in the synthesis of the UPRs on the particle size and particle size distribution on the MVPs.

4.1.2 Results and discussion – UPRs

The effects of the following parameters were considered in the DoE:

A: %PA,

B: %MA,

C: Heating rate 1 (°C/min),

D: Maximum process temperature (°C),

E: Heating rate 2 (°C/min),

F: Agitation speed (rpm),

G: Exotherm rate (°C/min).

These parameters were evaluated to determine the effect on the Brookfield viscosity, acid-value, number and weight average molecular weights (M_n and M_w) and polydispersity index (PDI) of the UPRs. These properties were investigated as it is known that the viscosity of UPRs, which is a function of the polymer molecular weight and PDI (degree of polymerization, DP_n) and degree of chain branching, affects the droplet/particle formation during the suspension polymerization (Section 2.2.3) of the MVPs. The acid-value is also of great importance due to the interaction between the carboxylic groups of the UPRs with the base, DETA, resulting in the water-filled vesicles of the MVPs during the suspension polymerization (see Section 2.3.3.1).

Table 4.1 shows the experimental design space and summarizes the results/ properties of the 27 UPRs. These results were entered into the Design Expert 7 program to determine the significance of the parameters on the specific properties of the UPRs, via analysis of variance (ANOVA).

A factor (or interaction between factors) with a p-value (Prob > F) less than 0.05, indicates that the factor is significant at a 95 % and higher confidence level. Futhermore, the lower the p-value the more significant the particular factor is. Factors or interactions with p-values more than 0.05 indicate that the model terms are significant at much lower confidence levels.

Table 4.1: Experimental design space for UPR synthesis.

RUN	PA (%)	MA (%)	Heating rate 1	Heating rate 2	Exotherm rate	Maximum temperature (°C)	Agitation speed (rpm)	Brookfield viscosity (cPs)	Acid-value (mgKOH/g)	M_n (Dalton)	M_w (Dalton)	PDI
1	9.24	30.13	-1	-1	fast	260	300	1612	40.37	1172	4751	4.05
2	13.18	26.19	1	1	slow	240	300	1370	38.16	1407	3153	2.24
3	13.18	26.19	0	0	fast	250	400	1735	25.31	1329	6247	4.70
4	17.12	22.25	1	1	slow	260	300	2000	32.91	1025	3046	2.97
5	13.18	26.19	1	1	fast	251	500	3311	25.94	1596	17068	10.69
6	17.12	22.25	-1	1	slow	240	500	1509	28.15	1351	4979	3.68
7	13.18	26.19	1	-1	fast	260	300	2199	27.59	1319	7661	5.81
8	11.21	28.16	-0.7	-1	slow	257	475	1507	27.56	1309	6431	4.91
9	13.18	26.19	-1	1	slow	260	500	830.2	28.65	1270	3716	2.92
10	17.12	22.25	1	-1	slow	260	500	1430	20.13	1547	5552	3.59
11	13.18	26.19	0	0	fast	250	400	1728	23.44	1230	4956	4.03
12	9.24	30.13	-1	1	slow	260	500	1452	29.08	1102	3849	3.49
13	17.12	22.25	-1	-1	slow	260	300	746.2	32.07	1055	3079	2.92
14	17.12	22.25	1	-1	fast	240	300	1111	32.46	1015	2896	2.85
15	13.18	26.19	-1	1	fast	247	300	1564	35.18	1253	4715	3.76

RUN	PA (%)	MA (%)	Heating rate 1	Heating rate 2	Exotherm rate	Maximum temperature (°C)	Agitation speed (rpm)	Brookfield viscosity (cPs)	Acid-value (mgKOH/g)	Mn (Dalton)	Mw (Dalton)	PDI
16	17.12	22.25	-1	1	slow	240	500	1668	24.31	1141	4156	3.64
17	9.24	30.13	-1	-1	slow	240	300	1207	33.07	1093	3476	3.18
18	13.18	26.19	0	0	slow	250	400	1365	27.43	1423	3682	2.59
19	13.18	26.190	0	0	slow	250	400	1658	30.17	1149	4026	3.50
20	13.18	26.19	-1	-1	fast	240	500	1651	24.09	1101	4279	3.89
21	17.12	22.25	-1	1	fast	260	500	1821	19.28	1232	5497	4.46
22	9.24	30.13	1	-1	fast	240	500	2318	29.16	1158	4489	3.88
23	9.24	30.13	1	-1	slow	260	300	5075	31.99	1146	4482	3.91
24	9.24	30.13	0.04	-0.2	fast	249	384	1879	39.1	1388	5384	3.88
25	17.12	22.25	-1	1	fast	260	500	1908	23.47	1210	4970	4.11
26	17.12	22.25	1	-1	fast	240	300	1207	28.92	1246	3288	2.64
27	9.24	30.13	1	1	fast	240	300	1411	47.64	992	2659	2.68

4.1.2.1 Brookfield viscosity

Table 4.1 shows the Brookfield viscosity data determined for the UPR-STY mixtures. The results show that the values ranged from ± 700 cPs to ± 5000 cPs (mean = 1732.46 cPs ± 332.49). Table 4.2 shows the significant factors (and interaction between factors) affecting the Brookfield viscosity of the UPR-STY mixtures.

Table 4.2: Significant factors affecting the Brookfield viscosity of UPR-STY mixtures.

Factor	Significance (p-value: Prob > F)
AB	0.0029
AE	0.0295
BC	< 0.0001
BD	0.0007
BE	0.0058
BG	0.0062
ABD	0.0322
ABG	0.0023

Table 4.2 shows that the most significant factors and interactions that affect the Brookfield viscosity of the UPR-STY mixtures are AB which is the MA:PA mole ratio, BC and BD, i.e. interactions between %MA and heating rate 1; and maximum process temperature.

Figure 4.1 shows a two component mix graph where the effect of varying the MA:PA mole ratio on the Brookfield viscosity of the UPRs or UPR-STY mixtures at fixed process parameters is presented. In other words, all other parameters are at their intermediate levels values given in Table 3.2. Figure 4.1 clearly shows that an increase in the %MA leads to an increased viscosity of the UPR-STY mixtures. The increased viscosity of the UPR-STY mixtures can be explained by the fact that the maleic groups in the UPR chains undergo a side reaction with PG (Ordelt reaction) leading to chain

branches, which influence the viscosity. An increase in the degree of unsaturation (maleic groups) in the UPR chains leads to an increase in the probability of the Ordelt reaction which in turn leads an increase in the degree of branching, leading to an increase in the viscosity of the UPR-STY mixtures. However, the DB-values of the UPRs are also a function of the degree of polymerization (DP_n), i.e. number-average and weight-average molecular weights (M_n and M_w) and the polydispersity index (PDI). The relationships between the viscosity and molecular weight and molecular weight distribution of the UPRs are discussed in sections 4.1.2.3 and 4.1.2.4.

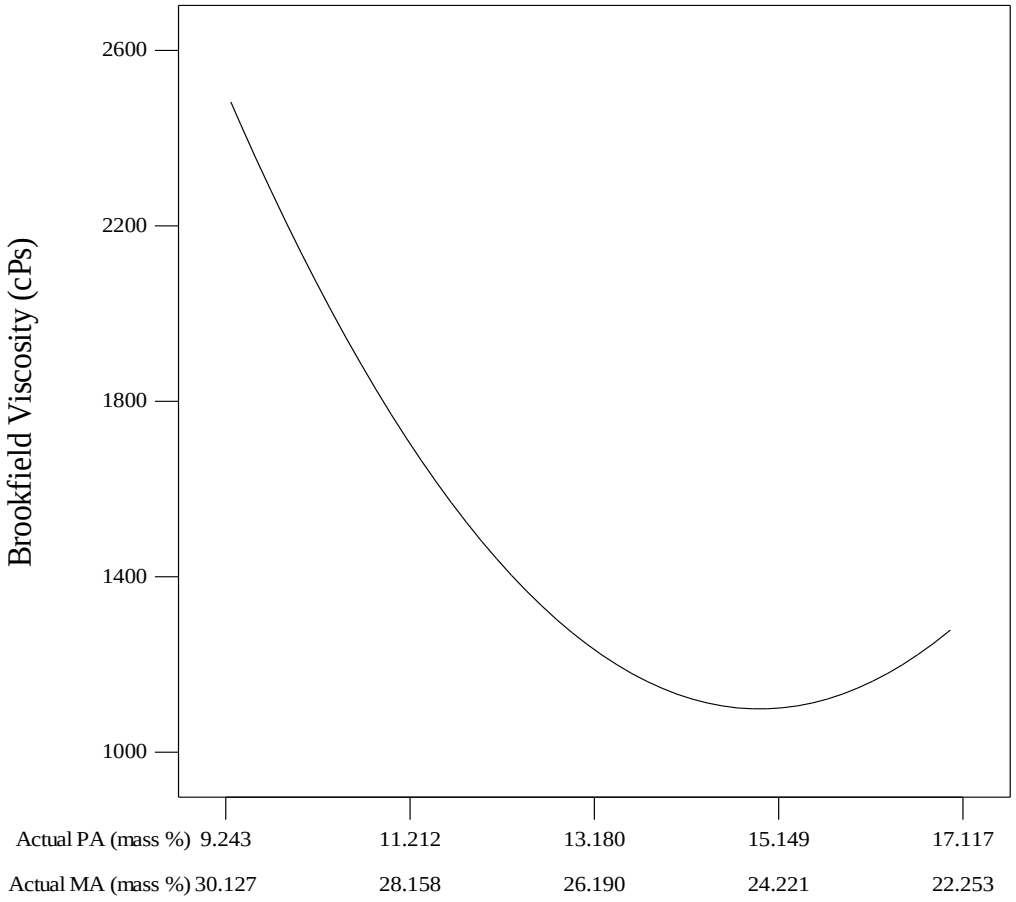

Figure 4.1: Two component mix graph for the formulation factors affecting the viscosity of the UPR-STY mixtures.

Figure 4.2 shows a "contour mix-process" graph where the interaction effect of %MA and heating rate 1 (BC) on the Brookfield viscosity of the UPR-STY mixtures, is presented.

It should be noted that a contour mix-process graph illustrates the effect of varying the MA:PA mole ratio together with a single process parameter (e.g. heating rate 1), on the properties of the UPRs and UPR-STY mixtures. All other parameters are kept constant at the default values given by the Intermediate level (0) in Table 3.2 with a "slow" exotherm rate (unless stated otherwise). An interaction between factors increases the value of a particular property following the color spectrum from blue to red, i.e. a blue region in the contour plot represents a low value of a particular property, whereas a red region represents a high value of that particular property. The values of a given property are displayed on the contours.

Figure 4.2 shows that an increase in the %MA and heating rate 1 leads to an increase in the Brookfield viscosity of the UPR-STY mixtures. It can also be seen that a slow heating rate 1 together with low percentages of MA leads to very low Brookfield viscosities of the UPR-STY mixtures. Heating rate 1 influences the melting and ring-opening of MA (by reaction with PG), i.e. a fast heating rate 1 (20 – 120 °C) allows for improved ring-opening of MA. Thus, a higher percentage MA is incorporated in the UPR chains, leading to an improved probability of Ordelt branching and an increase in the viscosities of the UPR-STY mixtures.

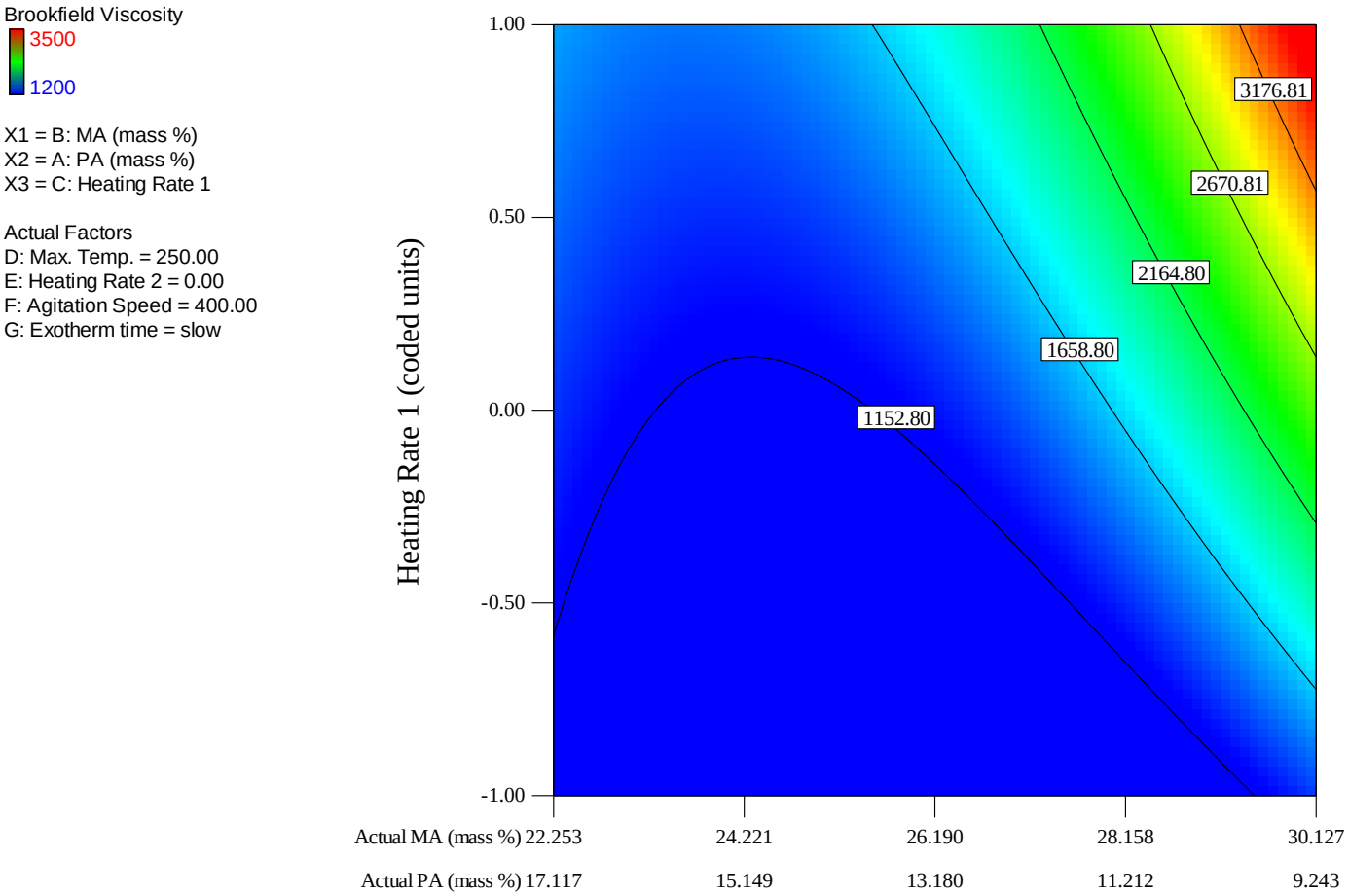

Figure 4.2: Contour mix-process graph of the interaction effect (BC) of heating rate 1 and %MA in MA:PA mole ratio on the Brookfield viscosity of UPR-STY mixtures.

Figure 4.3 shows a contour mix-process graph where the interaction effect of %MA and maximum temperature (BD) on the Brookfield viscosity of the UPR-STY mixture is presented. Figure 4.3 shows that an increase in the %MA and maximum reaction temperature leads to an increase in the viscosity of the UPR-STY mixtures. A high concentration of MA together with a high maximum temperature leads to an increased probability of the Ordelt side reaction, leading to an increased degree of branching and increased viscosity of the UPR-STY mixtures.

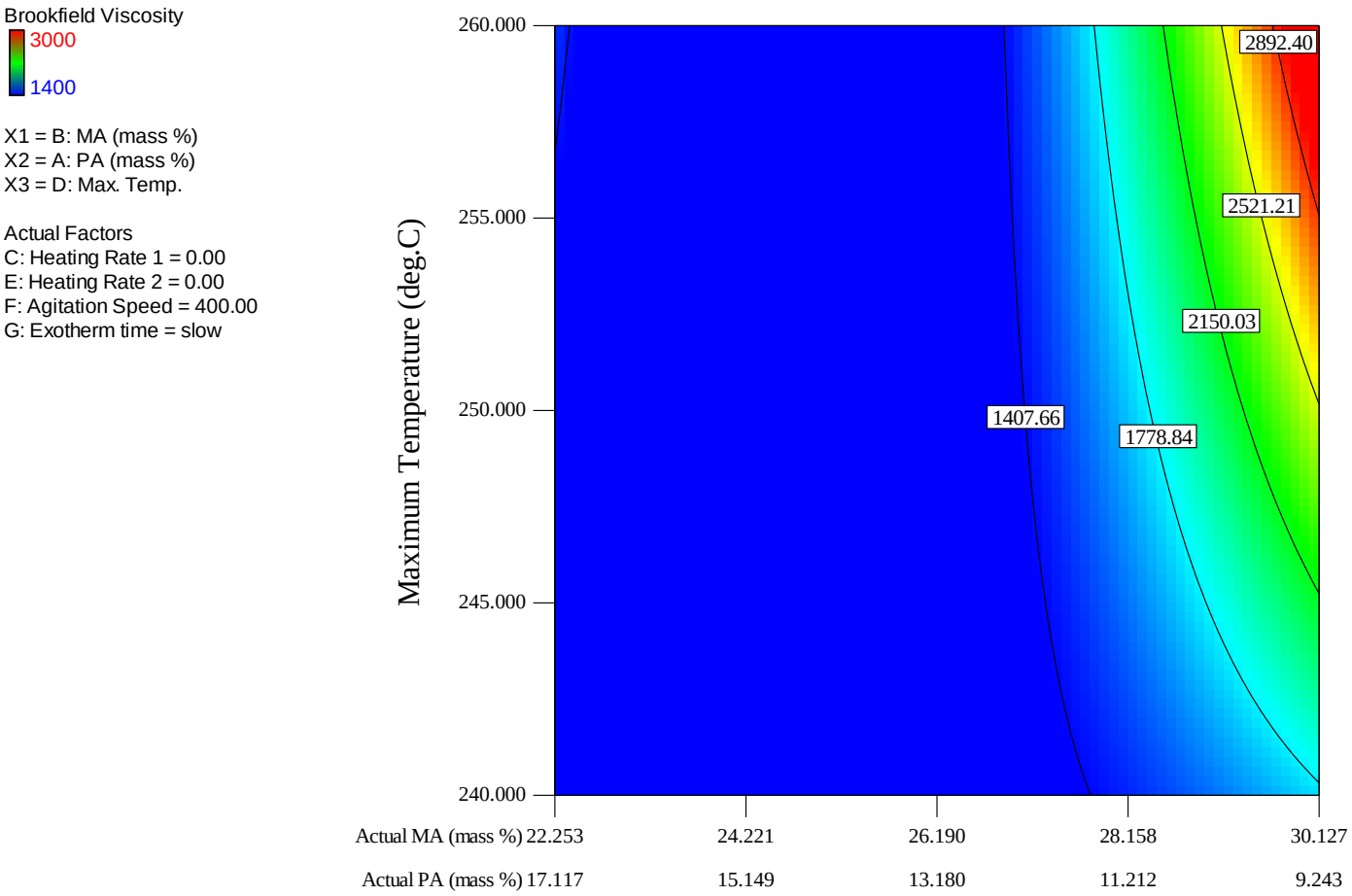

Figure 4.3: Contour mix-process graph of the interaction effect (BD) maximum temperature and %MA in MA:PA mole ratio on the Brookfield viscosity of UPR-STY mixtures.

Figure 4.4 shows a pertubation graph where the individual effects of the process parameters on the Brookfield viscosity of the UPR-STY mixtures (at a fixed UPR formulation) is presented.

It should be noted that a pertubation graph compares the effect of the process factors (at fixed MA:PA mole ratio) at a particular point in the design space. All the pertubation results are for the main effects only and do not consider any **interaction effects**. For example, the effect of the combination of maximum temperature and agitation speed on the Brookfield viscosity of the UPR-STY mixtures. These results represent the effect of varying each parameter on a one-factor-at-a-time basis, e.g. C = heating rate 1 will be

varied from minimum to maximum level whilst the other parameters are kept constant. The default values of the parameters used to construct the pertubation graph are given by the Intermediate level (0) in Table 3.2 with a "slow" exotherm rate. A steep gradient of the line indicates that the particular property is sensitive to this factor. A relatively flat line indicates that the factor has very little influence on the particular property. The x-axis of the Pertubation graph is labeled "process parameter" in coded units and not the actual units of the parameters to account for the fact that multiple parameters are analyzed simultaneously.

Figure 4.4 illustrates that an increase in heating rates 1 and 2 as well as the agitation speed leads to an increase in the Brookfield viscosity of the UPR-STY mixtures.

It can also be seen that the maximum reaction temperature appears to have no significant effect on the Brookfield viscosity (indicated by the relatively flat line), although its interaction with other factors is significant, i.e. only a high maximum process temperature and high %MA in the MA:PA mole ratio, significantly affect the Brookfield viscosity of the UPR-STY mixtures (see Figure 4.3).

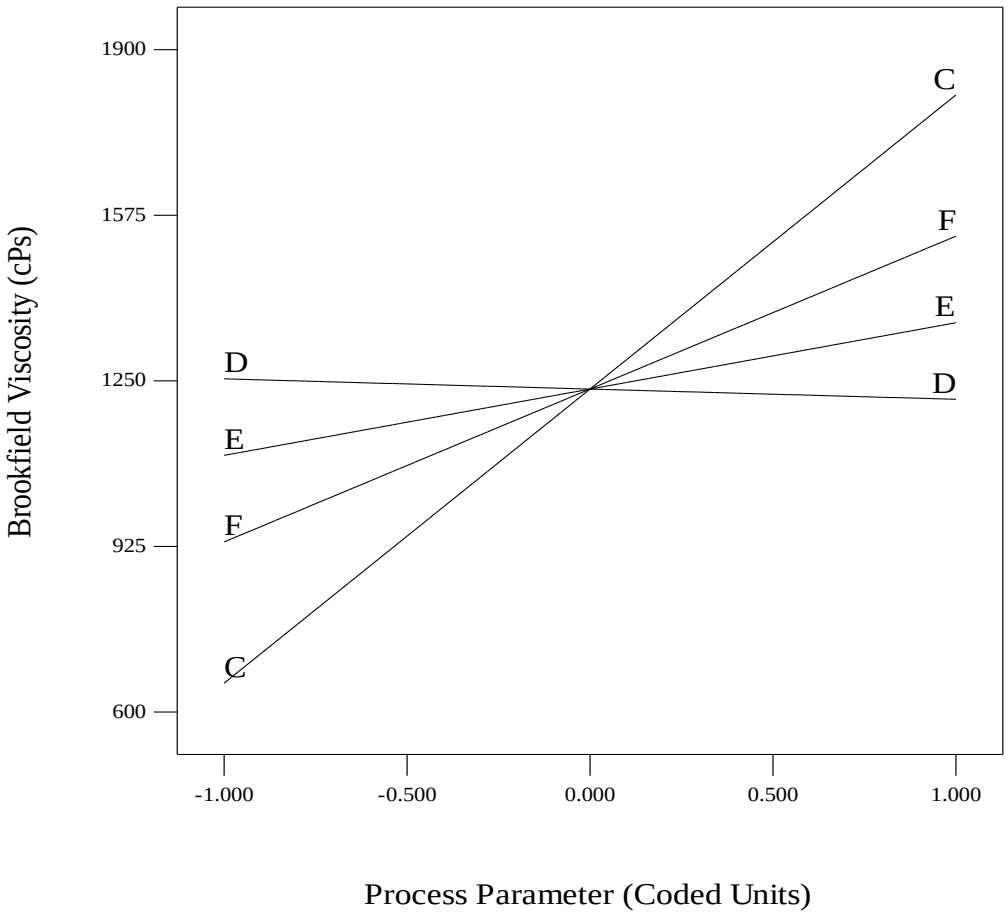

Figure 4.4: Pertubation graph for the process factors affecting viscosity of the UPR-STY mixtures (fixed MA:PA ratio at 26.19: 13.18).

4.1.2.2 Acid-value

As previously mentioned in Section 3.6.7, the acid-value or concentration of the carboxyl end-groups of the UPRs was determined by an acid-base titration method. The titration method is effective in determining the carboxyl end-group concentration of the UPRs in the DoE space, but does not allow the determination of the hydroxyl end-groups. Section 4.6 describes the determination of both end-groups of selected experimental runs by isocyanate derivatization coupled with ^{1}H NMR.

Table 4.1 shows that the acid-values determined for the UPRs by acid-base titration, ranged from 19 – 47 mgKOH/g resin (mean = 29.84 mgKOH/g resin ± 3.44). Table 4.3 shows the factors (and interaction between factors) affecting the acid-value of the UPRs.

Table 4.3: Significant factors affecting the acid-value of UPRs.

Factors	Significance (p-value: Prob > F)
AB	0.0002
AF	0.0028
AG	0.0388
BE	0.0329
BF	0.0023

Table 4.3 suggests that the most significant factors affecting the acid-value of UPRs, are the MA:PA mole ratio and interactions AF and BF between %MA, %PA and agitation speed.

Figure 4.5 shows a two component mix graph where the interaction effect of the MA:PA mole ratio on the acid-value of the UPRs is presented. It can be seen from Figure 4.5 that a decrease in the %MA (or increase in %PA) leads to a lower acid-value of the UPRs. The two anhydrides, MA and PA, have different reactivities towards PG, i.e. MA has a higher reactivity towards PG compared to PA. Thus, a UPR formulation with a high concentration of MA relative to PA, results in an increased concentration of carboxyl

end-groups relative to hydroxyl end-groups as more MA reacts with PG. A UPR formulation with a high concentration of PA relative to MA results in a higher concentration of hydroxyl end-groups (or lower concentration of carboxyl groups/ acid-value) due to a decreased reactivity of PA towards PG (see Section 2.3.1.1).

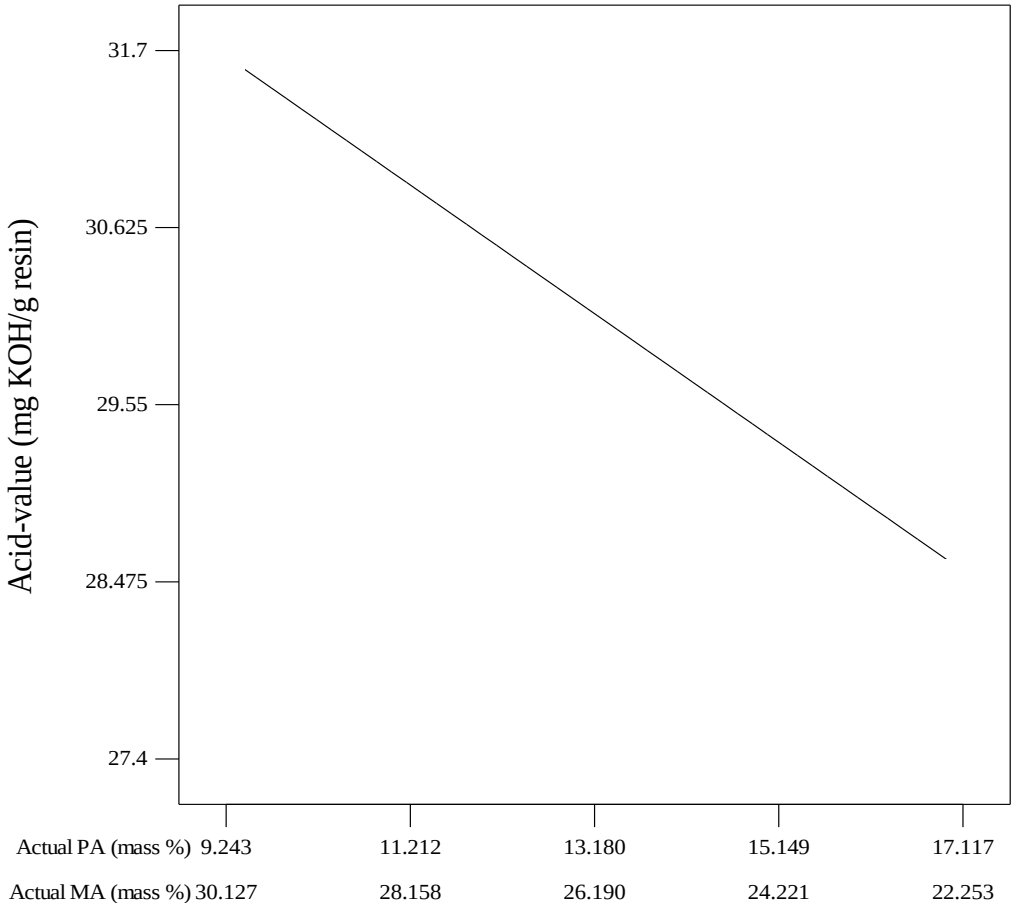

Figure 4.5: Two component mix graph for the formulation factors affecting the acid-value of UPRs.

Figures 4.6 and 4.7 show the contour mix-process graphs where the interaction effects of % PA and % MA with the agitation speed on the acid-value of the UPRs are presented.
It can be seen in Figures 4.6 and 4.7 that an increase in the %PA and agitation speed leads to a decrease in the acid-value of the UPRs. The agitation speed greatly affects the reaction rate of PA and MA with PG, i.e. a high agitation speed with a high concentration of PA in the UPR formulation leads to an improved reaction between PA and PG, which

effectively leads to a higher concentration of hydroxyl end-groups or lower concentration of carboxyl end-groups (acid-value). On the other hand, a high %MA and high agitation speed, may lead to a higher concentration of carboxyl end-groups due to the improved reaction between MA and PG compared to PA and PG.

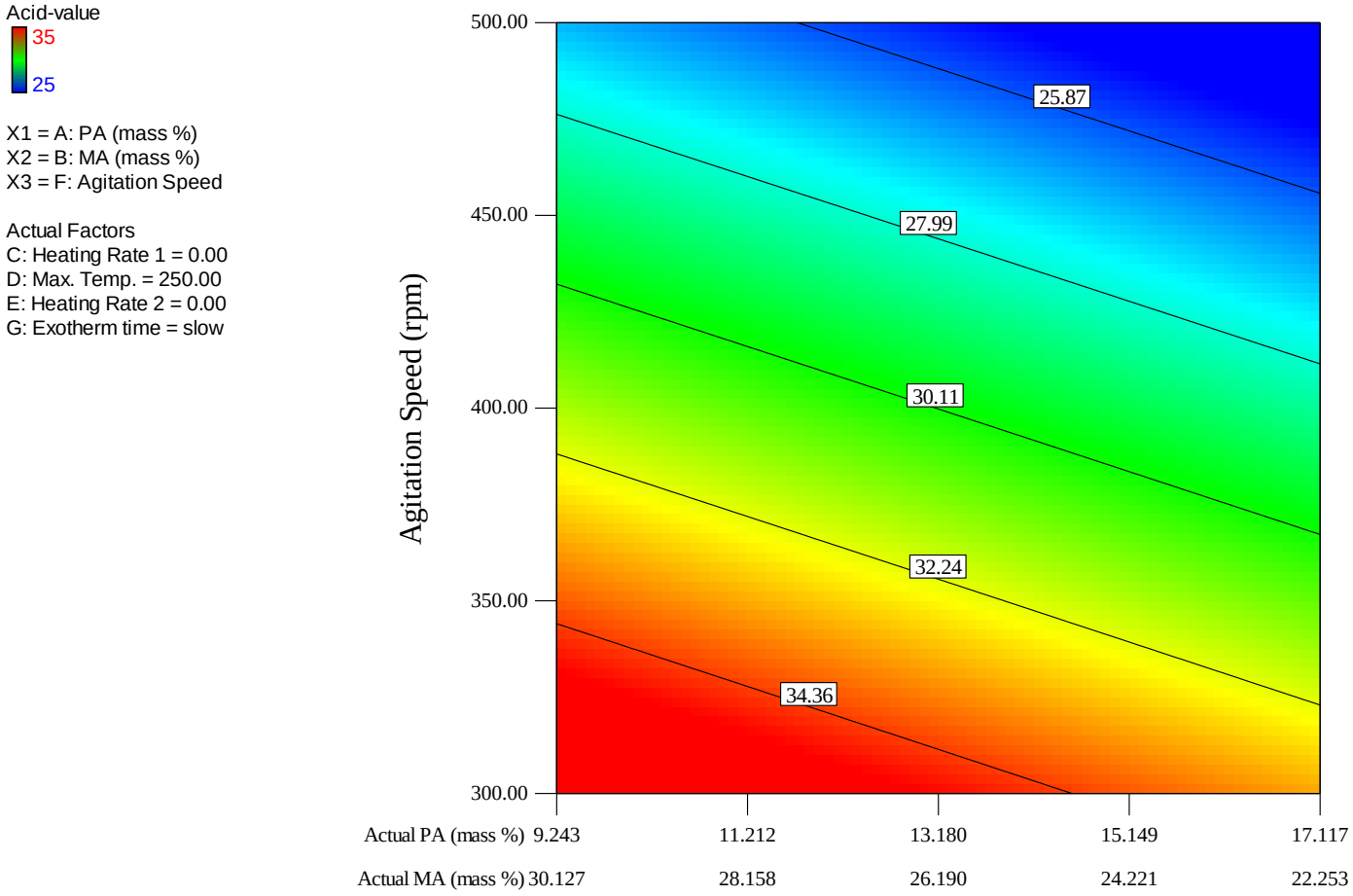

Figure 4.6: Contour mix-process graph of the interaction effect (AF) of %PA in MA:PA mole ratio and agitation speed on the acid-value of UPRs.

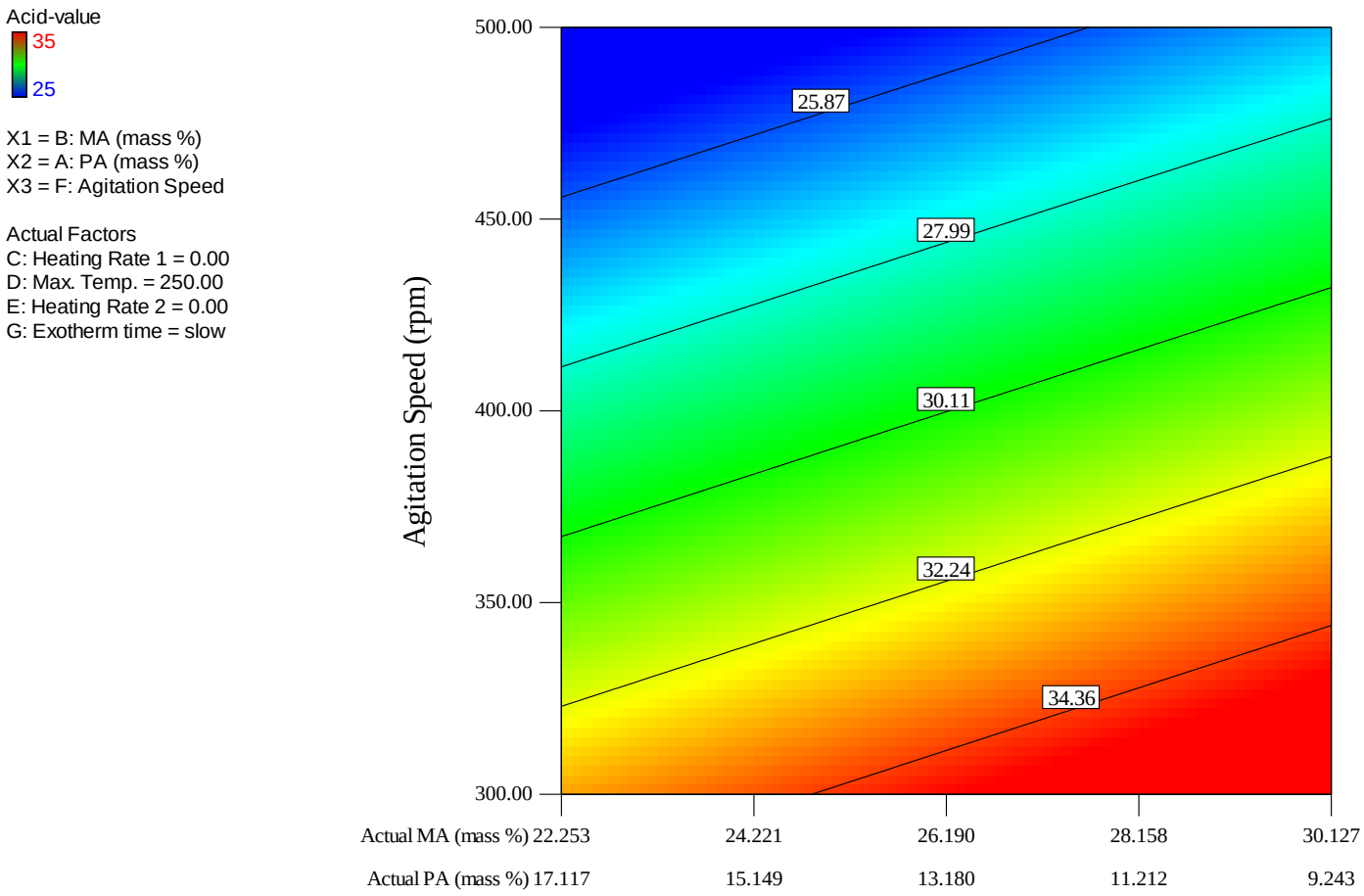

Figure 4.7: Contour mix-process graph of the interaction effect (BF) of %MA and agitation speed on acid-value of UPRs.

4.1.2.3 Number and weight-average molecular weights (M_n and M_w)

Statistical analysis of the M_n values of the UPRs, revealed that the MA:PA mole ratio and process parameters do not affect the M_n value significantly, as all the parameters or interaction between parameters have p-values greater than 0.05, which is important as it implies that the DP_n of the UPRs are relatively similar.

Table 4.1 shows the M_w values of the UPRs determined by SEC. The results show that the values ranged from 2659 Dalton to 17068 Dalton (mean = 4725.94 Dalton ± 2446.39). Table 4.4 shows the factors (and interaction between factors) affecting the M_w-value of the UPRs.

Table 4.4: Significant factors affecting the M_w-value of UPRs.

Factors	Significance (p-value: Prob > F)
AB	0.0013
AD	0.0009
AE	0.0039
AF	0.0011
AG	0.0006
BD	0.042
BG	0.0434
ABD	0.0006
ABE	0.0015
ABF	0.0025
ABG	0.0012
ACD	0.0020
ACE	0.0008

Table 4.4 shows that the most significant factors affecting M_w-value of the UPRs are the MA:PA mole ratio (AB), and interactions AG, AD and ABD, i.e. interactions between %PA and exotherm rate, %PA and maximum process temperature and the interaction between the MA:PA mole ratio and maximum process temperature.

Figures 4.8 and 4.9 shows the two component mix and contour mix-process graphs where the effect of the MA:PA mole ratio and its interaction with the maximum process temperature on the M_w-value of UPRs, is presented. Figure 4.8 shows that a decrease in the %PA (or increase in %MA) leads to an increase in the M_w-value of the UPRs. Figure 4.9, on the other hand, shows that an increase in the maximum process temperature (at MA:PA mole ratio of 26.19 : 13.18) leads to increase in the M_w-value of the UPRs.

The M_w-value of polymers is sensitive not only to the number of molecules (as with M_n-value), but also to the size or weight of the molecules. Thus the M_w-value is sensitive to

the degree of polymerization and branching extent, i.e. a branched molecule has a greater size or weight compared to a linear molecule of the same length.

Due to the fact that the DP_n of the UPRs is fairly similar, the M_w-value, as with the Brookfield viscosity of the UPRs is greatly affected by the degree of chain branching which is affected by the MA:PA mole ratio (AB) and its interaction with maximum reaction temperature (ABD). A high concentration of MA relative to PA or high MA concentrations with high maximum reaction temperatures lead to an increase in the degree of chain branching, and hence a higher M_w-value (and Brookfield viscosity) of a given UPR.

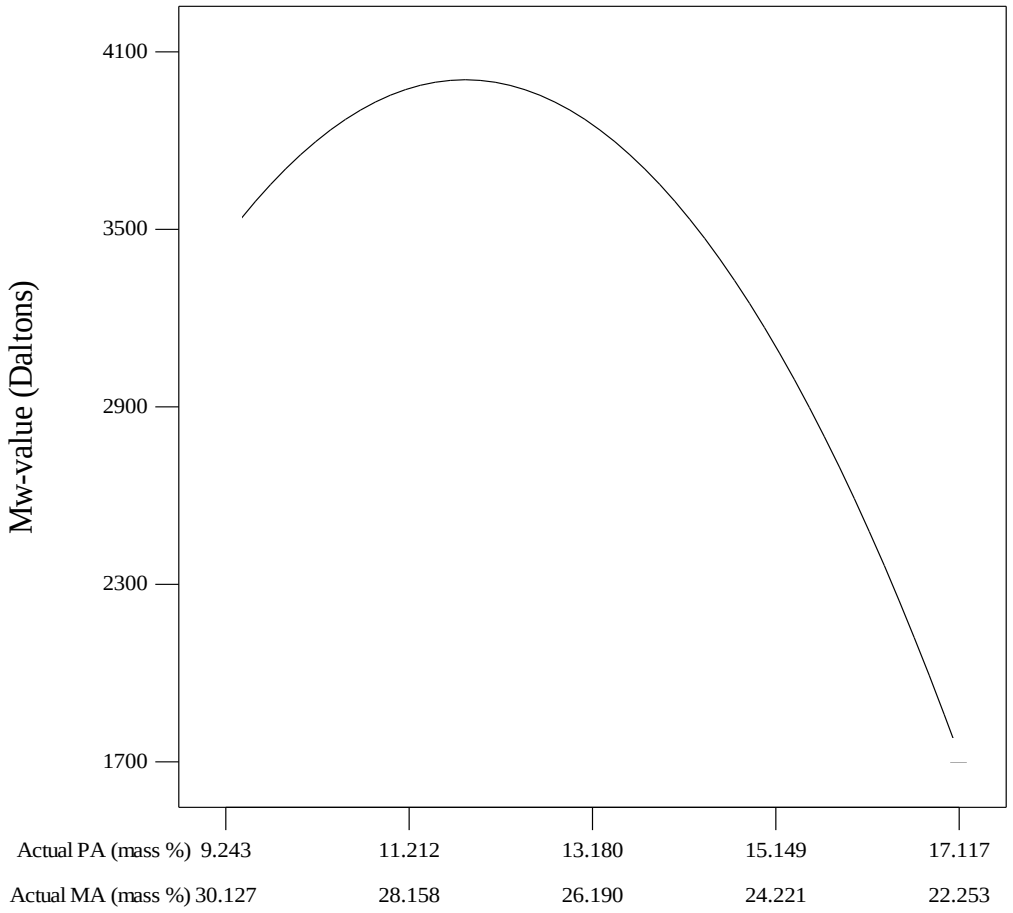

Figure 4.8: Two component mix graph for the formulation factors affecting the M_w-value of UPRs.

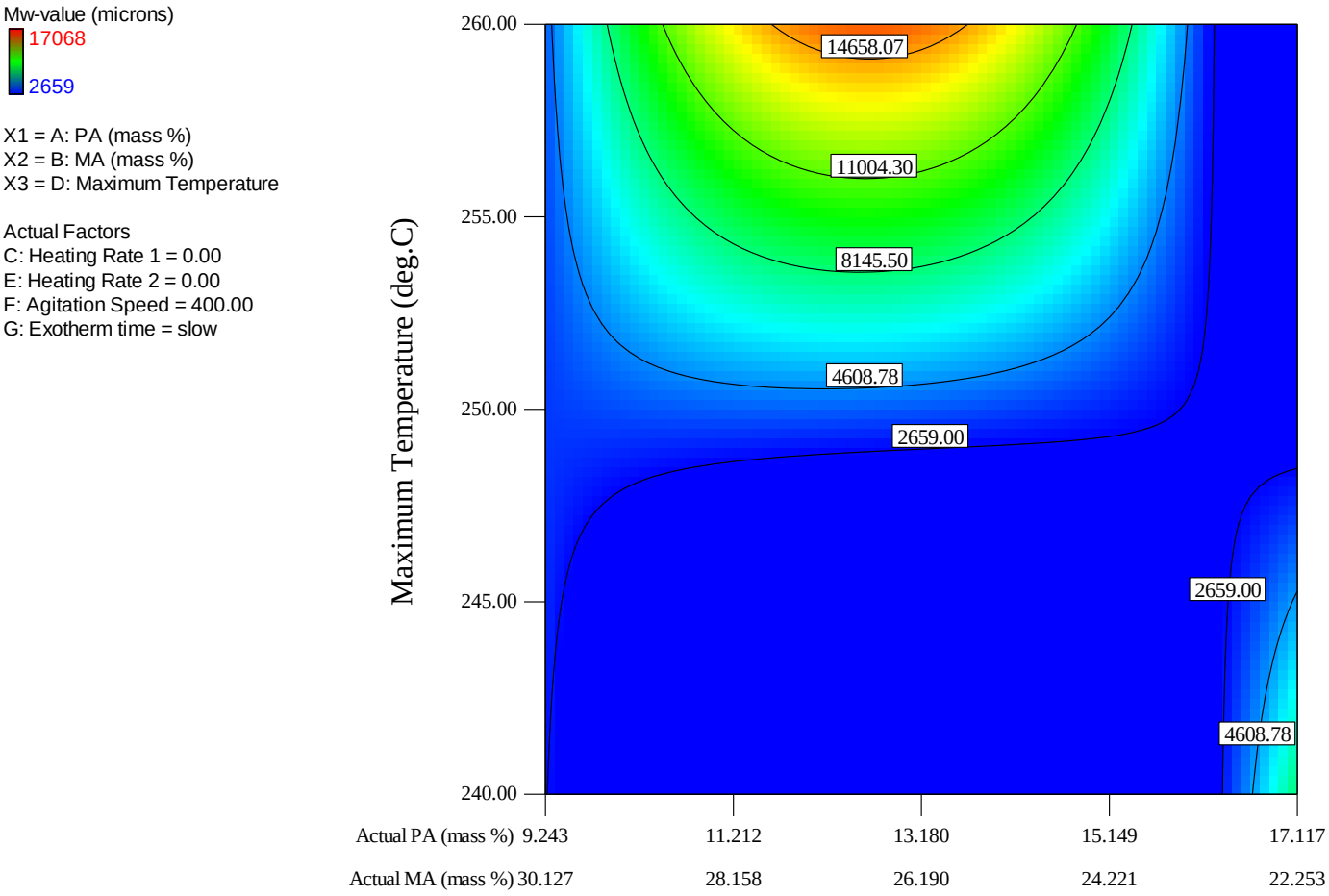

Figure 4.9: Contour mix-process graph of the interaction effects AD and ABD, i.e. interactions between % PA, MA:PA mole ratio and maximum temperature on M_w-value of UPRs.

The effect of the interaction AG between % PA and the exotherm rate cannot be shown graphically in a contour mix-process graph as the exotherm rate was not varied at multiple levels, i.e. the UPRs were only synthesized with a "slow"- and "fast" exotherm rate. However, the interaction effect between the % PA and exotherm rate is important, as a slow exotherm rate would improve the reaction between PA and PG, effectively increasing the incorporation of PA in the UPR chains. The increased incorporation of PA would indirectly influence the MA incorporation into the UPR chains, which influences chain-branching and therefore the M_w-value of the UPRs.

4.1.2.4 Polydispersity index (PDI)

Table 4.1 shows the PDI values of the UPRs determined by SEC. The results show that the values ranged from 2.21 to 10.69 (mean = 3.79 ± 1.43). Table 4.5 shows the factors (and interaction between factors) affecting the PDI values of the UPRs.

Table 4.5: Significant factors affecting the PDI-value of UPRs.

Factors	Significance (p-value: Prob > F)
AB	0.0035
AC	0.0445
AD	0.0033
AE	0.0096
AF	0.0043
AG	0.0013
ABD	0.0017
ABE	0.0041
ABF	0.0092
ABG	0.0034
ACD	0.0036
ACE	0.0024

It can be seen from Table 4.5 that the PDI-value of the UPRs is significantly affected by the MA:PA mole ratio (AB), and the interactions AG and ABD, i.e. interactions between %PA and exotherm rate and MA:PA mole ratio and maximum temperature.

Figures 4.10 and 4.11 show the two component mix and contour mix-process graphs where the effect of the MA:PA mole ratio (and its interaction with the maximum process temperature) on the PDI-value of UPRs, is presented. Figure 4.10 shows that a decrease in the %PA (or increase in %MA) leads to an increase in the PDI-value of the UPRs. Figure 4.11, on the other hand, shows that an increase in the maximum process

temperature (at MA:PA mole ratio of 26.19 : 13.18) leads to increase in the PDI-value of the UPRs.

The PDI-value of polymers is the ratio of M_w- and M_n-values, and is therefore a measure of the degree of polymerization (DP_n) and degree of branching of the UPR chains. The ANOVA evaluation of the M_n-values revealed that the DP_n of the UPRs is relatively similar, which means that the PDI value of the UPRs is significantly affected by the M_w contribution. Thus, the PDI value (as with the M_w value) is significantly affected the MA:PA mole ratio, interactions between %PA and exotherm rate; and MA:PA mole ratio and the maximum reaction temperature.

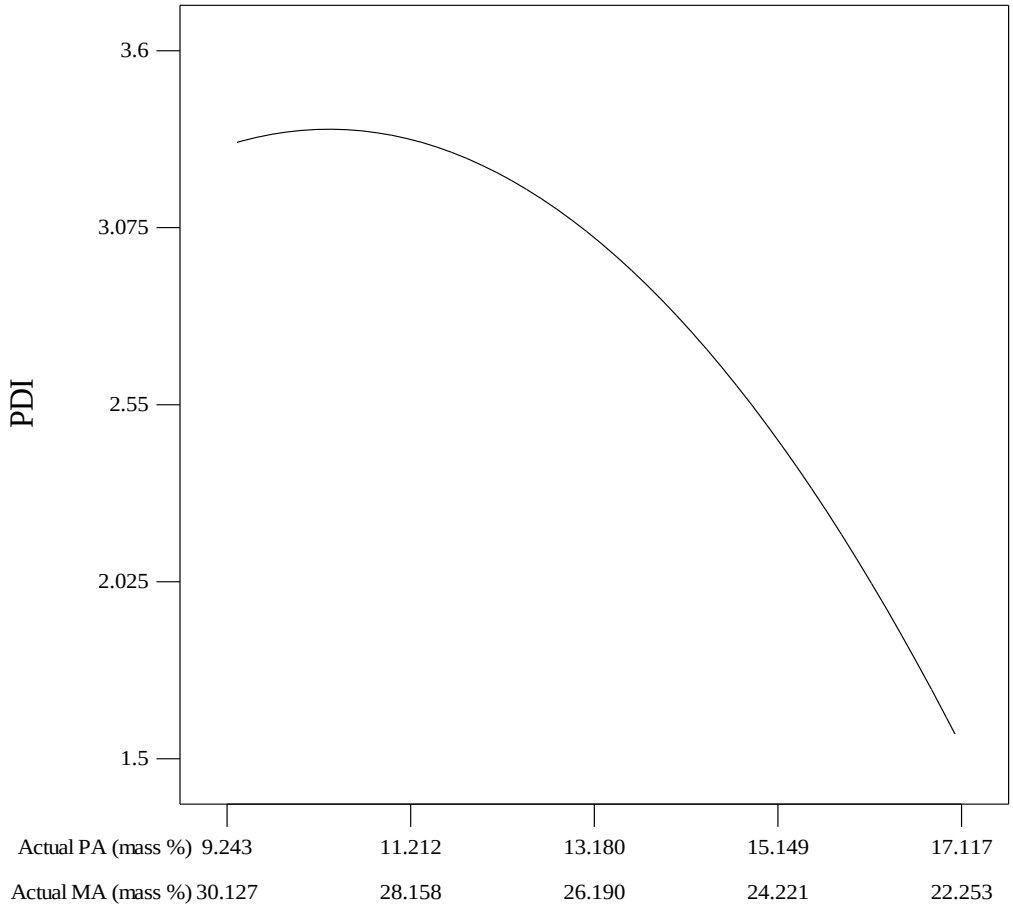

Figure 4.10: Two component mix graph for the formulation factors affecting the PDI-value of UPRs.

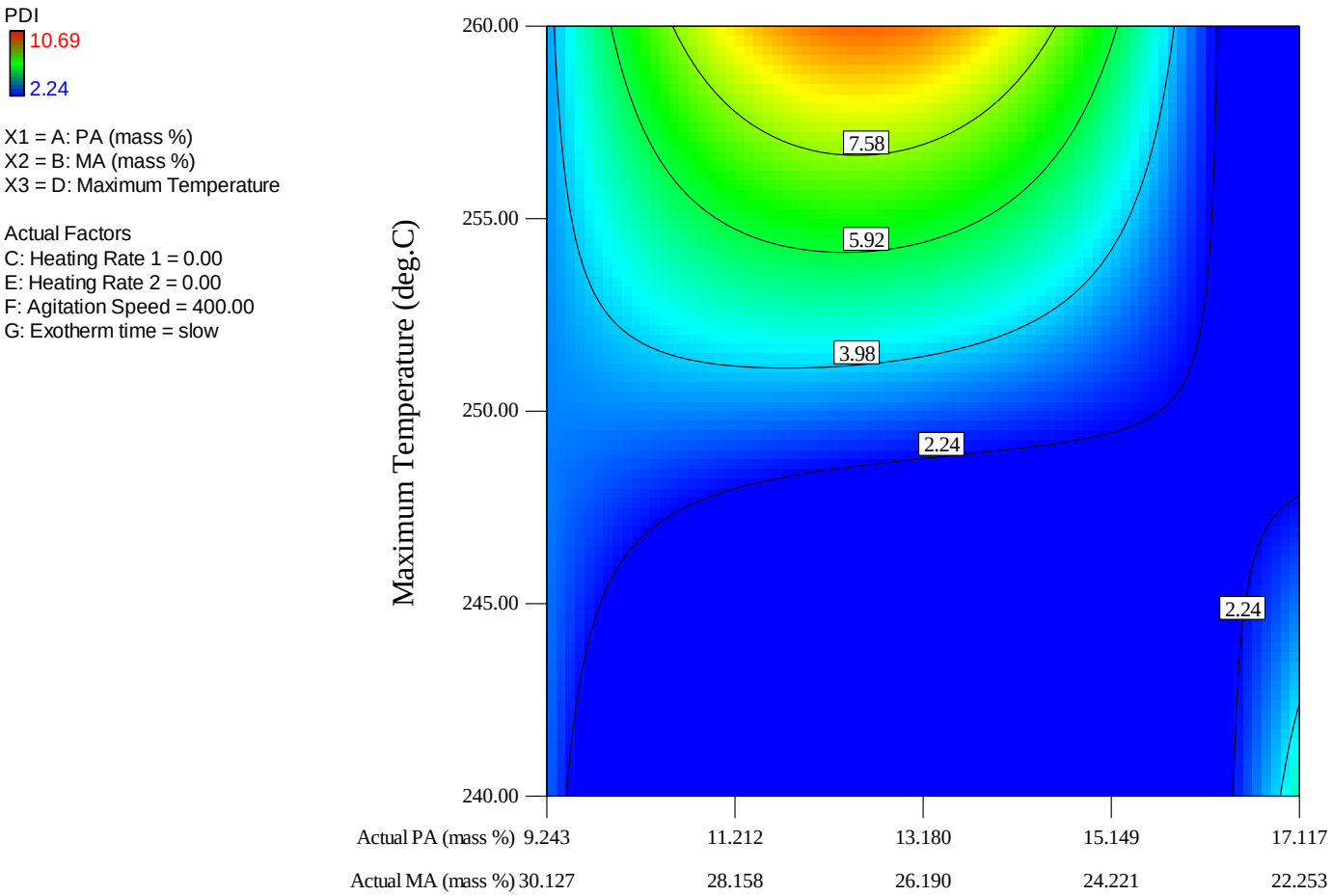

Figure 4.11: Contour mix-process graph of the interaction effect ABD, interaction between MA:PA ratio and the maximum temperature on PDI-value of UPRs.

4.1.2.5 Preliminary conclusion: UPRs

The MA:PA mole ratio and its interaction with the maximum process temperature were found to be the most significant factors affecting the degrees of unsaturation and chain branching, which in turn affects the viscosity, acid-value, M_w- and PDI-value of the UPRs.

4.1.3 Results and discussion – MVPs

Following the synthesis of the MVPs with the UPR-STY mixtures, the particle size and particle size distribution of the MVPs were determined using the Sympatec SUCELL HELOS/BF-OM laser diffraction sensor. The SUCELL machine determines the particle size of the MVPs by calculating the Sauter mean diameter (SMD) and the De Brouckere mean diameter (VMD) values, which are independent of the number of particles. The SMD (Equation 4.1) and VMD (Equation 4.2) values are calculated based on the surface area and mass or volume of the particles, respectively [1]:

$$\text{SMD} : D_{[3,2]} = \frac{(1^3 + 2^3 + 3^3)}{(1^2 + 2^2 + 3^2)} = 2.57 = \frac{\sum d^3}{\sum d^2} \qquad (4.1)$$

$$\text{VMD} : D_{[4,3]} = \frac{(1^4 + 2^4 + 3^4)}{(1^3 + 2^3 + 3^3)} = 2.72 = \frac{\sum d^4}{\sum d^3} \qquad (4.2)$$

where d = diameter.

The SMD and VMD-values of the 27 MVPs runs are given in Table 4.6. These results were also entered into the Design Expert 7 program (as with the data of the UPRs) to determine the significance of the polyester synthesis parameters (and resulting properties) on the particle sizes of the MVPs, via ANOVA.

It is known that a small particle has a greater surface area per unit volume compared to a larger particle. Thus, due to the fact that the SMD-value is calculated based on the surface area of the particles, relatively smaller diameter particles will contribute more toward this value.

The VMD-value, on the other hand, is calculated based on the volume or mass of the particles, which means that relatively large diameter particles will contribute more toward this value. Thus, the VMD-value will always be greater than the SMD-value for a given group of particles.

Table 4.6: Particle size results of MVPs.

RUN	SMD (µm)	VMD (µm)
1	21.03	67.43
2	23.23	48.32
3	30.15	79.13
4	29.93	57.97
5	20.03	50.57
6	40.33	61.15
7	25.03	69.45
8	21.14	65.49
9	28.47	57.06
10	28.62	79.00
11	20.17	55.13
12	15.87	56.35
13	17.84	41.47
14	17.75	40.17
15	26.64	71.76
16	29.35	70.49
17	31.61	98.36
18	18.94	67.06
19	22.10	63.00
20	25.28	68.25
21	26.89	84.01
22	34.07	117.44
23	21.09	67.70
24	29.92	78.91
25	33.58	71.06
26	12.72	30.31
27	22.28	64.59

4.1.3.1 SMD-values

Table 4.6 shows that the SMD-values of the MVPs ranged from 12.72 – 40.33 μm (mean = 24.97 μm ± 4.67). Table 4.7 shows the significant factors (and interaction between factors) affecting the SMD-value of the MVPs.

Table 4.7: Significant factors affecting SMD-value of the MVPs.

Factors	Significance (p-value: Prob > F)
AE	0.0198
BD	0.0467
BE	0.0414

Table 4.7 shows that the interactions AE, BD and BE i.e., interactions between %PA and Heating rate 2, %MA and maximum process temperature, and %MA and exotherm rate are the significant terms affecting the SMD-value of the MVPs.

Figures 4.12 and 4.13 show the two component mix and contour mix-process graphs where the effects of the MA:PA mole ratio and the interaction between %MA and maximum process temperature of the UPRs, on the SMD-value of the MVPs are presented. It can be seen from Figure 4.12 that an increase in the %PA of the UPRs leads to an increase in the SMD-value of the MVPs. Figure 4.13 shows that an increase in the %PA and decrease in the maximum process temperature of the UPRs lead to an increase in the SMD-value of the MVPs.

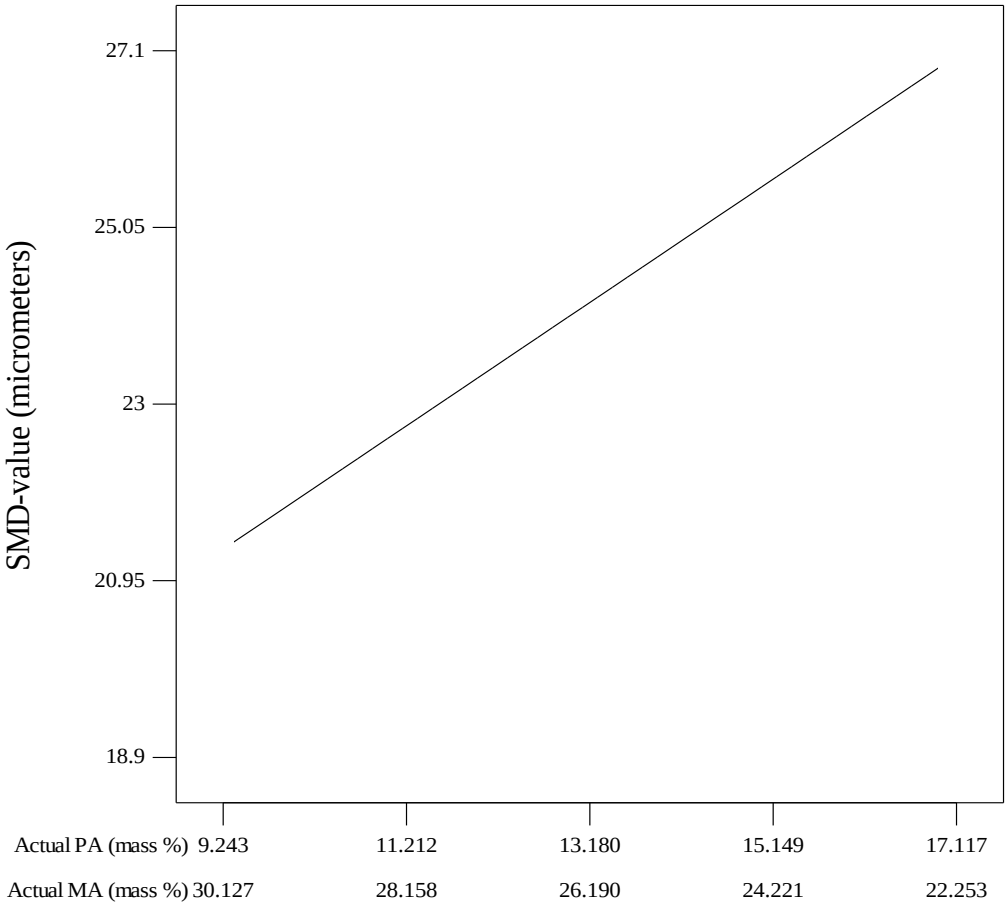

Figure 4.12: Two component mix graph for the formulation factors of the UPRs affecting SMD-value of the MVPs.

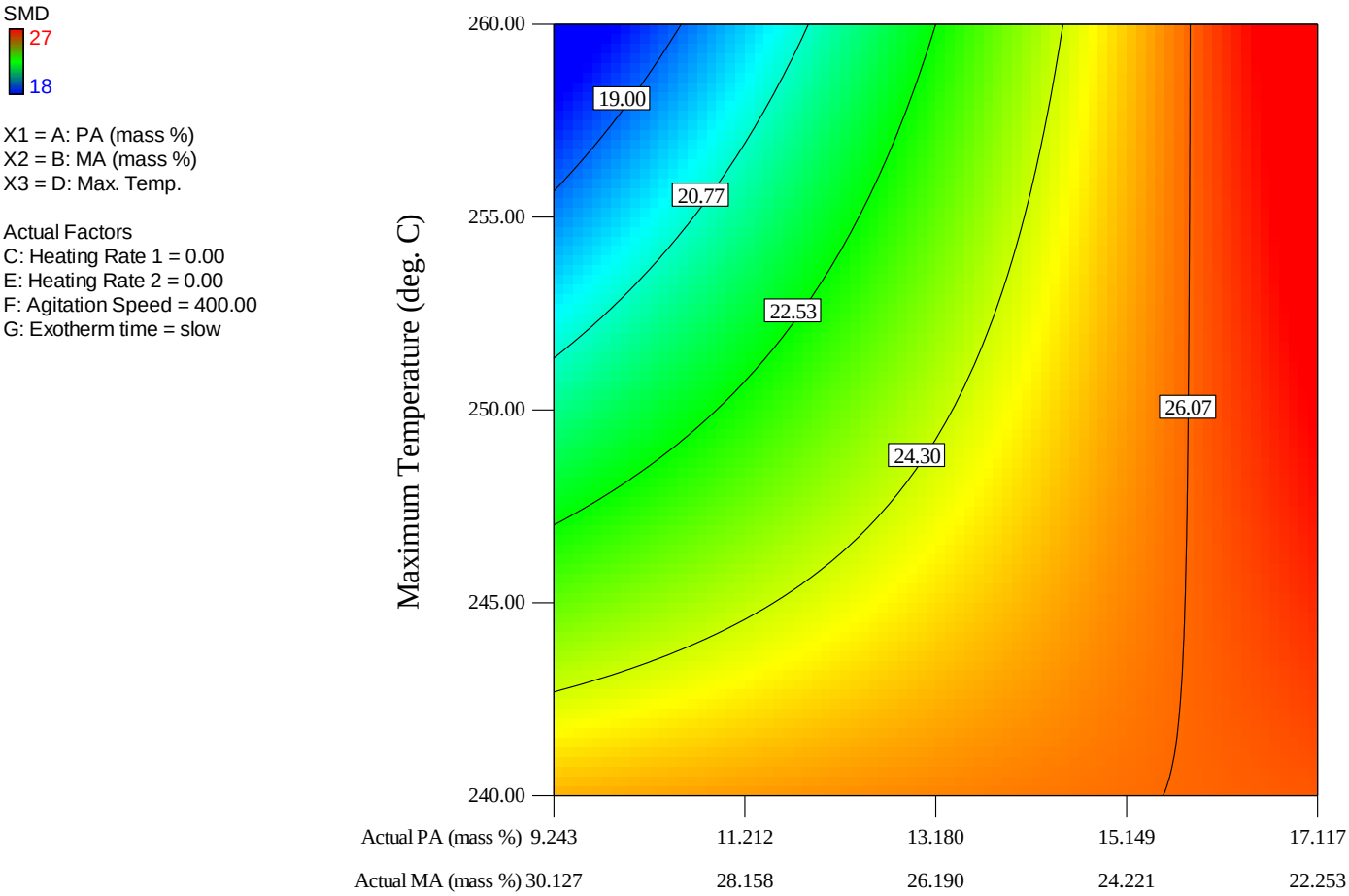

Figure 4.13: Contour mix-process graph of the interaction effect BD, i.e. interaction between %MA and the maximum temperature of the UPRs on SMD-value of MVPs.

The droplet or particle size during the suspension polymerization of MVPs is determined by the droplet break-up – coalescence equilibrium which is affected by the viscosity and surface tension of the oil droplet dispersed phase. In the suspension polymerization of MVPs, the dispersed phase comprises the UPR-STY mixture, LMA and DETA. The viscosity and surface tension of the dispersed phase is determined by the inherent viscosity of the UPR-STY mixture and the neutralization reaction between the carboxyl end-groups of the UPRs and DETA, i.e. a high viscosity mixture is achieved when UPRs with a high concentration of carboxyl end-groups are neutralized by the ammonium groups of the DETA. Thus a high SMD-value (high surface area particles with small diameter) will be the result of a UPR-STY mixture with a low viscosity and low acid-

value, which can be achieved with a high %PA (or low %MA) in the MA:PA mole ratio, and low maximum reaction temperature, which has been shown in the Section 4.1.2.

4.1.3.2 VMD-values

Table 4.6 also shows that the VMD-values of the MVPs ranged from 30.31 – 117.44 μm (mean = 64.599 μm ± 11.12). Table 4.8 shows the factors (and interaction between factors) affecting the VMD-value of the MVPs.

Table 4.8: Significant factors affecting VMD-value of the MVPs.

Factors	Significance (p-value: Prob > F)
AB	0.005
AF	0.0466
BD	0.0071
BE	0.0035

Table 4.8 shows that the most significant factors affecting the VMD-values of the MVPs are the MA:PA mole ratio (AB), and the interactions BE and BD, i.e. interactions between %MA and heating rate 2 and interaction between %MA and maximum process temperature.

Figures 4.14 and 4.15 show the two component mix and contour mix-process graphs where the effects of the MA:PA mole ratio and the interaction between the %MA and maximum process temperature of the UPRs are presented. It can be seen from these figures that an increase in %MA and decrease in the maximum reaction temperature of the UPRs leads to a high VMD-value of the MVPs.

A high VMD-value will be the result of a UPR-STY mixture with a high viscosity and/ or high acid-value, which can be achieved by a high % MA with a low maximum reaction temperature and agitation speed. Thus, the MA:PA mole ratio and interaction

between % MA and maximum reaction temperature of the UPRs are highly significant factors affecting the VMD-value of the resultant MVPs.

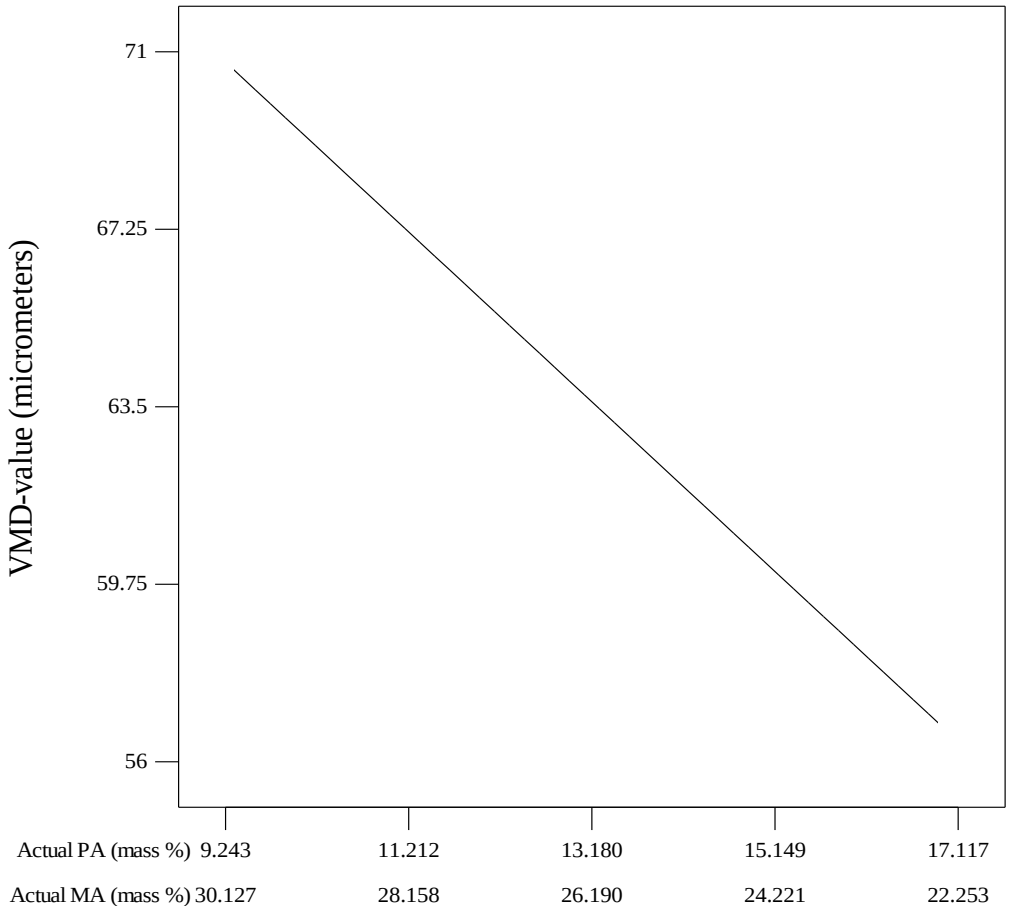

Figure 4.14: Two component mix graph for the formulation factors of the UPRs affecting VMD-value of the MVPs.

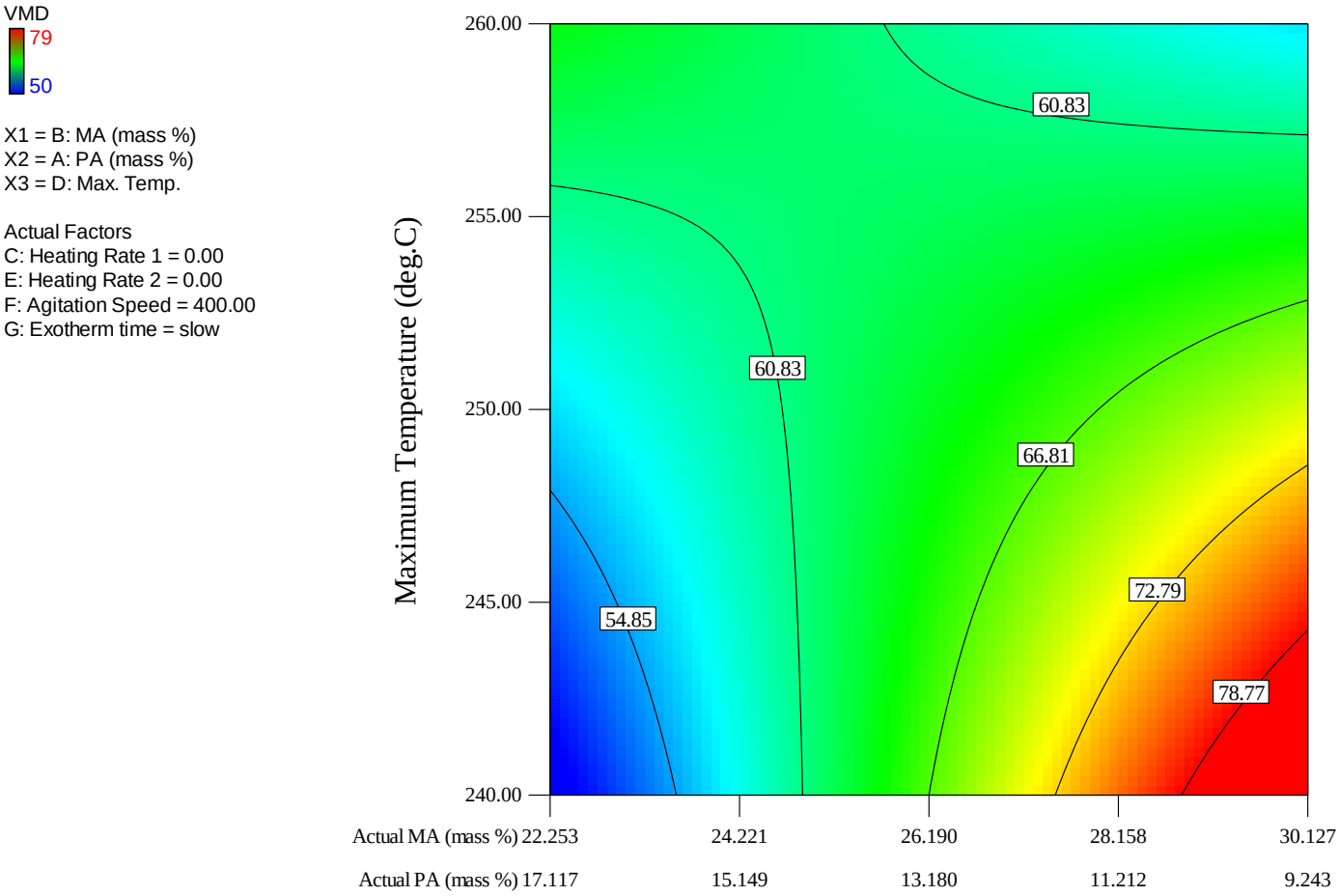

Figure 4.15: Contour mix-process graph of the interaction effect BD, i.e. interaction between %MA and the maximum temperature of the UPRs on VMD-value of MVPs.

Figure 4.16 shows a contour mix-process graph where the interaction effect of %MA and heating rate 2 is presented. It can be seen from Figure 4.16 that an increase in the %MA and decrease in the heating rate 2 of the UPRs lead to an increase in the VMD-value of the MVPs. The slow heating rate 2 leads to improved reaction of the MA with PG, which increases the degree of chain branching and viscosity of the UPRs (and UPR-STY mixtures), and subsequently high VMD-values of the MVPs.

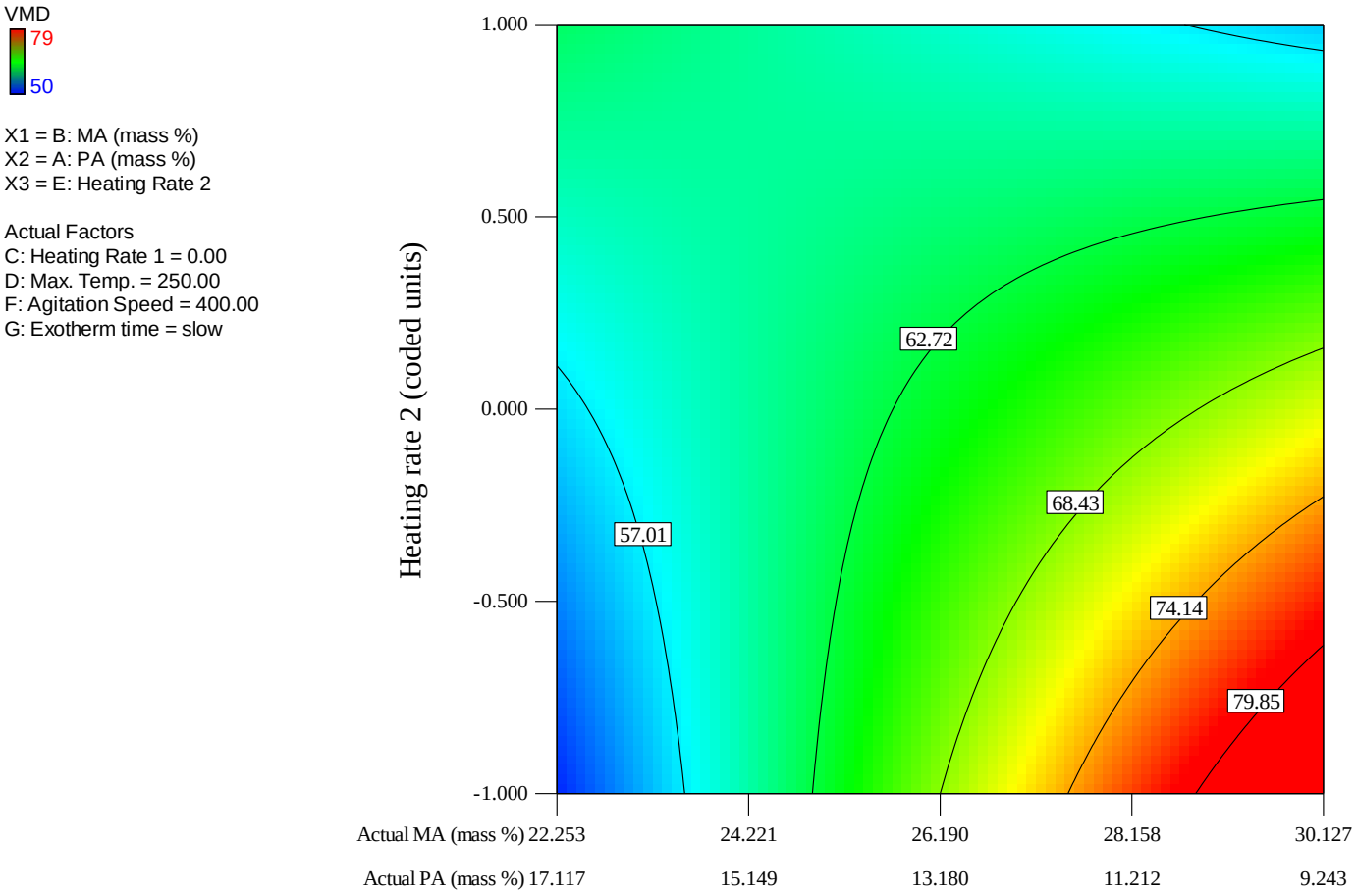

Figure 4.16: Contour mix-process graph of the interaction effect BE, i.e. interaction between %MA and the heating rate 2 of the UPRs on VMD-value of MVPs.

4.1.3.3 Preliminary conclusion: MVPs

The significant factors affecting the particle sizes (SMD and VMD-values) of the MVPs include the MA:PA mole ratio and its interaction with the maximum process temperature. The particle size of suspension-based polymers is controlled by the droplet/particle coalescence-break-up equilibrium during the polymerization. The coalescence-break-up equilibrium is determined by the viscosity and surface tension of the oil droplets, which are affected by the MA:PA mole ratio and maximum process temperature.

4.2 Detailed analysis of selected DoE runs

Detailed analysis of experimental runs 6 and 26 (UPRs and resulting MVPs) was performed. These polymers were selected since the particle sizes of MVPs of these runs are vastly different, although they have been synthesized from UPRs according to the same formulation, but slightly different process parameters, i.e. heating rates 1 and 2, exotherm rate and agitation speed. Table 4.9 shows the MA:PA mole ratio and process parameters used in the synthesis of the UPRs of runs 6 and 26. Tables 4.10 and 4.11 show the properties of the two UPRs and the corresponding MVPs, respectively.

Table 4.9: Formulation and process parameters of DoE runs 6 and 26.

RUN	PA (%)	MA (%)	Actual heating rate 1 (˚C/min)	Exotherm rate	Maximum exotherm temperature (°C)	Actual heating rate 2 (˚C/min)	Maximum temperature (°C)	Agitation speed (rpm)
6	17.12	22.25	4.0	slow	147.4	1.1	240	500
26	17.12	22.25	6.0	fast	174.0	0.8	240	300

Table 4.10: Properties of UPRs of DoE runs 6 and 26.

RUN	Viscosity (cPs)	Acid-value (mgKOH/g)	M_n (Dalton)	M_w (Dalton)	PDI	Tg (°C)	Degree of branching[#]
6	1509	28.15	1351	4979	3.68	-5.59	0.47
26	1207	28.92	1246	3288	2.64	-6.50	0.47

[#]Degree of chain branching was determined by ^{1}H NMR (Section 4.5).

Table 4.11: Properties of MVPs with UPRs of DoE runs 6 and 26.

RUN	SMD (µm)	VMD (µm)
6	40.33	61.15
26	12.72	30.31

Table 4.10 shows that RUN 6 has a greater viscosity and molecular weight and molecular weight distribution compared to RUN 26. RUN 6 was processed with a higher agitation

speed and heating rate 2 which leads to an increase in the overall reaction rate, and therefore an increase in the viscosity, molecular weight and molecular weight distributions.

It can also be seen from Table 4.10 that a higher Tg-value is obtained for RUN 6, which is possibly due to the increase in the concentration of bulky PA groups incorporated in the chains due to a (1) slower exotherm rate and (2) faster agitation speed, which lead to improved reaction between PA and PG, compared to RUN 26. The improved PA incorporation results in reduced main-chain motion and hence a higher Tg-value of the UPR compared to RUN 26.

Table 4.10 also shows that the UPRs of runs 6 and 26 have very similar acid-values and degree of chain branching, which means that the carboxylic acid distribution of the polyester chains is similar (see Section 4.5). Consequently, when DETA is added to the UPRs (during the synthesis of the corresponding MVPs) they will have similar concentrations of neutralized carboxylic groups and therefore similar micelle concentrations in the organic phase (see Section 2.3.3.1), which in turn leads to similar concentrations of the aqueous voids (and degrees of vesiculation) in the organic phase droplets in the dispersion stage (see Section 3.5).

Figures 4.17(b) and 4.18(b) show the SEM images of the microtomed MVPs of runs 6 and 26, respectively, illustrating the degree of vesiculation of the MVPs. The MVPs of runs 6 and 26 have similar degrees of vesiculation due the fact that the UPRs have similar acid-values and degrees of chain branching as they were synthesized at the same maximum temperature (maximum process temperature and its interaction with MA:PA mole ratio determine the degree of chain branching and acid-value) (see Section 4.1.2).

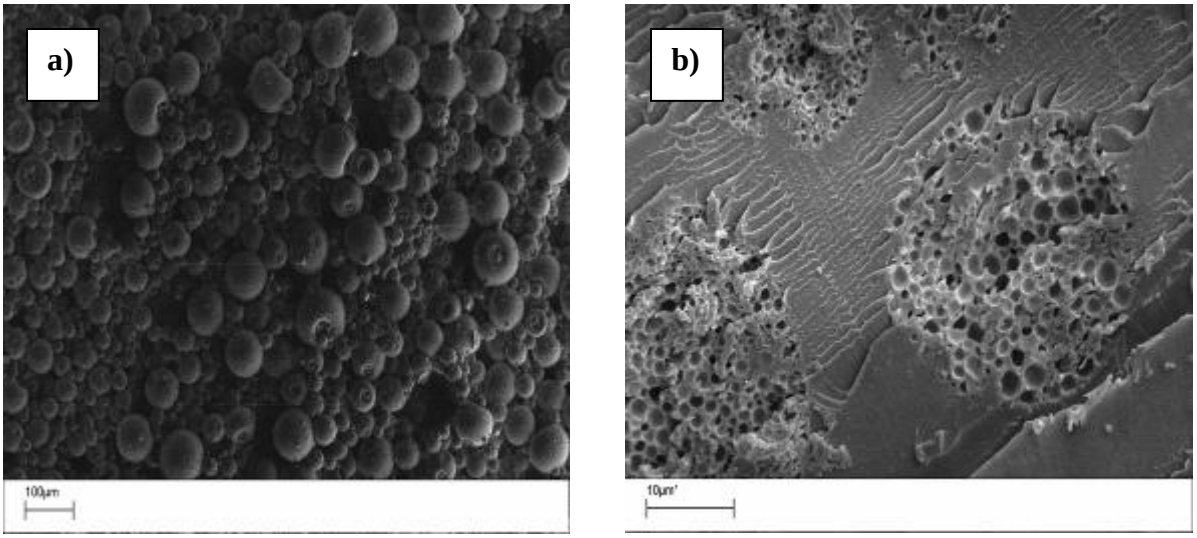

Figure 4.17: SEM images of (a) MVPs of RUN 6 at 100× magnification and (b) microtomed MVPs of RUN 6 at 1790 × magnification.

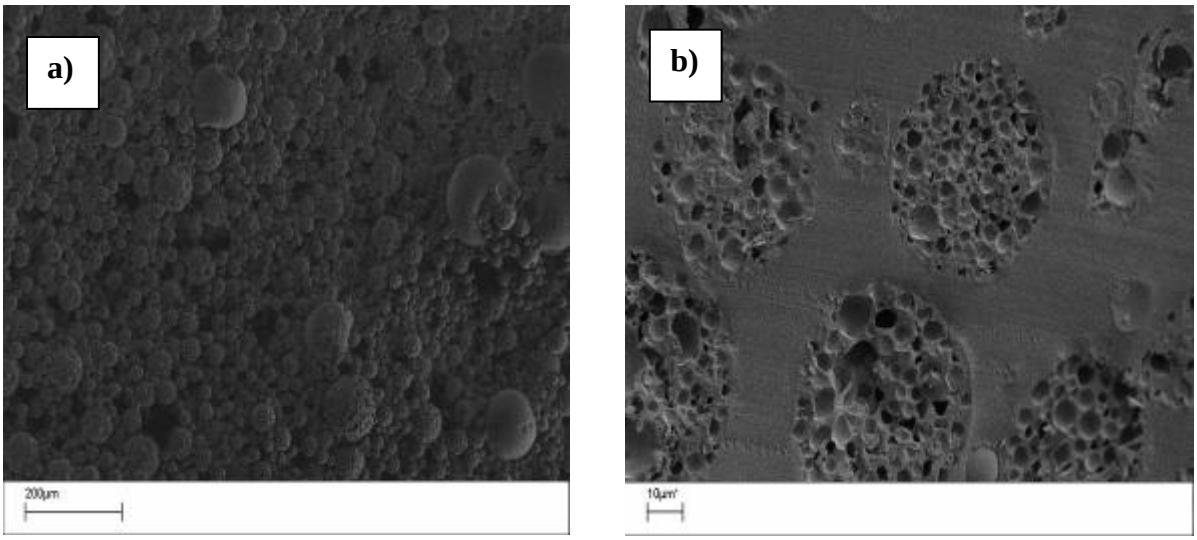

Figure 4.18: SEM images of (a) MVPs of RUN 26 at 100× magnification and (b) microtomed MVPs of RUN 26 at 735 × magnification.

Table 4.11 also indicates that the high molecular weight/ viscosity of the UPR of RUN 6 results in larger particle sizes (SMD and VMD-values) of the MVPs compared to RUN 26. The SEM images in Figures 4.17(a) and 4.18(a) confirm the larger particle size of the MVPs of RUN 6.

Figure 4.19 shows the bimodal particle surface area distributions ("Density" distributions) and cumulative distributions of the particle sizes of the MVPs of runs 6 and 26 determined by light scattering. It can be seen from Figure 4.20 that the MVPs of RUN 6 have a greater percentage of larger particles, indicated by a greater intensity of the larger particle size region of the distribution. The SEM images in figures 4.17 and 4.18 also indicate the bimodal nature of the particle size distributions of runs 6 and 26.

The MVPs of RUN 6 have larger particle sizes due to the high viscosity of the polyester/ organic phase (during the suspension polymerization of the MVPs) which reduces the droplet break-up, resulting in larger dispersed droplets in the aqueous phase, and ultimately larger MVPs.

The effect of processing the UPRs at different maximum process temperatures on the properties of the UPRs and MVPs is investigated in Section 4.3.

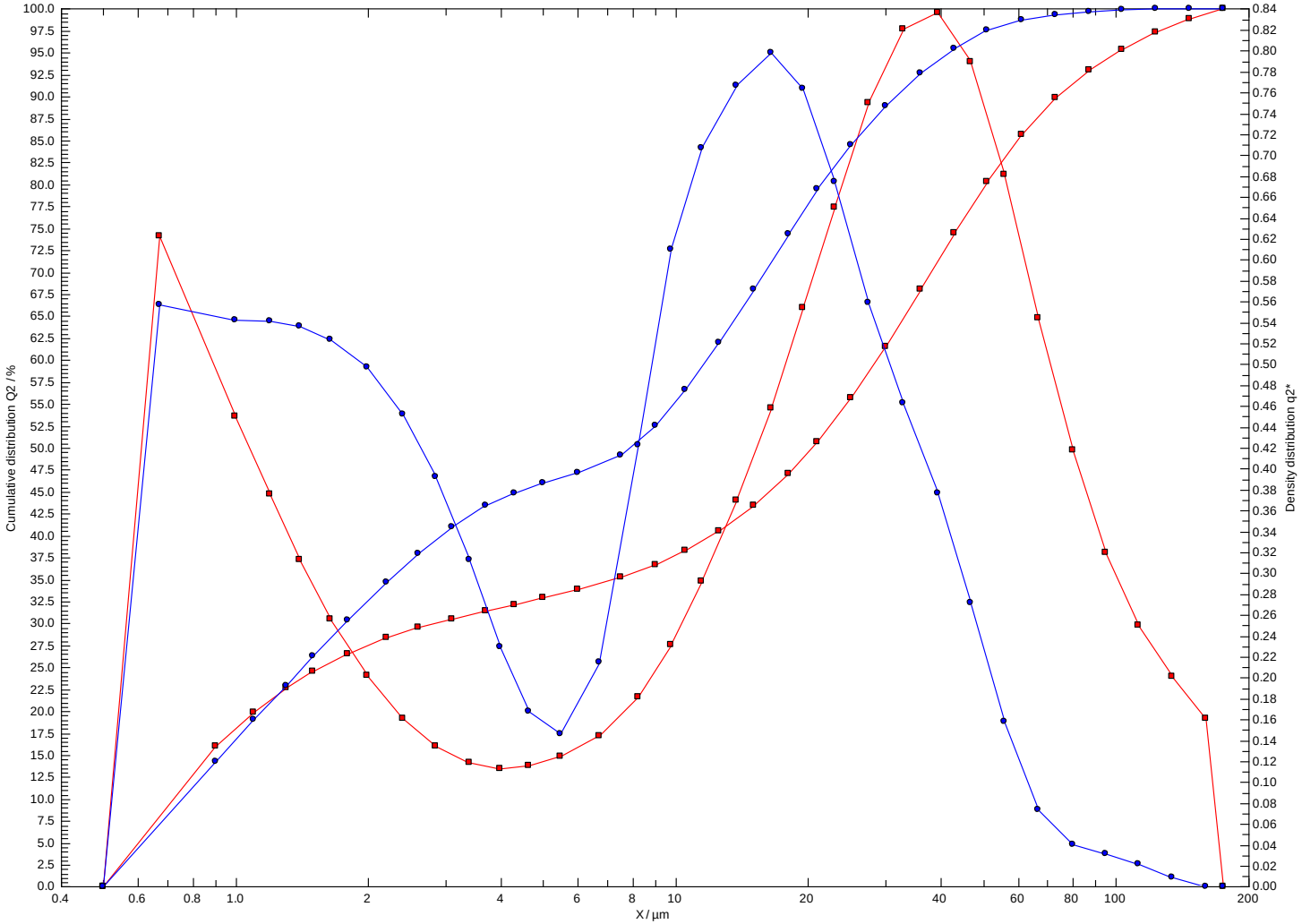

Figure 4.19: Surface area and cumulative distributions of the particle sizes of MVPs of DoE run 6 (red) and DoE run 26 (blue).

4.3 Effect of UPR maximum processing temperature on properties of the UPR and the resultant MVPs.

Fairly anomalous results were obtained with regards to the particle size values (SMD and VMD) of the MVPs in Section 4.1.3. ANOVA evaluation of particle sizes of these MVPs revealed that a high SMD-value can be achieved with a low UPR maximum reaction temperature, whilst a high VMD-value can be achieved with a high UPR maximum temperature. To investigate the individual effect of the UPR maximum temperature on the particle size (and other properties) of the MVPs, a series of UPRs and MVPs were synthesized with a variation in the maximum reaction temperature while the other parameters are kept constant.

The UPR series were synthesized according to the standard formulation (See Table 3.1) and experimental procedure (i.e. standard heating rates, agitation, and exotherm time/ temperature) (see Section 3.3) but with different maximum temperatures, i.e. 220, 230, 240, 250, and 260 °C. These UPRs were also analyzed for viscosity, acid-value, molecular weights (M_n, M_w), PDI and T_g-values. The five resultant UPR-STY mixtures were used to synthesize MVPs to determine the effect of the maximum process temperature of the UPRs on the particle sizes of the MVPs. The properties of the five UPR-STY mixtures are given in Table 4.12.

Table 4.12: Effect of UPR maximum processing temperature on properties of the UPRs of runs 29 – 33.

RUN	Maximum temperature (°C)	Viscosity (cPs)	Acid-value (mgKOH/g)	M_n (Dalton)	M_w (Dalton)	PDI	Tg (°C)	Degree of branching*
29	220	791.8	65.09	746	1556	2.08	-8.77	0.323
30	230	566.3	57.83	821	1783	2.17	-6.00	0.299
31	240	777.4	50.84	992	2406	2.43	0.01	0.387
32	250	861.4	41.82	1081	3328	3.08	4.56	0.407
33	260	1346	39.96	1273	6950	5.46	6.96	0.413

*Degree of chain branching (DB) of the UPRs was determined by ^{1}H NMR (see Section 4.5).

Table 4.12 shows that an increase in the polyester maximum process temperature results in an increase in the viscosity, M_n-, M_w-, PDI-, T_g-values, degree of chain branching and a decrease in the acid-value of the UPR-STY mixtures.

The increase in the viscosity can be attributed to an increase in molecular weight, PDI value and the degree of chain branching of the UPR chains (see Section 4.5). Figure 4.20 shows the molecular weight distributions of the five UPRs obtained by SEC.

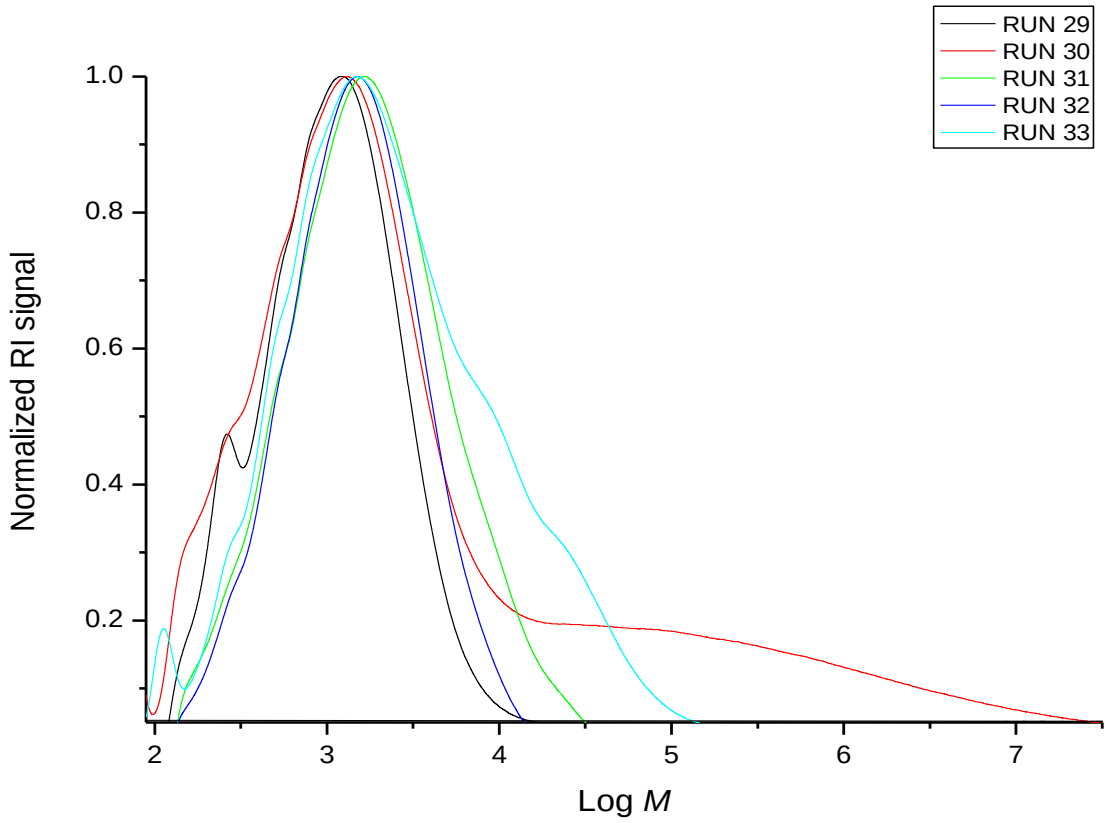

Figure 4.20: SEC chromatograms of UPRs prepared at different maximum processing temperatures.

The decrease in the acid-value of the UPRs can be explained by the fact that the carboxylic acid concentration decreases as the polyesterification reaction progresses. However, the degree of chain-branching increases as the polyesterification reaction progresses at a higher process temperature, which means that the carboxylic acid concentration per chain increases. In other words, the concentration of carboxylic acid

groups of the individual chains increases due to the acid end groups of the branches/side chains. The schematic diagram in Figure 4.21 illustrates this phenomenon.

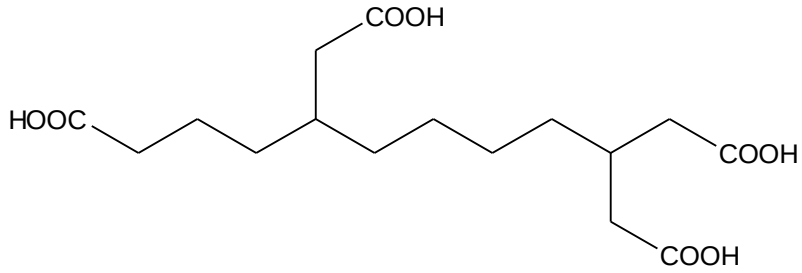

Low degree of chain branching

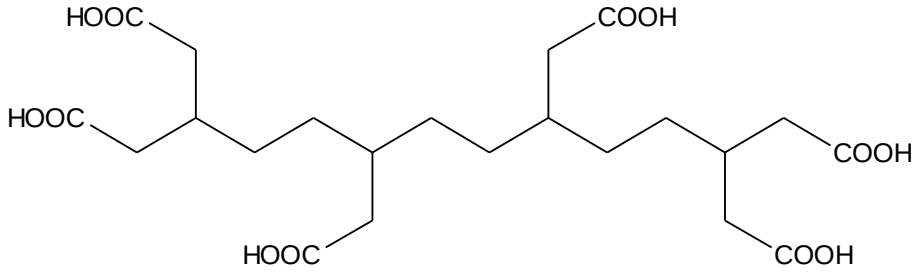

High degree of chain branching

Figure 4.21: Schematic diagram of the effect of chain branching on the acid-value of the UPRs.

The increase in the T_g values of the UPRs may be attributed to the increased molecular weight, degree of chain-branching as well as the increased incorporation of the bulky phthalate groups in the chains at higher temperatures. These factors decrease the main-chain mobility of the UPRs, which leads to an increase the T_g value. Figure 4.22 shows the DSC thermograms with the T_g values of the UPRs.

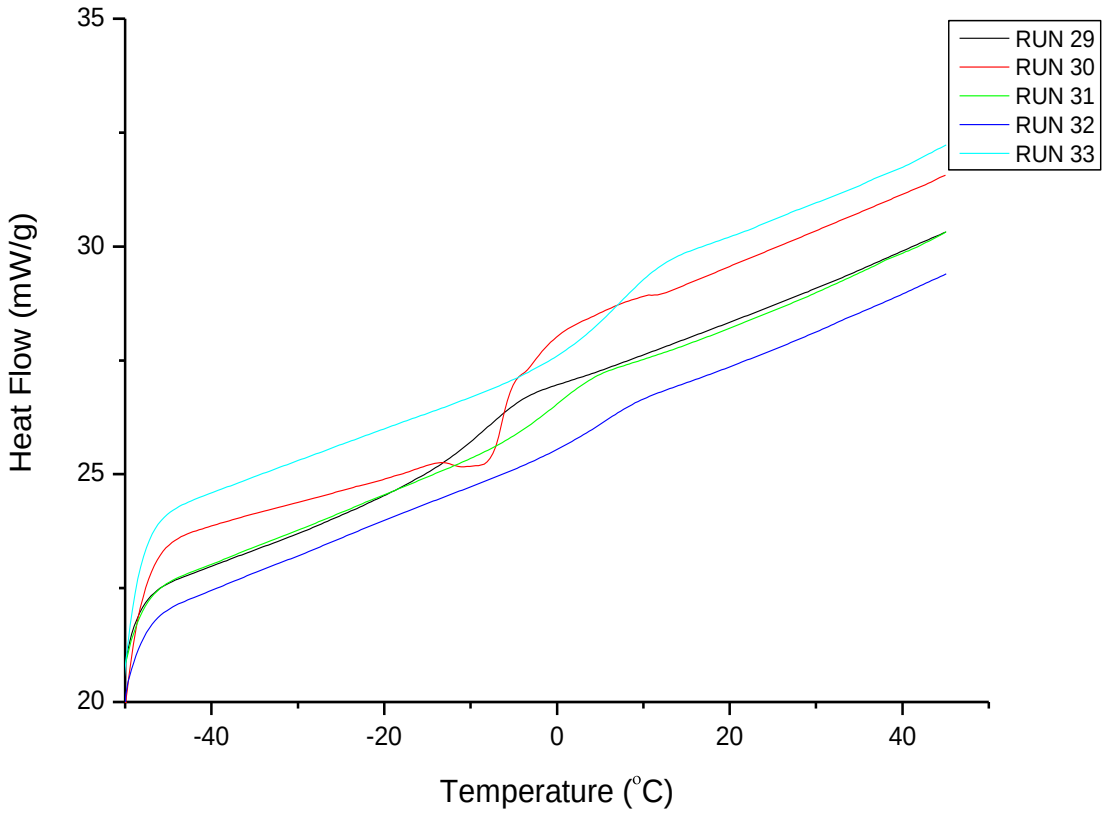

Figure 4.22: DSC curves of the UPRs prepared at different maximum processing temperatures.

Table 4.13: Effect of UPR maximum processing temperature of runs 29 – 33 on properties of the MVPs.

RUN	SMD (µm)	VMD (µm)	Contrast ratio
29	11.76	53.24	0.17
30	8.47	41.64	0.30
31	13.93	47.35	0.24
32	28.87	56.28	0.57
33	37.58	93.65	0.61

It is known that an increase in the maximum processing temperature of the polyester leads to an increase in the percentage chain branching of the polyester. An increase in the chain branching leads to an increase in the concentration of carboxylic groups per chain

and therefore an increase in the concentration of neutralized carboxylic groups per main chain with the addition of DETA to the polyester mixture (see Section 2.3.3.1). The increased concentration of neutralized groups leads to an increase in the concentration of micelles in the organic phase, which in turn leads to an increase in the concentration of the aqueous voids in the organic phase droplets, and eventually an increase in the concentration of vesicles or degree of vesiculation of the dried MVPs. In other words, the concentration of vesicles or degree of vesiculation increases as the polyester chain branching increases, which in turn increases as the polyester maximum processing temperature increases. Figure 4.23 shows the SEM micrographs of microtomed MVPs of experimental runs 29 and 33, indicating the difference in the degree of vesiculation of the runs.

Figure 4.23(a) clearly shows that the MVPs of RUN 29 have a lower degree of vesiculation compared to those of RUN 33 in Figure 4.23(b). RUN 29 has a low degree of vesiculation due to the lower degree of chain-branching of the polyester chains, resulting in a low concentration of neutralized carboxylic groups (micelles). On the other hand, the MVPs of RUN 33 has a higher degree of vesiculation due to a high percentage of chain-branching, as a result of a high polyester processing temperature.

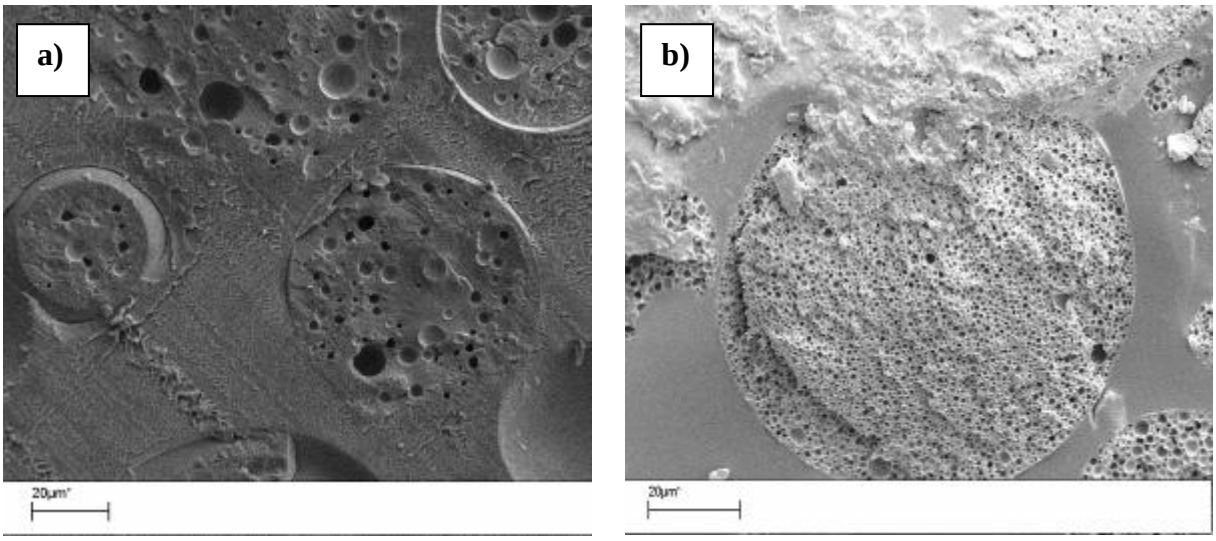

Figure 4.23: SEM micrograph of microtomed MVPs of a) RUN 29 at 622× magnification and (b) RUN 33 at 913× magnification.

Table 4.13 indicates that RUN 33 has a higher contrast ratio/ opacity value (at the same film wet-film thickness) than RUN 29. The opacity of RUN 33 is higher due to the higher degree of vesiculation and light scattering ability of the MVPs (see Section 2.3.1).

Table 4.13 also shows that the UPR maximum temperature indirectly affects the particle size of MVPs. As previously concluded from Section 4.1.3, a low maximum reaction temperature with a high %PA or a high maximum temperature with a high %MA of the UPRs, can lead to a large particle size (SMD or VMD-values) under certain circumstances. Table 4.13, however, shows that an increase in the UPR maximum temperature leads to an overall increase in the particle size (SMD and VMD values) of MVPs at a MA:PA mole ratio = 26.19:13.18.

Figure 4.24 illustrates the bimodal particle surface area distributions of MVP runs 29 and 33. It can be seen from Figure 4.24 that the MVPs of RUN 33 have a greater percentage of larger particles compared to smaller particles, indicated by a greater intensity of the larger particle size region of the distribution.

The larger particle size of the MVPs of RUN 33 can be explained by the high viscosity of the UPR processed at a higher maximum temperature. The UPR of RUN 33 has a higher viscosity than RUN 29 due to increased DP_n and DB-values at the high maximum process temperature. The higher viscosity of the UPR reduces the droplet break-up and increases the probability of droplet coalescence, resulting in larger dispersed droplets in the aqueous phase, and ultimately larger MVPs.

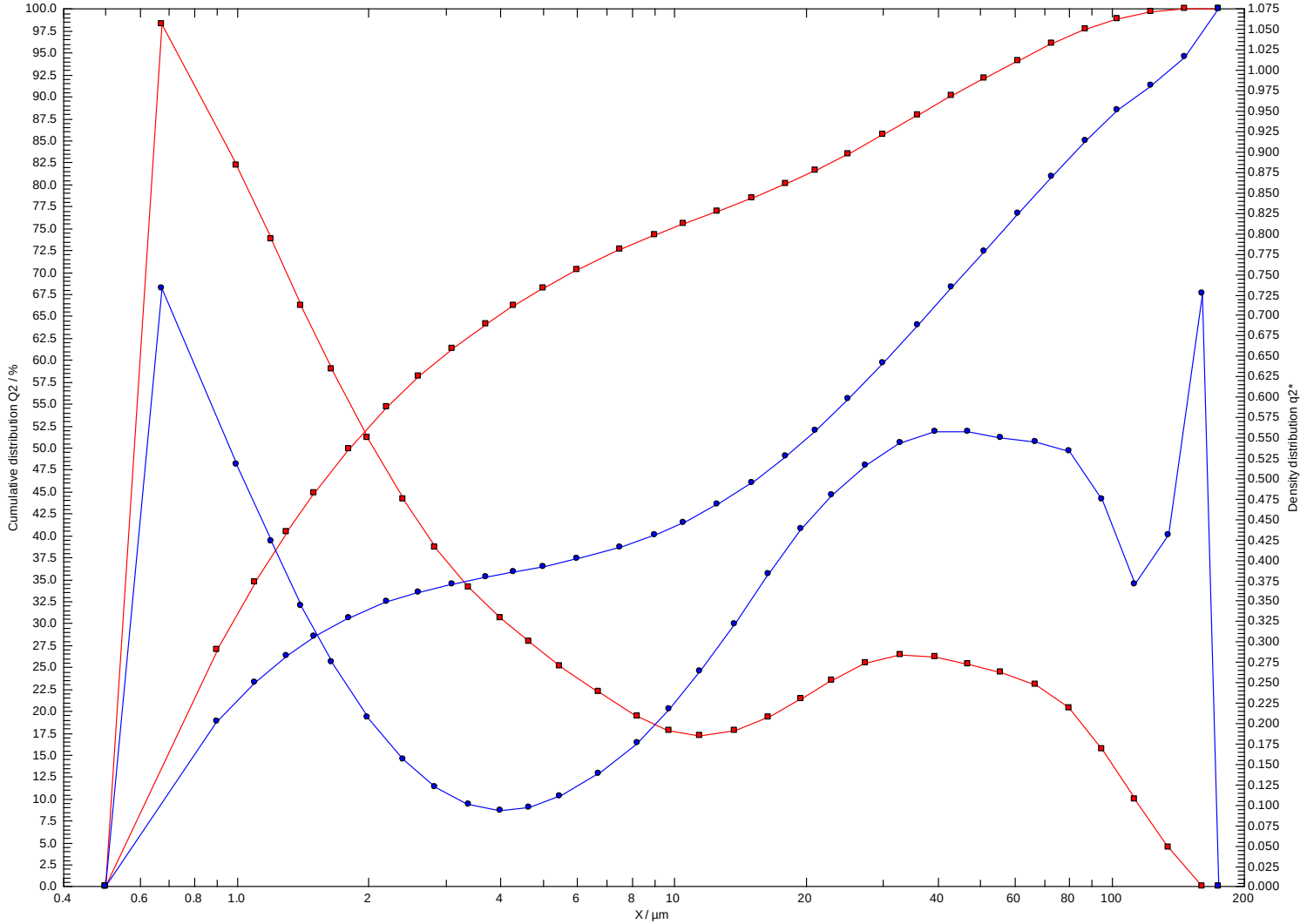

Figure 4.24: Surface area and cumulative distributions of the particle sizes of MVPs of runs 29 (red) and 33 (blue).

4.4 Determination of hardness of MVPs

Attempts were made to determine the hardness/ stiffness of the MVPs to quantitatively determine the effect of the crosslink density, degree of vesiculation, and particle size on the hardness of the MVPs to confirm the following postulates:

- The crosslink density of the MVPs is determined by the reaction between the MA of the UPR and STY, i.e. a high MA:PA mole ratio in the UPR leads to a high crosslink density, which in turn results in harder MVPs. The impact resistance of the MVPs is however compromised.
- The degree of vesiculation (size and concentration of vesicles) of the MVPs is determined by the interaction between the COOH-groups of the UPR and DETA during the synthesis of the MVPs. Thus a high concentration of COOH-groups leads to a high degree of vesiculation due to increased interaction with the DETA. The degree of vesiculation would affect the hardness and impact resistance of the MVPs, e.g. highly porous MVPs will have lower impact resistance compared to those with low porosity.
- MVPs with different particle sizes will have different hardness values.

The microhardness tester and Atomic Force Microscopy (AFM) in contact mode were used to determine the hardness of the MVPs.

As previously mentioned in Section 3.6.11, the microhardness testing of the dried MVPs involved indenting the individual MVPs with the micro-indenter. The MVPs were sprinkled onto the surface of a liquid alkyd resin before it was allowed to cure completely. The resin was cured to keep the MVPs stationary during testing. The sprinkling of the MVPs onto the resin surface meant that not all the MVPs were at the same depth at the resin surface. Thus, when the micro-indenter was applied to the MVPs, erratic results were obtained. In other words, erratic microhardness values were obtained as the surfaces of the MVP-resin disks were not homogeneous.

AFM was found to be effective to determine the hardness of the MVPs smaller than 1 micron, although the mean particle size of the MVPs is approximately 25µm. In other words, AFM is not a suitable technique to determine the hardness of MVPs due to their relatively large particle size. AFM was however performed on the sub-micron sized MVPs of runs 29 (low degree of vesiculation) and 33 (high degree of vesiculation) to determine the effect of degree of vesiculation on the hardness of the MVPs. For example, Figures 4.26 and 4.27 show the AFM software-generated 3D-images and "Force-Distance" curves of sections of individual MVPs of runs 29 and 33, respectively. The force-distance curves approaches from -1µm towards 20nm on the z-axis as the cantilever tip moves towards the MVPs. Adhesion between the cantilever tip and the MVP is indicated by the sharp dip in the retracting curve. The cantilever is thereafter deflected from the MVP, where the angle of the deflection slope indicates the hardness of the MVP.

It can be seen from Figures 4.25(b) and 4.26(b) that the deflection angle (of the slope) of the approaching curve of the MVP from RUN 29 (45.94°) is greater than that of RUN 33 (33.89°), indicating that the MVP from RUN 29 is relatively harder than that of RUN 33. The MVP of RUN 29 is possibly harder due to the lower degree of vesiculation of the MVPs.

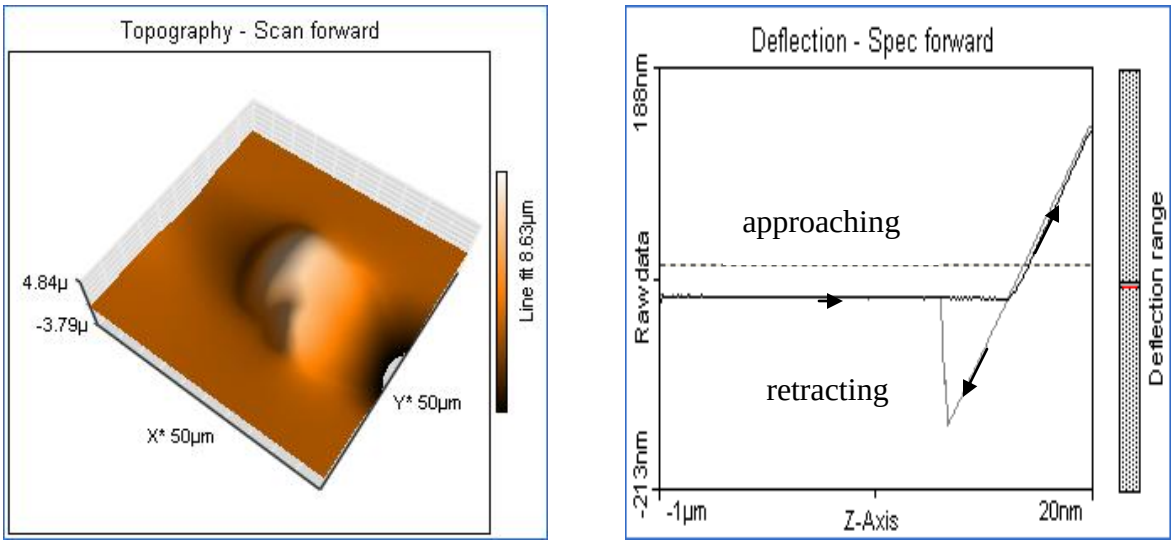

Figure 4.25: AFM 3D image (a) and force-distance curve (b) of a sub-micron MVP of RUN 29.

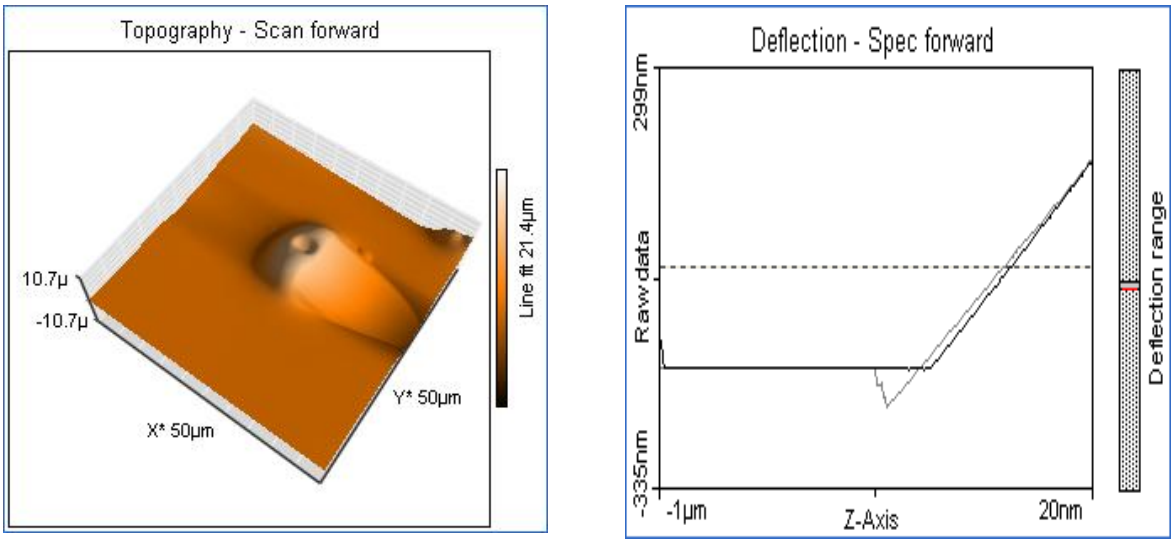

Figure 4.26: AFM 3D-image (a) and force-distance curve (b) of a sub-micron MVP of RUN 33.

4.5 Chain-branching

As mentioned in Section 4.1, the Ordelt reaction is the main side reaction in the polyesterification reaction. The Ordelt reaction involves the double bonds of the maleate or fumarate component becoming saturated and leading to branched structures or side chains. The degree of branching can be determined by size-exclusion chromatography using the PDI as a measure of the branching extent, whereby the greater the PDI, the greater the branching extent [2]. Zetterlund et. al. [3], on the other hand, studied the Ordelt reaction by ^{1}H NMR by using the work of Paci et. al. [4] and Judas et. al. [5] together with the NMR spectra of polyesters with only PG and PA (Figure 4.27) as well as polyesters with only PG and MA (Figures 4.28). It was concluded that the shoulder of the resonance peak at 5.2 ppm in Figure 4.28 was related to the Ordelt reaction, as no shoulder was observed for the resonance peak in the spectrum of PA in Figure 4.27.

.

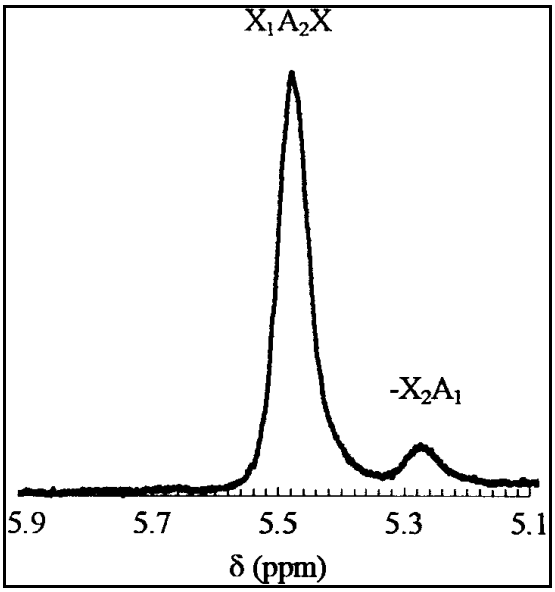

Figure 4.27: ^{1}H NMR spectrum of polyester with phthalic anhydride [3].

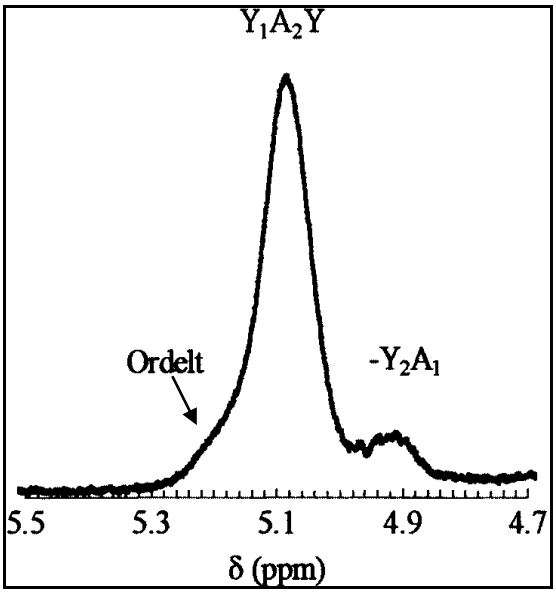

Figure 4.28: ^{1}H NMR spectrum of polyester with maleic anhydride [3].

Holter et. al. [6] derived an equation to determine the degree of branching based ratio of the ^{1}H NMR signal intensities of branched (due to the Ordelt reaction) units and the linear units of the unsaturated polyester chains. The ratio is as follows:

$$\text{Degree of Branching (DB)} = \frac{2D}{2D + L} \qquad (4.3)$$

Where

D = NMR intensity of a branched unit in the polyester chains

L = NMR intensity of a linear unit in the polyester chains

The DB values were determined by using the ^{1}H NMR intensities of the shoulder of the methine peak at 5.2 – 5.4 ppm as D and the methine peak at 5.1 – 5.2 ppm as L in Equation 4.3 (e.g. ^{1}H NMR spectrum of the UPR of RUN 29 in Figure 4.29). Table 4.14 shows the DB- and PDI-values obtained from ^{1}H NMR and SEC of runs 29 to 33, respectively.

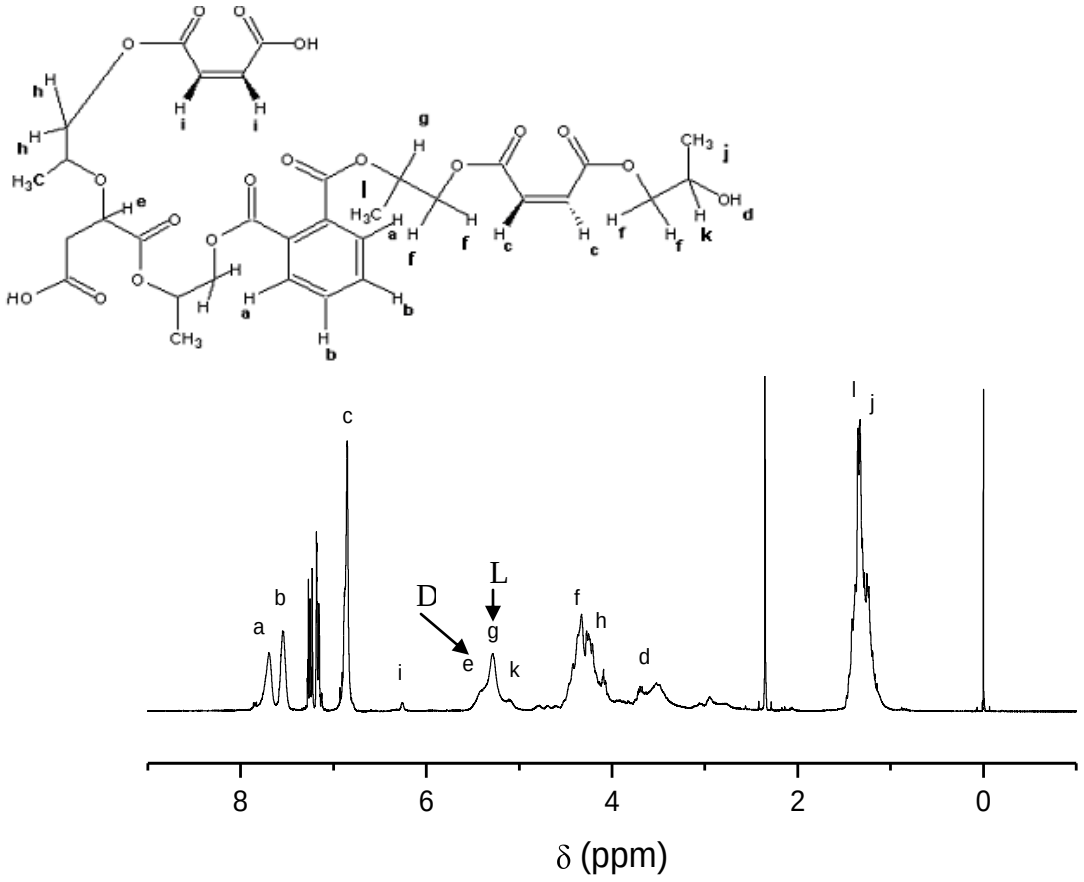

Figure 4.29: ^{1}H NMR spectrum of UPR of RUN 29.

Table 4.14: DB results of UPRs of runs 29 and 33 via ^{1}H NMR and SEC.

RUN	^{1}H NMR			SEC
	Intensity of methine unit (g)	Intensity of branched unit (e)	DB	PDI
DoE 6	11.877	5.160	0.465	3.68
DoE 26	11.779	5.188	0.468	2.64
29	2.040	0.486	0.323	2.08
30	1.488	0.318	0.299	2.17
31	2.779	0.877	0.387	2.43
32	2.976	1.022	0.407	3.08
33	0.577	0.203	0.413	5.46

Table 4.14 clearly shows that the DB values of the UPRs of DoE runs 6 and 26 are very similar, because they were synthesized at the same maximum temperature (240 °C). However, the DB values of the UPRs from runs 29 – 33 increase from run 29 (0.323) to 33 (0.413) due to the increased probability of the Ordelt reaction (chain-branching) at higher maximum processing temperatures of the UPRs.

The DB results of runs 29 to 33 are in good agreement with the PDI values obtained from SEC. The PDI- and DB-values were not in good agreement for runs 6 and 26, because these UPRs were synthesized according to different process protocols, i.e. different exotherm rates, agitation speeds and heating rates 1 which affect the molecular weights (and therefore PDI-values) of the UPRs. These parameters (unlike the maximum process temperature) do not significantly affect the degree of branching of the UPRs.

4.6 End-group analysis by isocyanate derivatization and ^{1}H NMR

Historically, numerous methods have been employed to analyze the end-groups of polyesters, including classical titration methods [7-8], Fourier Transform Infra-red spectroscopy (FTIR) [9-10], Matrix-Assisted-Laser-Desorption-Ionization-Mass-Spectrometry (MALDI) [11] and High Performance Liquid Chromatography (HPLC) [12].

NMR spectroscopy is an attractive method for the quantitative and qualitative determination of end-groups of polyesters, providing these resonances can be resolved from those attributed to the backbone signals [13-14]. ^{13}C NMR spectroscopy have been used to determine the end-groups of PET [13, 15], but the technique is complex and does not have general applicability. Derivatization of the polyester chains with various chemical compounds followed by ^{19}F NMR [16] and ^{31}P NMR [17] has also been used, but these methods require complex experimental protocols.

The method used to determine the end-groups of the UPRs synthesized in this study is an efficient and quantitative method developed by Donovan and Moad [18]. The method

entails the characterization of the COOH and OH end-groups by ^{1}H NMR after derivatization of these groups by trichloroacetyl isocyanate (TAI). The TAI-derivatized end-groups have imidic NH resonances in a clear region of the ^{1}H NMR spectrum, i.e. the COOH-groups have resonances at 10–11.5 ppm for C(O)–O–C(O)–NH–C(O)CCl_3 groups, and the OH-groups at 8–9 ppm for O–C(O)–NH–C(O)CCl_3 groups. The reaction schemes involved are given in Figures 4.30 and 4.31.

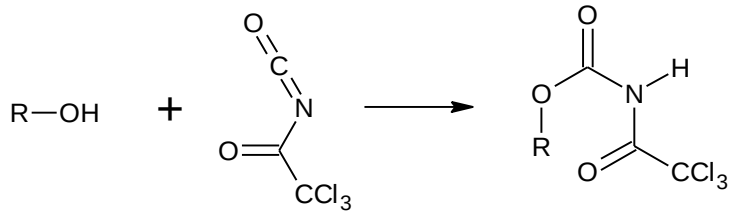

Figure 4.30: Derivatization of OH-groups of UPRs with TAI.

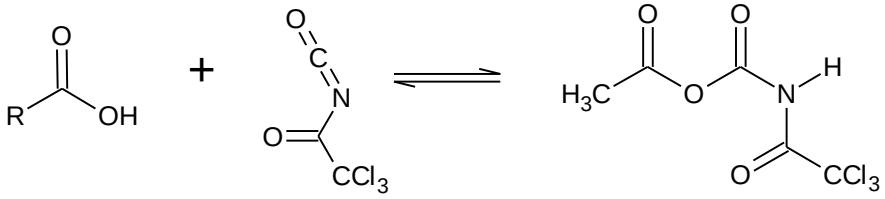

Figure 4.31: Derivatization of COOH-groups of UPRs with TAI.

The derivatization reaction is performed by dissolving a sample of the polyester (300 mg) in deuterated chloroform $CDCl_3$ (2 mL) in a NMR tube, after which an excess of trichloroacetyl isocyanate (TAI) (0.5 mL) is added and the ^{1}H NMR spectrum is recorded for 32 scans. The derivatization reaction is instantaneous and any excess TAI, being aprotic, causes no additional resonance signals in the spectra. Figure 4.32 shows the FTIR spectrum which confirms the derivatization reaction of the UPR of RUN 29 with TAI.

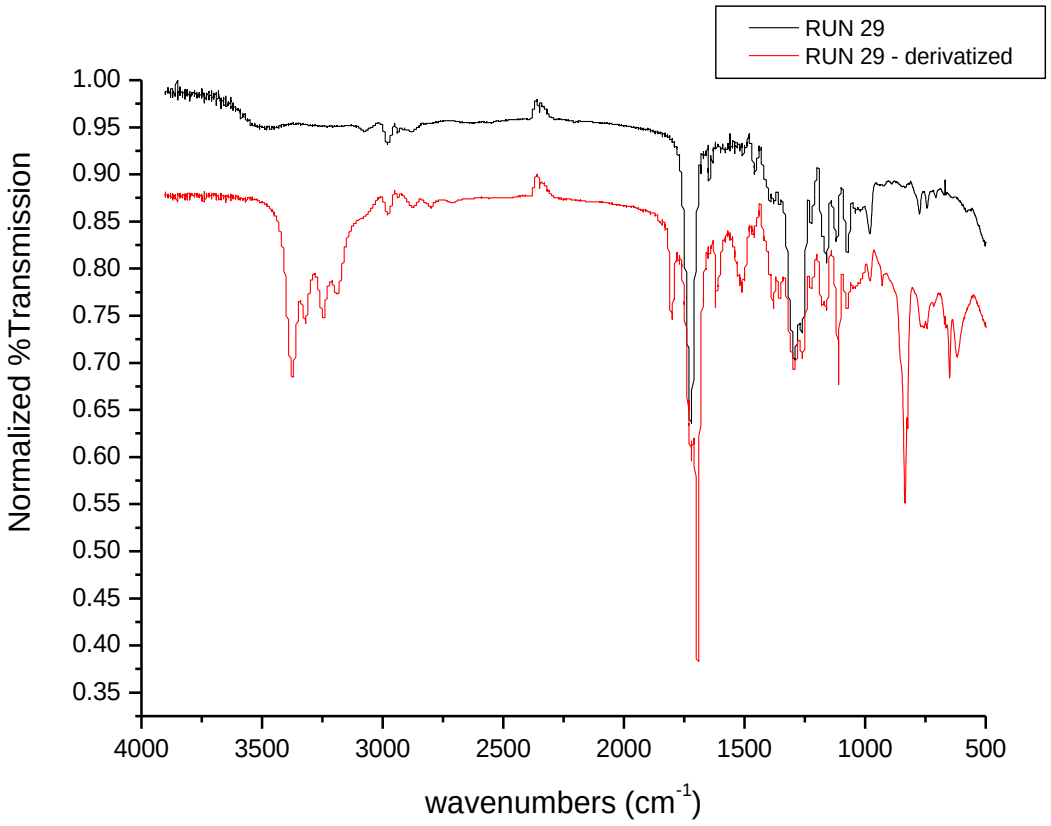

Figure 4.32: FTIR spectrum of the UPRs of RUN 29 (black) and RUN 29 derivatized with TAI (red).

Figure 4.32 clearly shows that the UPR chains of RUN 29 were derivatized by TAI due to the presence of N-H stretch vibrational frequencies at 3500-3100 cm^{-1} and the absence of O-H vibrational frequency at 3500cm^{-1} which is present in the spectrum of the un-derivatized sample.

Figure 4.33 shows the ^{1}H NMR spectrum of TAI-derivatized UPR of RUN 29. It can be seen from Figure 4.33 that the TAI-derivatized OH-groups at 9.0 ppm -and COOH-groups at 11 ppm are in a clear region of the NMR spectrum. Integration of these resonance signals corresponding to the OH- and COOH end-groups relative to the linear units (e.g. fumarate unit signal at 6.8 – 7.0 ppm) provides the relative percentages of the COOH -and OH-groups. Table 4.15 shows the relative percentages of the OH- and COOH-groups of runs 29 to 33.

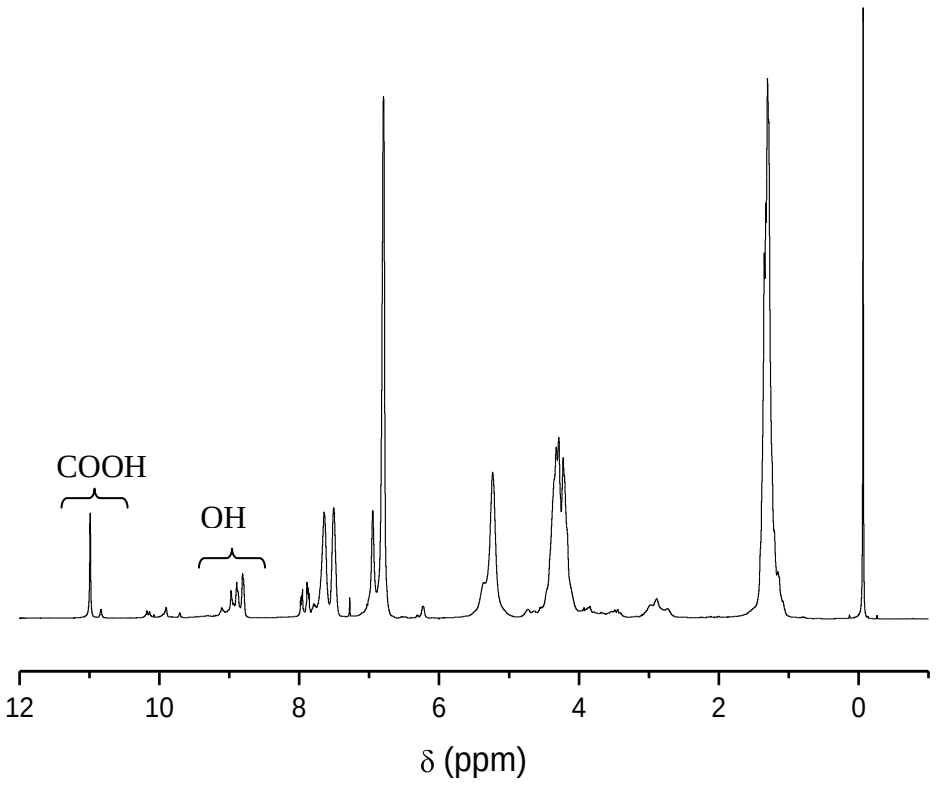

Figure 4.33: ^{1}H NMR spectrum of UPR of RUN 29 derivatized by TAI.

Table 4.15: Relative OH- and COOH-group percentages of UPRs of runs 29 to 33.

RUN	Integrated -COOH peak	Integrated –OH peak	Fumarate	%COOH	%OH
29	0.90	2.30	11.70	7.69	19.66
30	0.00	1.10	36.90	0.00	2.98
31	0.90	2.90	18.90	4.76	15.34
32	1.00	4.50	32.20	3.11	13.98
33	1.20	3.80	26.00	4.62	14.62

Table 4.15 shows that the OH- and COOH-group concentrations of the UPRs decrease as the maximum processing temperature increases. In other words, a higher conversion is achieved at higher processing temperatures. The latter is supported by the acid-value results in Section 4.3.2.

Table 4.15 also indicates that the UPRs have higher concentrations of OH-groups compared to COOH-groups, because they were synthesized with excess PG. In other words, the probability of an OH-terminated polyester chain is higher than COOH-terminated chain. It should be noted that the derivatization technique was not successful for all UPR samples, e.g. the %COOH of RUN 30 could not be determined, as the COOH-peak had an integration-value of zero in multiple ^{1}H NMR spectrums.

4.7 References

1. Rawle, A. *Basic Principles of Particle Size Analysis*; Malvern Instruments Limited: Worcestershire, pp 1 - 8.
2. Podzimek, S.; Hanus, J.; Klaban, J.; Kitzler, J. *Journal of Liquid Chromatography* **1990,** 13, 1809.
3. Zetterlund, P. B.; Gosden, R. G.; Weaver, W.; Johnson, A. F. *Polymer International* **2003,** 52, 749.
4. Paci, M.; Crescenzi, V.; Supino, N. *Makromolekulare Chemie* **1982,** 183, 377.
5. Judas, D.; Fradet, A.; Marechal, E. *Makromolekulare Chemie* **1983,** 184, 1129.
6. Holter, D.; Burgath, A.; Frey, H. *Acta Polymer* **1997,** 48, 30.
7. Ubranski, J.; Czerwinski, W.; Janicka, K.; Majewska, F.; Zowall, H. In *Handbook of analysis of synthetic polymers and plastics*, 1st ed.; Cameron, G. G., Ed. Halsted Press: London, **1977**; pp 223 - 272.
8. Price, G. F. In *Techniques of polymer characterisation*, Allen, P. W., Ed. Butterworths Scientific: London, **1959**; pp 209 -229.
9. Koenig, J. L. In *Spectroscopy of polymers*, Elsevier: New York, **1999**.
10. Al-AbdulRazzak, S.; Lofgren, E. A.; Jabarin, S. A. *Polymer International* **2002,** 51, 174.
11. Guittard, J.; Tessier, M.; Blais, J. C.; Bolbach, G.; Rozes, L.; Marechal, E. *Journal of Mass Spectrometry* **1996,** 31, 1409.
12. Rissler, K. *Journal of Chromatography A* **1997,** 786, 85.

13. Fox, B.; Moad, G.; Diepen, G. V.; Willing, R. I.; Cook, W. D. *Polymer* **1997,** 38, 3035.
14. Bovey, F. A.; Mirau, P. *NMR of polymers*. In Academic Press: New York, **1996**; pp 199 - 212.
15. Petiaud, R.; Waton, H.; Pham, Q. T. *Polymer* **1992,** 33, 3155.
16. Kenwright, A. M.; Peace, S. K.; Richards, R. W.; Bunn, A.; MacDonald, W. A. *Polymer* **1999,** 40, 2035.
17. Spyros, A.; Argyropoulos, D. S.; Marchessault, R. H. *Macromolecules* **1997,** 30, 327.
18. Donovan, A. R.; Moad, G. *Polymer* **2005,** 46, 5005.

CHAPTER 5

CONCLUSIONS AND RECOMMENDATIONS

5.1 Conclusions

The first objective of the study was to investigate the effects of varying MA:PA mole ratio and process parameters, e.g. heating rates, agitation speed, etc. on the properties of the UPRs, via Design of Experiments (DoE).

Statistical analysis of the DoE results revealed that the process and formulation parameters/factors (as well as interactions between the factors) had significant effects on the basic properties (e.g. viscosity, acid-value) of the UPRs. In particular, the MA:PA mole ratio and its interaction with the maximum process temperature significantly affect most of the UPR properties as these factors control the degree of chain branching, concentration of carboxyl groups and viscosity.

The second objective was to determine the molecular composition/ structure of the UPRs and relate to specific properties of MVPs.

The molecular weights (M_n and M_w values) and molecular weight distribution (PDI) of the UPRs were successfully determined by SEC; glass-transition temperature (T_g) by DSC; degree of chain branching by ^{1}H NMR; and the percentage carboxyl- and hydroxyl end-groups via isocyanate derivatization coupled with ^{1}H NMR.

The particle sizes (SMD and VMD-values) of the MVPs were found to be significantly affected by viscosity, molecular weights and molecular weight distribution of the UPRs. The properties mentioned are affected by the MA:PA mole ratio and its interaction with the maximum process temperature, due to the fact that the particle size of suspension-based polymers is controlled by the droplet/particle coalescence-break-up equilibrium during the polymerization. The coalescence-break-up equilibrium is determined by the

viscosity and surface tension of the oil droplets, which are affected by the MA:PA mole ratio and maximum process temperature.

It was found that UPRs synthesized with a low %MA and low maximum reaction temperature can result in MVPs with a high SMD-value, and those synthesized with a high %MA and high maximum reaction temperature can result in MVPs with a high VMD-value.

To determine the effect of maximum reaction temperature (at fixed MA:PA mole ratio) on the properties of the UPRs and MVPs, a detailed evaluation was conducted. The evaluation revealed that an increase in the magnitude of the maximum process temperature results in an increase in the viscosity, molecular weight (M_n and M_w values) and molecular weight distribution (PDI), T_g value and degree of chain branching; and a decrease in the acid-value of the UPRs.

The evaluation also revealed that an increase in the maximum process temperature (at fixed MA:PA mole ratio) of the UPRs resulted in larger MVPs in terms of their SMD and VMD-values. Furthermore, it was found that the degree of vesiculation (or opacity) of the MVPs is dependent on the MA:PA mole ratio and maximum reaction temperature in the UPR synthesis. These parameters control the distribution of the carboxylic groups (and degree of branching) of the UPR chains, and therefore their interaction with DETA, and the formation of the MVP vesicles.

In addition, an attempt was made to determine the hardness of the MVPs using the microhardness tester and AFM. The relative hardness of the MVPs were determined to establish a relationship between the properties of the hardness and the crosslink density, particle size and degree of vesiculation of the MVPs.

Unfortunately, the microhardness testing was found to be unsuccessful due to the fact that not all the MVPs were homogeneously distributed at the surface of the cured resin, which led to erratic results during testing.

AFM was only found to be effective to determine the hardness of MVPs smaller than 1μm, which means that the hardness of MVPs with an average particle size e.g. 25μm could not be determined.

5.2 Recommendations for future work

As mentioned in Section 4.1, the screening design involved a minimum of experimental points to determine the main effects affecting the properties of the UPRs and MVPs. Future work may include augmenting the design, i.e. broadening the experimental space by adding additional experiments to the existing data to be able to optimize the synthesis and properties of the UPRs and MVPs.

As mentioned in Section 4.5, the end-group analysis via isocyanate derivatization coupled with ^{1}H NMR was not successful for all samples. Future work may include investigating alternative techniques e.g. ^{19}F NMR and ^{31}P NMR to quantitatively determine the hydroxyl -and carboxyl end-groups of the UPRs.

Great difficulty was experienced in determining the physical properties (e.g. hardness) of the MVPs. AFM and microhardness testing were unsuccessful, but other mechanical tests may be attempted in the future to determine the physical properties of MVPs.